

Self-Assembly, Spatial-, and Size- Control of Gold Nanoparticle/Block Copolymer Conjugates

Dissertation

zur Erlangung des akademischen Grades eines Doktors der

Naturwissenschaften (Dr. rer. nat.)

im Fach Chemie

an der Bayreuther Graduiertenschule

für Mathematik und Naturwissenschaften (BayNAT)

der Universität Bayreuth

vorgelegt von

Dipl. Chem. Melissa S. Köhn Serrano

aus

Mexiko-Stadt

Bayreuth, 2015

Die vorliegende Arbeit wurde in der Zeit von September 2011 bis Juli 2012 in Marburg am Lehrstuhl für Makromolekulare Chemie und in der Zeit von August 2012 bis Juli 2015 in Bayreuth am Lehrstuhl für Makromolekulare Chemie II unter Betreuung von Herrn Prof. Dr. Andreas Greiner angefertigt.

Vollständiger Abdruck der von der Bayreuther Graduiertenschule für Mathematik und Naturwissenschaften (BayNAT) der Universität Bayreuth genehmigten Dissertation zur Erlangung des akademischen Grades eines Doktors der Naturwissenschaften (Dr. rer. nat.).

Dissertation eingereicht am:	21. Juli 2015
Zulassung durch das Leitungsgremium:	28. Juli 2015
Wissenschaftliches Kolloquium:	18. November 2015

Amtierender Direktor: Prof. Dr. Stephan Kümmel

Prüfungsausschuss:

Prof. Dr. Andreas Greiner	(Erstgutachter)
Juniorprof. Dr. Markus Retsch	(Zweitgutachter)
Prof. Dr. Birgit Weber	(Vorsitz)
Prof. Dr. Peter Strohrig	

When obstacles arise, you change your direction to reach your goal; you do not change your decision to get there.

Zig Ziglar

List of publications

Parts of this work were previously published:

[1] M. S. Köhn Serrano, T. A. F. König, J. S. Haataja, T. I. Löbbling, H. Schmalz, S. Agarwal, A. Fery, A. Greiner, Self-Organization of Gold Nanoparticle Assemblies with 3D Spatial Order and Their External Stimuli Responsiveness, *Macromol. Rapid Commun.* **2015**, DOI: 10.1002/marc.201500509.

[2] Z. Fan, X. Chen, M. Köhn Serrano, H. Schmalz, S. Rosenfeldt, S. Förster, S. Agarwal, A. Greiner, Polymer Cage as Universal Tools for the precise Bottom-up Synthesis of Metal Nanoparticles, *Angew. Chem. Int. Ed.* **2015**, *54*, 14539-14544, *Angew. Chem.* **2015**, *127*, 14747-14752.

[3] Z. Fan, M. Köhn Serrano, A. Schaper, S. Agarwal, A. Greiner, Polymer/Nanoparticle Hybrid Materials of Precise Dimensions by Size-Exclusive Fishing of Metal Nanoparticles, *Adv. Mat.* **2015**, *27*, 3888-3893.

Contents

1	Introduction	1
2	Theoretical Background and Literature Overview	2
2.1	Anionic Polymerization	2
2.2	Block Copolymers and Self-Assembly	4
2.3	Functional Block Copolymers	7
2.4	Nanotechnology and Gold Nanoparticles	9
2.4.1	Historical Background	9
2.4.2	Stabilization of Gold Nanoparticles	12
2.4.3	Preparation Methods of Gold Nanoparticles	13
2.5	Polymer/Gold Nanoparticle Nanocomposites	16
2.5.1	S4VP/AuNP Nanocomposites	19
3	Motivation, Aim, and Scope of the Thesis	23
4	Results and Discussion	26
4.1	Synthesis of S4VP Block Copolymers	26
4.2	Synthesis of Citrate-stabilized Gold Nanoparticles Citrate@AuNP	30
4.3	Synthesis of Citrate-stabilized Silver Nanoparticles Citrate@AgNP	33
4.4	Ligand Exchange Reactions of Citrate@AuNP with S ₂₆ 4VP ₁ , S ₇₇ 4VP ₁ , and S ₇₇ 4VP ₃₄ with Variation of AuNP/4VP Ratio	35
4.4.1	Hypothesis and Motivation	35
4.4.2	Ligand Exchange Reactions with Monodentate Ligands; Variation of AuNP Ratio	40
4.4.3	Ligand Exchange Reactions with Multidentate Ligands; Variation of AuNP Ratio	54

4.4.4	Reverse Experiment: Ligand Exchange Reactions of Citrate@AuNP; Variation of 4VP Ratio	58
4.4.5	Ligand Exchange Reactions with Monodentate Ligands; Variation of 4VP	58
4.4.6	Ligand Exchange Reactions with Multidentate Ligands; Variation of 4VP Ratio	62
4.4.7	Conclusion	65
4.5	<i>In situ</i> Reactions of AuNP with S ₇₇ 4VP ₁ , S ₇₇ 4VP ₁₇ , and S ₇₇ 4VP ₃₄	67
4.5.1	Hypothesis and Motivation	67
4.5.2	<i>In situ</i> Formation of AuNP	67
4.5.3	Characterization of Monodentate Ligands	69
4.5.4	Characterization of Multidentate Ligands	73
4.5.5	Conclusion	79
4.6	Synthesis, Characterization, and Application of α -Hydroxypolystyrene- <i>b</i> -poly-4(vinylpyridine) (α -HO-S4VP)	81
4.6.1	Synthesis of <i>t</i> BDMSOPrLi	82
4.6.2	Synthesis and Characterization of α -Hydroxypolystyrene- <i>b</i> -poly-4-vinylpyridine (α -HO-S4VP) Block Copolymer <i>via</i> Living Anionic Polymerization	86
4.6.3	Click Reactions of α -OH-S ₈₅ 4VP ₂ with Coumarin	99
4.7	Ligand Exchange Reactions of Citrate@AuNP with CM-O-S ₈₅ 4VP ₂	103
4.8	Ligand Exchange Reactions of Citrate@AgNP with CM-O-S ₈₅ 4VP ₂	105
5	Summary	107
6	Zusammenfassung	110
7	Outlook	113
8	Acknowledgments	116
9	Experimental section	118
9.1	Materials and Methods	118
9.1.1	Chemicals and Solvents	118
9.1.2	Instrumentation	120

9.2	General Synthetic Procedures	124
9.2.1	Synthesis of S4VP Block Copolymers	124
9.2.2	Synthesis of <i>t</i> BDMSOPrCl	127
9.2.3	Synthesis of <i>t</i> BDMSOPr as an Internal Standard for GC	128
9.2.4	Synthesis of <i>t</i> BDMSOPrLi	129
9.2.5	Synthesis of α -HO-S4VP Block Copolymer	129
9.2.6	Synthesis of Coumarin-3-Carboxylic Chloride	131
9.2.7	Synthesis of CM-O-S ₈₅ 4VP ₂	132
9.2.8	Synthesis of Citrate@AuNP	133
9.2.9	Ligand Exchange Reactions of Citrate@AuNP with S4VP	133
9.2.10	<i>In situ</i> Synthesis of S4VP@AuNP	133
9.2.11	Synthesis of Citrate@AgNP	134
9.2.12	Ligand Exchange Reactions of Citrate@AuNP and Citrate@AgNP with CM-O-S ₈₅ 4VP ₂	134
	List of Abbreviations	135
	Bibliography	138

1 Introduction

The combination of organic and inorganic compounds at the nanoscopic scale has existed since the origin of life. Bone, nacre, corals, and membranes of living cells are only a few examples that nature has been fabricating. These bio-materials show extraordinary properties due to the particular arrangement, or so called self-assembly of molecules, which inspired scientists to challenge this field and develop novel synthetic nanocomposites with better and controlled properties^[1].

The field of polymers, especially block copolymers (BCP) has been studied for many decades, and various morphologies have been observed in bulk and in solution. The use of combined BCP and gold nanoparticles (AuNP) has attracted a strong research interest due to the different and controlled morphologies, self-assembly, and unique properties, respectively, which hold great expectations for developing novel materials with enhanced optical, electronic or magnetic properties^[2].

For many applications, polymer/AuNP nanocomposites require a precise control over the size, morphology, and self-assembly of nanoparticles and pronounced stimuli-responsive properties^[3]. The ability to functionalize AuNP with BCP and to control their exact location within a polymer matrix has opened new developments for the fabrication of genuine polymer/AuNP nanocomposites with tailored structures, where their properties can be manipulated^[4]. The latter implies an appropriate molecular composition of the BCP with a correct balance of intermolecular interactions between the polymer and the metal nanoparticles.

The aim of this work is to explore the self-assembly and surface modification of AuNP with BCP in suspension, leading ordered structures of polymer/AuNP nanocomposites with characteristic optical properties.

2 Theoretical Background and Literature Overview

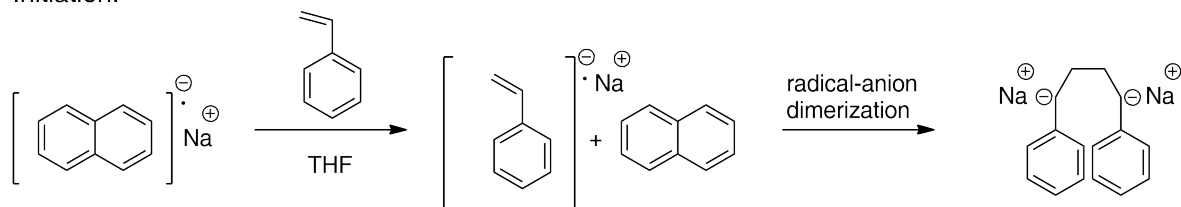
2.1 Anionic Polymerization

One of the most important methods to synthesize well defined polymers with narrow molar mass distributions is the living anionic polymerization, which embraces a chain-growth mechanism of the reaction process. This method has been used since a century ago, when SCHLENK and co-workers reported for the first time the anionic polymerization of styrene in 1914^[5,6]. However, the term „living“ anionic polymerization was highlighted by MICHAEL SZWARC and co-workers in 1956^[7]. SZWARC demonstrated the mechanism of the anionic polymerization by polymerizing styrene in tetrahydrofuran (THF) using sodium naphthalene as initiator^[8] (Scheme 1). It was shown that the formed polymer can spontaneously resume its propagation by addition of the same or of a different monomer in the absence of chain termination and chain transfer. This was carefully analyzed by measuring the viscosity after the addition of a second aliquot of a monomer, which showed an increment due to the growth of the polystyrene chain. In addition the red color of the solution proved the „living“ species of the active styryl anions in solution. This reaction marked the beginning of a new area of research regarding living polymers^[7,9-11].

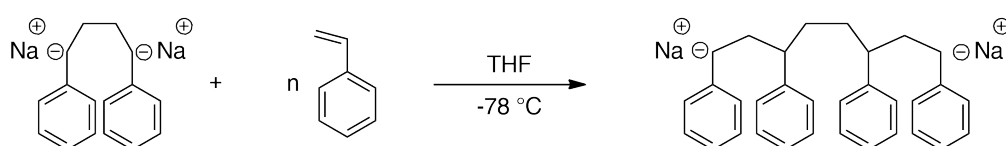
Subsequently, the anionic polymerization of styrene was further investigated using organolithium compounds as initiators, which showed an improvement and raised an interest in this field^[12-14]. The reaction is composed of three main steps: (i) initiation of a single monomer molecule to the reactive species, (ii) propagation of the polymeric chains by consecutive incorporation of monomer, and (iii) termination by deactivation of the chain-end. Scheme 2 shows the anionic polymerization of styrene using *sec*-butyllithium

(*sec*-BuLi) as initiator.

Initiation:

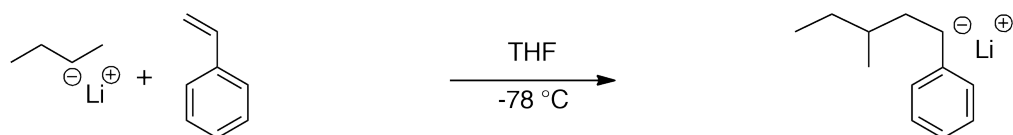


Propagation:

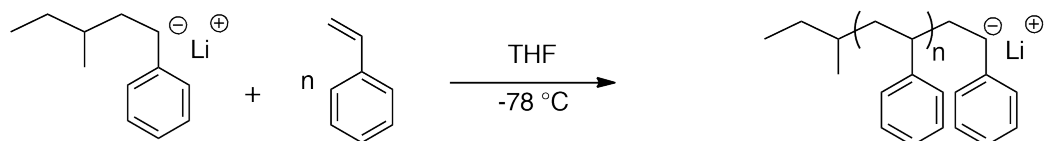


SCHEME: 1 Anionic polymerization of styrene using sodium naphthalene as initiator in THF, reported by SZWARC^[8].

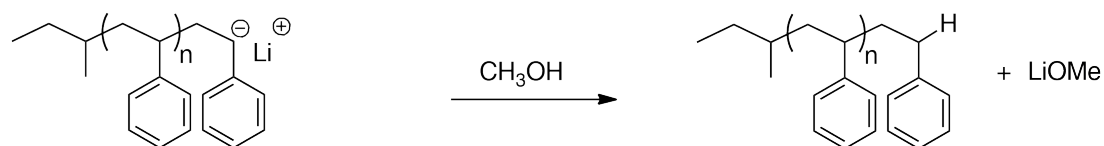
Initiation



Propagation



Termination



SCHEME: 2 Anionic polymerization of styrene using *sec*-BuLi as initiator in THF.

Living anionic polymerization distinguishes itself from conventional chain polymerizations by the absence of termination and chain transfer reactions, which results in a highly controlled polymer architecture. The relative molar mass (M_n) is determined by the amount of consumed monomer and the initiator employed. Polymers synthesized by anionic polymerization exhibit in general a narrow molar mass distribution with dispersity between 1.0 and 1.1. This narrow distribution is obtained only if the rate of initiation is much faster than the rate of propagation. However, a molar mass distribution over 1.1 might be observed due to the end-group reactivity of the monomers used^[15]. Though, the main obstacle of this reaction is its sensitivity to impurities or contaminants, which influence the molar mass distribution and restrict the propagation of the living polymer. For this reason it is very important to work under strictly controlled reaction conditions, such as absence of water or air contact, as well as the avoidance of contaminated monomers.

The main benefit of the anionic polymerization is the possibility to tailor and control properties, such as polymer molar mass (M_n and M_w), architecture, composition, and chain-end functionality by simply varying the initiator amounts or adding different monomers^[6]. The precise tailoring of these properties has opened windows for the development of unique materials with a wide range of applications.

2.2 Block Copolymers and Self-Assembly

BCP are a class of macromolecules composed of two or more chemically distinct and most frequently immiscible polymer blocks, covalently bound together^[16–18]. The most simple and widely employed BCP are the AB-type diblock and ABA-type triblock copolymers, which consist of a linear chain of type A monomers bound to one end to a linear chain of type B monomers. With two different homopolymers it is possible to prepare AB diblock, ABA triblock, multiblock, and star-block copolymers, which have been the focus of a very large number of well understood studies over the past two decades^[19–22]. Figure 2.1 illustrates schematically the conventional structures of AB block copolymers.

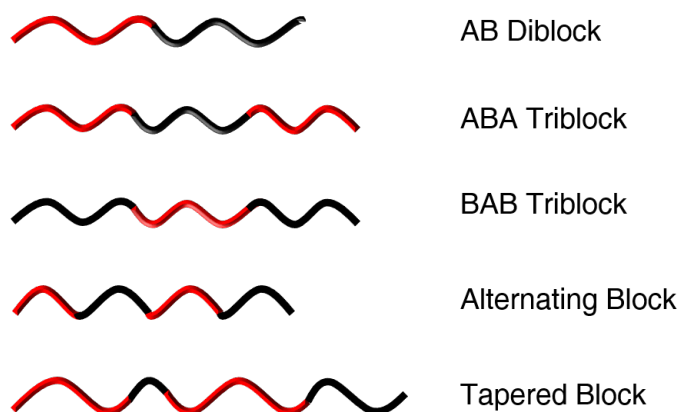


Figure 2.1: Conventional structures of BCPs composed of two types of blocks, A and B.

The most common used macromolecules in diblock copolymer synthesis are polystyrene (PS), poly(methyl methacrylate) (PMMA), polyvinylpyridine (PVP), polyisoprene (PI), polybutadiene (PB), polydimethylsiloxane (PDMS), and poly(ethylene oxide) (PEO)^[23]. Living anionic polymerization enables the controlled synthesis of block copolymers and the number of accessible monomers since its investigation has increased due to further developments in various types of controlled polymerization techniques^[24]. Since the 1980s block copolymers became an immense subject for theoretical and experimental studies due to the immiscibility of the blocks, which offers the ability of microphase separation in macrodomains of a nanometer scale, which displays self-assembly of BCPs^[17,23,25].

The term self-assembly is defined as a spontaneous organization of highly ordered molecules driven by an unfavorable force mixing enthalpy coupled with a small mixing entropy, while the covalent bond connects the two blocks preventing microphase separation^[26]. The microphase separation of block copolymers depends on three parameters: (i) the total degree of polymerization N ($N = N_A + N_B$), (ii) the volume fraction ϕ of the A and B blocks (ϕ_A and $\phi_B = 1$), and (iii) the FLORY-HUGGINS parameter, χ_{AB} ^[17,19]. The degree of polymerization (\bar{D}) is related to the radius of gyration (R_g) of the polymer and hence the size of the microdomains in an indirect way. N specifies the entropic contribution to the overall GIBBS energy of the block copolymer. The χ -parameter is responsible for the incompatibility of the blocks, which is a driving force of phase separation and is temperature dependent, so that it specifies the enthalpic contribution to the overall GIBBS energy^[19]. The degree of microphase separation can be determined by the

segregation product χN , which is governed by the volume fraction and is divided in the weak segregation limit (WSL) ($\chi N < 10$) and the strong segregation limit ($\chi N \gg 10$) (SSL). According to this χN BCPs emerge in a variety of morphologies, including spheres (S), cylinders (C), bicontinuous gyroids (G), and lamellae (L) depending on the composition of the BCP. Several theories have been developed to explain the different morphologies of BCPs. MATSEN and BATES described the different morphologies of BCPs with a phase diagram according to the self-consistent field theory (SCFT)^[16,19]. Figure 2.2 shows the phase diagram of BCPs with their corresponding morphologies predicted by MATSEN and BATES^[16,27].

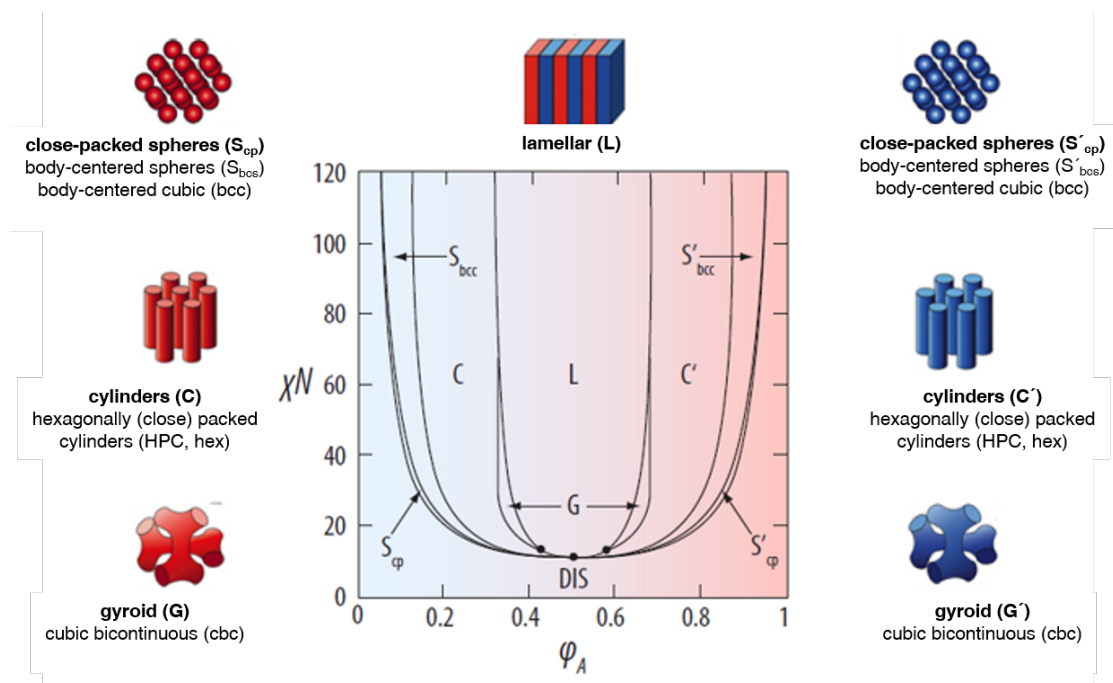


Figure 2.2: Phase diagram of BCPs in bulk predicted by MATSEN and BATES^[27].

The increase of the volume fraction of one of the blocks leads to a microphase separation starting from close packed spheres (CPS), passing through spheres (S), hexagonally packed cylinders (C), bicontinuous gyroids (G), and lamellae (L). An inversion of the morphology is also possible when the composition is inverted^[16,19].

In contrast to BCP self-assembly in bulk, BCP self-assembly in solution exhibits another kind of morphology due to the solvents, that can be selective or non-selective to one of the blocks. Also the use of polar and non-polar monomers increases the level of complexity of BCP self-assembly. Depending on the solubility of the blocks, BCPs can be cat-

egorized in non-polar block copolymers and amphiphilic block copolymers^[28–31]. The solubility of one of the blocks leads to the formation of micelles with different shapes. If the soluble block is predominant, the insoluble block aggregates to produce spherical micelles, showing a core-corona structure^[32–34]. By decreasing the soluble block relative to the insoluble block, cylindrical micelles or vesicles are formed.

Polymers that contain polar monomers are more challenging to synthesize due to their high reactivity and the formation of side products during the polymerization process^[35]. This can be avoided by using end-capping agents, such as 1,1-diphenylethylene (DPE) before the addition of the polar monomer to decrease the nucleophilicity of the active chain ends and create block copolymers with well defined properties^[15].

Over the past decade, the self-assembly of amphiphilic block copolymers has been immensely investigated and well established. They are a good choice, both in terms of thermodynamics and dynamics to create materials and patterns for potential applications as multifunctional devices^[3].

BCPs composed of styrene and 4-vinylpyridine (S4VP) have been well studied in bulk and in solution over the past decade^[19,32,36–41]. Due to the incompatibility of the blocks S4VP phase separates in bulk and self-assembles into sphere, cylinder, gyroidal or lamellar morphologies. Depending on the molecular composition of S4VP, the volume fraction of 4VP (χ_{4VP}), and solvent that is used, it is possible to control and tailor the morphology of S4VP^[39–43]. The ability to control the chemical composition and structure of block copolymers allows these materials to be ideal templates for hierarchical supramolecular control over the size, particle density, and spatial location of inorganic nanoparticles^[44]. Unlike the 2VP block, 4VP units are subject to stronger interactions between each other and with the inorganic compounds, which results in a significant difference in the micellization behavior of this block copolymer. In this thesis the block copolymer polystyrene-*block*-poly-4-(vinylpyridine) (S4VP) was employed as ligands for the stabilization of inorganic nanoparticles and will be highlighted in the next sections.

2.3 Functional Block Copolymers

In addition to the structural and topological control of polymers and their properties by living anionic polymerization, further properties can be enhanced by introducing

reactive functional groups into the polymers. The incorporation of functional groups can be achieved by different pathways, including the use of reactive monomers, such as ethylene oxide, or protected functional anionic polymerization initiators. The chemical properties of the polymers can be modified by quantitative functionalization at a particular point of the chain^[18,45].

The use of functional initiators for living anionic polymerization reactions are of major interest, because they possess the ability to generate facile telechelic monomers at the beginning of the polymer initiation and conclude with the addition of a numerous of different monomers to synthesize block copolymers with well defined molecular architectures. These kinds of telechelic block copolymers are suitable for applications in coatings, adhesives, and sealants^[46], or employed as templates for novel and simple routes for the attachment of dyes by click-reactions^[47].

In 1991, the organolithium compounds of type ω -(*tert*-butyldimethylsilyloxy)-1-alkyllithium were fabricated and introduced as „protected“ anionic polymerization initiators for the synthesis of α -hydroxy-functionalized semi-telechelic polystyrenes^[48]. These types of compounds have been widely used to prepare nearly monodisperse functional polymers with a hydroxyl end-group, as the silyl protecting group is easily removed with acidic or fluorene sources^[49–56]. HILLMYER used 3-*tert*-dimethylsilyloxy-1-propyllithium (*t*BDMSOPrLi) as initiator for the synthesis of 1,4-polybutadiene and 1,4-polyisoprene homopolymers^[51] in THF, while QUIRK and co-workers investigated the kinetics of the reaction and improved the polymerization to synthesize well defined telechelic block copolymers of styrene and 1,4-polydienes in nonpolar solvents^[49,54]. BATES and co-workers investigated the activity of the block copolymer α -hydroxy-poly(styrene/1,4-diene) with the initiator 3-triisopropylsilyloxy-1-propyllithium (TIPSOPrLi) and showed a control over regioselectivity of the 1,4-diene and well formed monodisperse telechelic block copolymers^[57]. The use of TIPSOPrLi was also successful for the synthesis of various functional macromonomers, e.g. the synthesis of the triblock copolymer composed of styrene-isoprene-styrene.

According to these reports, a functional block copolymer of styrene and 4-vinylpyridine is also possible to be synthesized by anionic polymerization using functional initiators. Functional α -hydroxy-polystyrene-*block*-poly-4-(vinylpyridine) (α -OH-S4VP) could be considered as a bifunctional polymer. On the one hand, the polystyrene block carries a reactive hydroxyl group in α -position of the polystyrene block, which is suitable for

further functionalizations. On the other hand, the lone pair of electrons of the pyridyl group of the 4VP block acts as a coordinating agent for metal nanoparticles. Basically, a modified S4VP block copolymer could be employed as a bifunctional polymer for the functionalization of metal nanoparticles and the attachment of reactive molecules such as chromophores by click reactions for the purpose of enhancing the physical and chemical properties of novel nanostructures.

2.4 Nanotechnology and Gold Nanoparticles

2.4.1 Historical Background

Nanotechnology is the science that deals with the design, characterization, production, and application of structures, devices, and systems by controlling shape and size at the nanometer scale^[37]. It embraces an interdisciplinary research in the fields of engineering, physics, chemistry, materials science, and molecular biology^[58]. In general, the size of a nanoparticle ranges in dimensions between 100 nm and 1 nm^[59]. These materials are composed of a few atoms and are intermediate in size between the molecular and atomic level, where the energy levels of the system become more discrete and the energy is quantified and they are referred to as quantum dots. In contrast, materials at the macroscopic level are composed of a valence and a conducting band, which are only separated by an energy gap^[60,61]. There are three major factors that are responsible for the differences of metal nanoparticles: high surface-to-volume ratio, quantum size effect, and electrodynamic interactions^[58,62]. This is why nanoparticles show extraordinary physical and chemical properties that differ from their bulk materials^[63]. The density of states between atomic and bulk level is schematically represented in Figure 2.3.

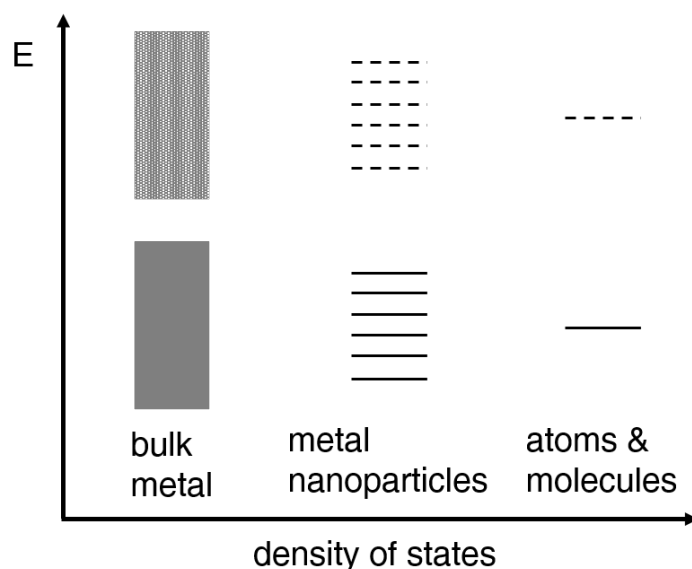


Figure 2.3: Electronic energy levels (E) in dependence of the density of states from macroscopic to atomic level^[60].

The properties of metal nanoparticles can be, for instance, strength, electrical and thermal conductivity, optical and catalytic response, or elasticity^[58,64]. Among the noble metals copper, silver, and gold, AuNP are probably the most exploited materials in research and applications, since they not only show resistivity against oxidation and corrosion but also show biocompatibility and are less cytotoxic than other metal nanoparticles^[65]. The use of AuNP has created a huge impact in society and science over the last century and are fundamental subjects in nanotechnology. Historically, AuNP are known since the ancient times to Middle Ages, where AuNP suspensions were used to stain glass or treat illnesses^[66,67]. Stained glass can be observed in most of Gothic European churches, where the windows are stained with colloidal gold or silver. The color changes depending on the size and shape of gold and silver nanoparticles. A photograph of one of the rose windows of the Cathédrale Notre-Dame de Chartres, France is appreciated in Figure 2.4^[59].

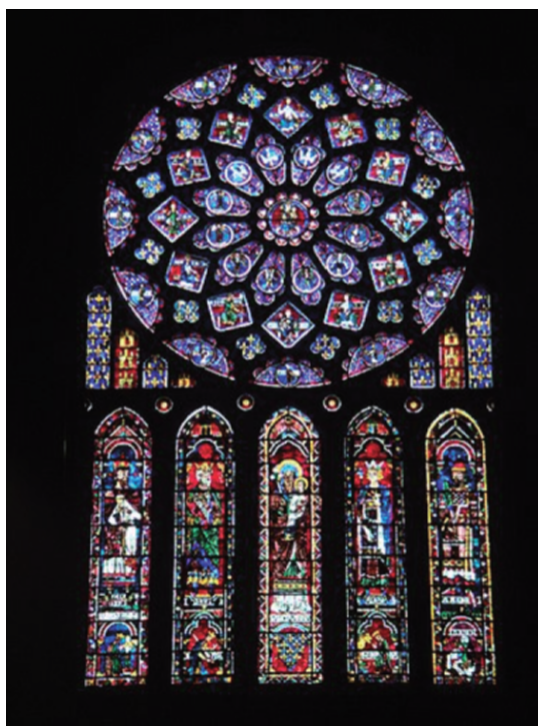


Figure 2.4: Rose window stained glass in the Cathédrale Notre-Dame de Chartres, France^[59].

The first scientific reports on metal nanoparticles originated in the 1850s, when MICHAEL FARADAY reported the formation of ruby-red gold colloids by reduction of an aqueous solution of tetrachloroaurate (AuCl_4^-) with phosphorus in carbon disulfide (CS_2) in a biphasic reaction. Moreover, he investigated the optical properties of thin films prepared from dried colloidal solutions and observed reversible color changes by mechanical compression^[68]. Furthermore, he investigated the interactions between light and colloidal solutions and observed that particles were much smaller than the wavelength of light. His work marked a new era for the research in the field of optics. At the beginning of the 20th century MAXWELL and MIE unraveled the theory for scattering and absorption of light by spherical nanoparticles^[69,70]. The reason for the special color of metal nanoparticles derives from the collective oscillation of the electron gas of the metal nanoparticles in the presence of an electric field, which in this case is the interaction with light. This phenomenon is called surface plasmon resonance (SPR), which is a unique optical property of metal nanoparticles. The SPR depends on shape, size, metal and dielectric environment of the nanoparticles and emerges in the whole electromagnetic spectrum^[71]. The control of shape and size of the nanoparticles has developed new challenges, which increases the possibility for a numerous of applications in the field

of nanotechnology^[72,73]. Figure 2.5a describes schematically the interaction of metal nanoparticles with light and Figure 2.5b shows SPR of different metal nanoparticles.

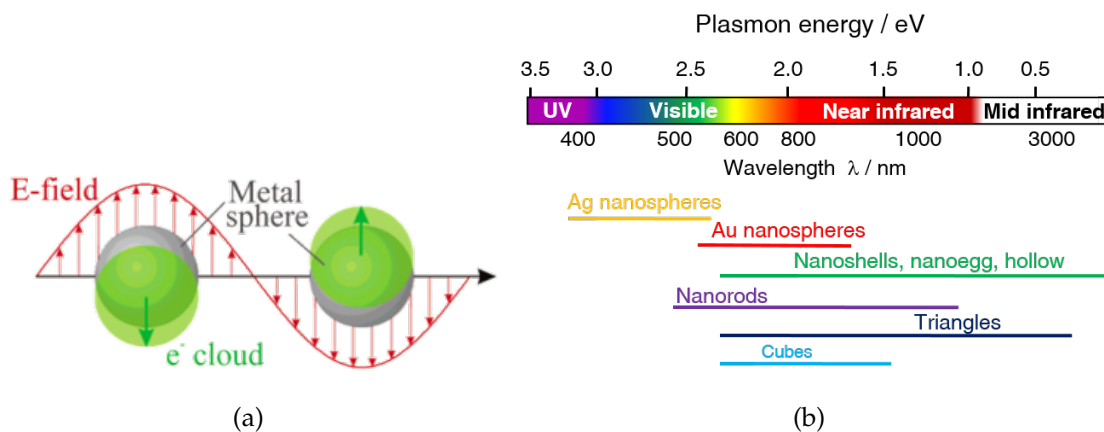


Figure 2.5: (a) Schematic representation of the electron gas of metal nanoparticles by interaction with light^[71]. (b) SPR of different metal nanoparticles and shapes.

2.4.2 Stabilization of Gold Nanoparticles

AuNP are only stable if their surface is surrounded by stabilizing agents. There are different types of stabilization for nanoparticles^[73]. By using anions and cations from the starting material in solution, the surface of the nanoparticles are electrostatic stabilized by an electrical double layer. This results in a COULOMB repulsion that prevents agglomeration. To prevent aggregation and unstable nanoparticles, large molecules, e.g. polymers or surfactants are used, causing a steric hindrance between the nanoparticles (Figure 2.6). The combination of steric and electrostatic effects is known as electrosteric stabilization^[74].

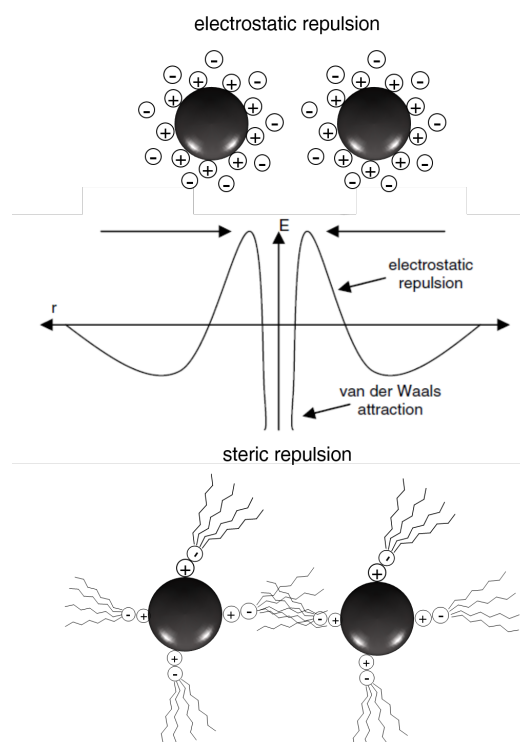


Figure 2.6: Electrostatic and steric stabilization of gold nanoparticles^[74].

2.4.3 Preparation Methods of Gold Nanoparticles

AuNP can be prepared by two different approaches, namely the „top-down“ and „bottom-up“ method.

The „top-down“ method comprises the breaking up of a solid substance in a wet or a dry atmosphere by ball mill techniques to generate AuNPs of the desired dimensions^[37]. However, this method leads to an uncontrolled size and shape formation of AuNP and restricts further functionalizations^[75]. In contrast, the „bottom-up“ approach offers a much better flexibility concerning material design. The formation of AuNP originates from individual molecules, which involves the chemical reduction of metal ions followed by nucleation and successive growth of nanoparticles. This growth mechanism is also called OSTWALD ripening, which describes the diffusion of atoms from smaller to larger particles leading to a more homogeneous diameter distribution with elevated mean diameters^[76,77]. When nucleation and growth takes place in the same reaction process, it is called *in situ* synthesis. Among all methods for *in situ* synthesis, the procedures developed by TURKEVICH and BRUST-SCHIFFRIN are the most popular methods

used for the preparation of AuNP.

In 1951 TURKEVICH presented a simple route for AuNP by reduction of the metal salt HAuCl_4 with citrate ligands, which also acted as stabilizing agents for AuNP^[78]. Particles were generated in diameter size of 20 nm. This reaction was refined by FRENS, who obtained stable AuNP in different sizes ranging from 15 nm to 150 nm by changing the molar ratio of citrate ligands^[79], that also showed significant changes of the SPR^[80]. Figure 2.7 shows the reaction scheme of citrate stabilized AuNP and a UV/Vis spectrum of AuNP synthesized in different sizes. Today exists a remarkable research on the mechanism of TURKEVICH-FRENS to synthesize AuNP to improve the control of shape and monodispersity of AuNP^[81–85].

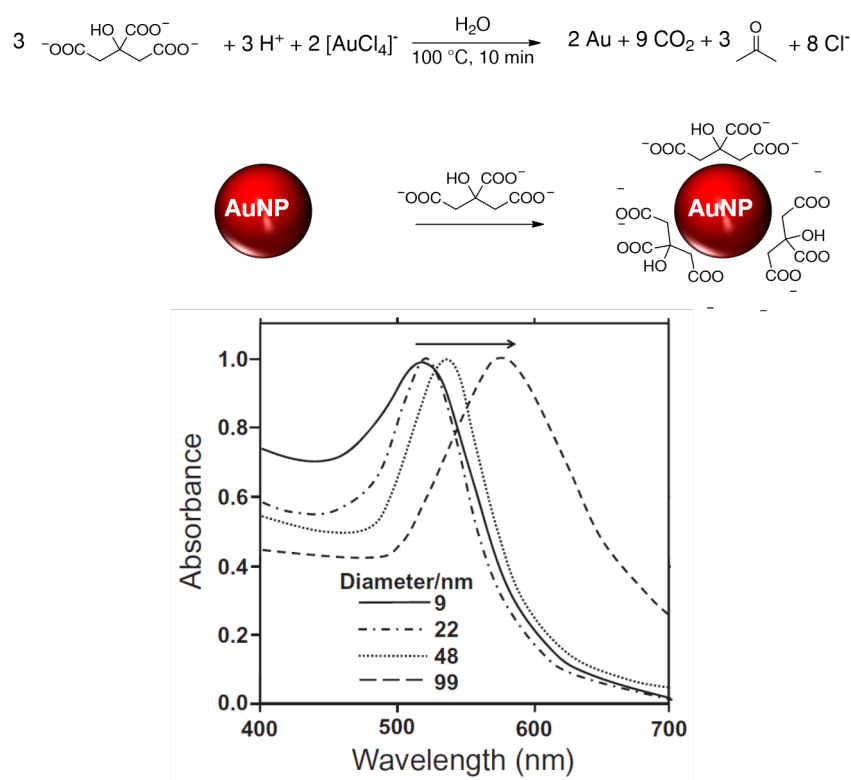


Figure 2.7: Synthesis of citrate-stabilized AuNP by the TURKEVICH-FRENS Method and corresponding UV/Vis spectrum of AuNP with different diameter sizes^[78,80].

In 1994 BRUST and SCHIFFRIN reported the synthesis of AuNP with alkylthiols of various chain lengths in a two-phase system (water/toluene) using tetraoctylammonium bromide (TOAB) as a phase transfer catalyst^[86]. This procedure induced great expectations for nanoparticle synthesis due to the control of monodisperse nanoparticles with

small sizes (5 nm), which also were isolated in form of a powder and redispersed in various organic solvents without aggregation or decomposition. The particles could also be kept in solid state under ambient conditions for a long time without significant aging effects. Thiol-functionalized AuNP showed great stability due to the strong affinity of the sulfur atoms to gold. The fact, that the reaction is carried out in a two phase system, provides the use of diverse thiol ligands for the functionalization of AuNP as described by MURRAY and co workers^[87] (Figure 2.8).

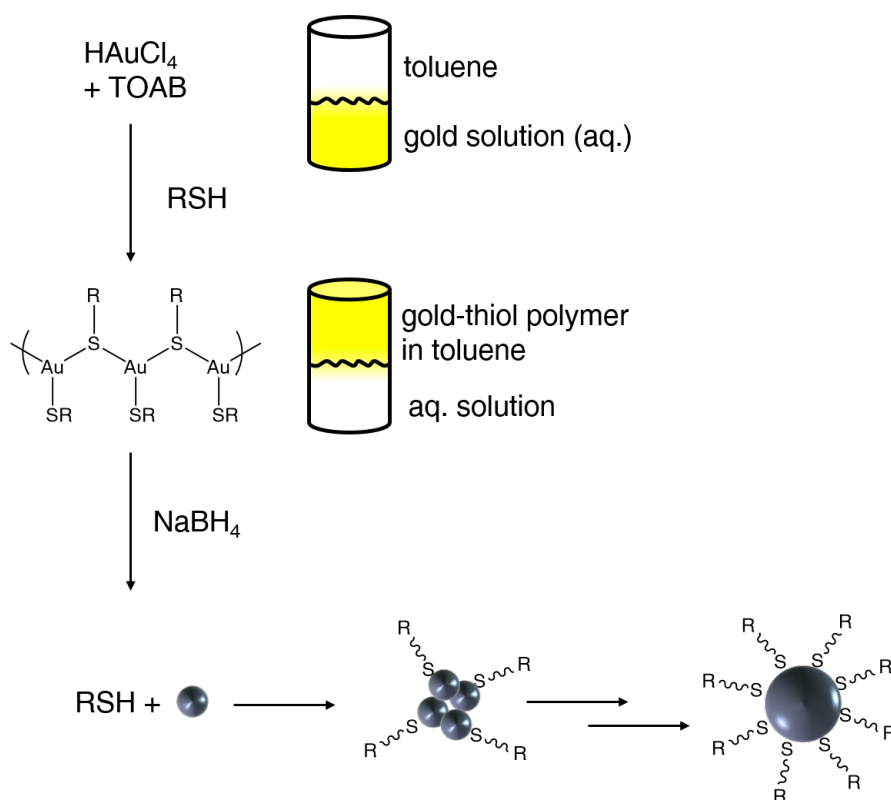


Figure 2.8: Scheme for AuNP synthesis by the BRUST-SCHIFFRIN Method^[86,87].

This method inspired scientists to improve the procedure to link ligands with a thiol end group onto the AuNP surface, that was further extended for the employment of phosphine-, amine-, and oxygen-based polymer ligands, which gave rise to the research of functionalized AuNP in the field of polymer chemistry. This routes opened a revolutionary path to create novel composites of polymers and metal nanoparticles, which will be explained in detail in the next section.

2.5 Polymer/Gold Nanoparticle Nanocomposites

As described before, metal nanoparticles, particularly AuNP are being considered in wide ranging applications, such as photonics, information storage, electronic and optical detection systems, therapeutics, diagnostics, photovoltaics, and catalysis^[67,88,89]. However, AuNP are thermodynamically unstable because of their high surface energy, which tend to spontaneously aggregate. This limits most industrial applications of nanoparticles^[90]. Most strategies of aggregation prevention are based on fixation on surfaces with small molecules, such as citrate or thiol ligands, or by functionalization with large molecules like polymers.

The conjugation of AuNP with polymer ligands to design polymer/AuNP nanocomposites has attracted much interest, not only to improve the stability and surface chemistry of AuNP but also as a way of accessing unique structures with desirable functionalities, synergistic properties and applications by combining the different characteristics of both components, which are not obtainable from one nanomaterial alone.

The use of polymeric stabilizers for metal nanoparticles has been known since 1718, when HELCHER observed how starch could stabilize AuNP dispersions^[91]. This inspired the studies of various synthetic routes to link all kind of polymers to metal nanoparticles and the investigations on properties as well as potential applications of the polymer/AuNP nanocomposites. The advantages of using polymers as stabilizers are not only the enhancement of long-term stability, adjustment of the solubility and amphiphilicity of AuNPs, but also the functionalization of AuNPs with polymers to achieve higher and tunable surface-density, and to tailor properties of AuNPs, as well as to promote compatibility and processability^[92].

The fabrication of functionalized AuNP with polymers has been well investigated and can be classified into three categories^[93]: the „grafting from“ method is accomplished when the polymerization occurs at the AuNP surface in the presence of initiators, e.g. the surface polymerization of PMMA on AuNP by living radical polymerization (ATRP), or the surface polymerization on AuNP with thiol-groups by azo-initiators^[94,95]. This technique provides the precise control of the molecular weight, a versatile structural design of a polymer layer, and effective introduction of polymer chains with high density. Figure 2.9 shows the fabrication of AuNP by surface polymerization exemplified with 4-vinylthiophenol moieties. This work was presented by GREINER and co-workers^[96,97].

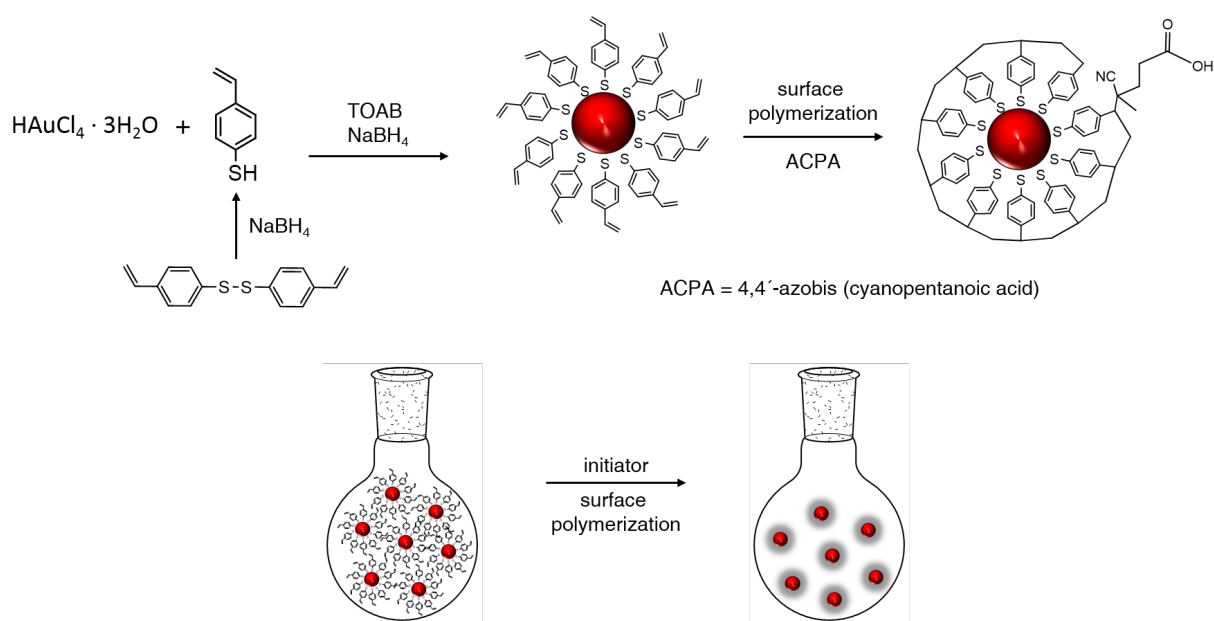


Figure 2.9: „Grafting from“ method: schematic synthesis of surface polymerization on AuNP with 4-vinylthiophenol according to the work of GREINER and co-workers^[96].

„Grafting to“ involves direct AuNP synthesis by attachment of thiol- or amine-functionalized polymers to the AuNP surface. Advantages of this method are the availability of many kinds of polymers with an anchor group for gold and the easy one-pot synthesis, which enables less impurities during the reaction. This reaction can also be described as an *in situ* reaction of AuNP in the presence of a functional polymer. Using anionic polymerization techniques, the groups of LENNOX, FÖRSTER, and GREINER reported on straightforward methods for the grafting of thiol-functionalized polystyrene (PS-SH) on gold or silver nanoparticles. The PS-SH was prepared by anionic polymerization of styrene followed by termination with ethylene sulfide. The addition of reducing agents, e.g. NaBH_4 , or lithium triethylborohydride (LiEt_3BH , Superhydride) resulted in PS-SH-grafted gold or silver nanoparticles, which showed remarkable dispersion in solvents or within the polystyrene matrix^[95,98]. A general reaction synthesis of the „grafting to“ method is schematically displayed in Figure 2.10.

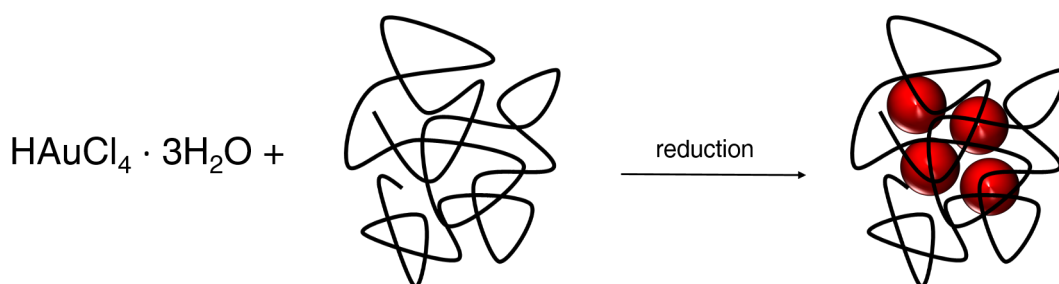


Figure 2.10: „Grafting to“ method: schematic representation of *in situ* synthesis of AuNP in the presence of thiol- or amine-functionalized polymers.

The post modification method is carried out with pre-synthesized AuNPs and polymers. This method is a common ligand exchange reaction by replacing weak ligands with stronger ligands on the AuNP surface. It is a very important and useful tool for preparing polymer/AuNP nanocomposites. Many groups have been working with this simple technique to exchange citrate anions attached to AuNP in aqueous solution with hydrophobic ligands, like PS-SH resulting on polymer nanocomposites with monodisperse AuNP^[99–102]. This reaction is schematically represented in Figure 2.11.

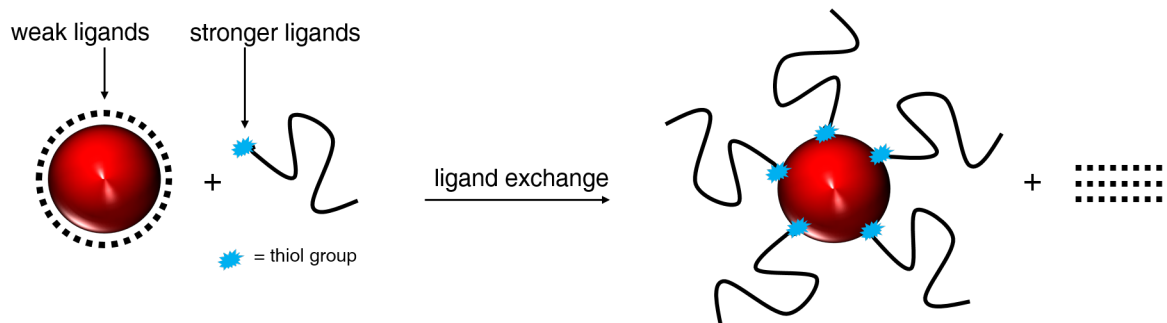


Figure 2.11: Post modification method: ligand exchange reactions of pre-synthesized AuNP with thiol-functionalized polymers^[103].

Today exists a large repertoire of functional polymers that can be bound to the AuNP surface. Homopolymers, such as polystyrenes^[99], PVP^[104], PMMA^[94], PNIPAM^[105], PEG^[106] as well as copolymers, like PS-PI^[107], PS-P2VP^[108], and PS-P4VP^[42] among others are the most popular used polymers due to their great physical and chemical properties, which results on the precise design of polymer/AuNP nanocomposites with desirable properties^[109]. There are three different approaches for the polymer-functionalized AuNP. Depending on the anchor group, ligands can act as monodentate or multidentate

ligands for AuNP^[110]. Monodentate ligands refer to a single anchor group, for example a thiol group at the end of the polymer chain. They cover the whole nanoparticle surface creating a „star like“-approach. When the polymer consists of several repeating units that can coordinate to the gold surface, the polymer acts as a multidentate ligand, which can be wrapped around one nanoparticle, assuming that in the average each particle is coordinated by only one polymer chain^[67,109]. If the polymer possesses a cross-linking group, it is possible to produce a network system, where AuNP are cross-linked with the polymer^[111]. Figure 2.12 shows the different functionalization approaches for AuNP.

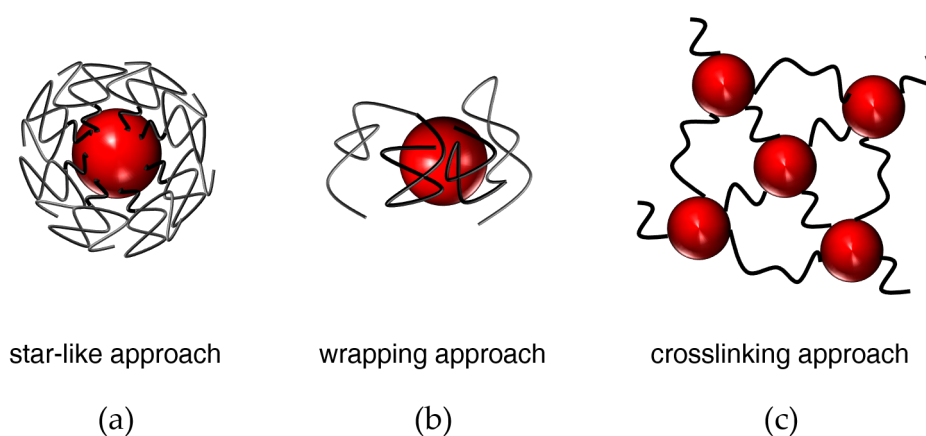


Figure 2.12: Schematic representation of different approaches for polymer-functionalized AuNP: (a) star-like approach, (b) wrapping approach, (c) cross-linking approach.

This thesis is focused on ligand exchange and *in situ* reactions of AuNP with monodentate and multidentate ligands using amphiphilic block copolymers of styrene and 4VP (S4VP). Therefore a historical and exemplary background of S4VP/AuNP nanocomposites will be introduced in the next section.

2.5.1 S4VP/AuNP Nanocomposites

There are additional potential benefits emanating from the use of functional amphiphilic block copolymers, not only because their structure can be tailored and undergo self-assembly but also because they can be used as templates or building blocks. Templates generated by the self-assembly of amphiphilic molecules are particularly attractive for the fabrication of nanocomposites because of their reproducible formation and tunable structure, and their characteristic dimensions in the nanoscale. Variation of the block

copolymer molecular characteristics, e.g. block length, block ratio, concentration, solvent quality (e.g. solvent type, mixtures of solvents), and temperature allows a unique tunability of the phase behavior and corresponding nanostructure^[112,113].

S4VP BCPs have been well studied in bulk and in solution over the past decade^[32,36,40,41].

Due to the incompatibility of the blocks the S4VP phase separates in bulk and self-assembles into sphere, cylinder, gyroidal or lamellar morphologies. Depending on the molecular composition of S4VP, the volume fraction of 4VP (χ_{4VP}), and solvent that is used, it is possible to control and tailor the morphology of BCPs. Groups of ANTONIETTI, FÖRSTER, and FAHMI have reviewed about the physical and chemical properties of this block copolymer^[39,43,113]. S4VP has been applied as building block for the incorporation of metal nanoparticles and have shown great advances for the fabrication of well-defined nanocomposite materials in the last years^[114–118]. These nanocomposite materials comprise a new platform for multifunctional devices for future applications in catalysis^[119], as memory devices^[120], or as thermoresponsive materials^[121]. The control of selectivity and distribution of metal nanoparticles in block copolymer domains is a well-established method in bulk^[90,122].

The work of FAHMI introduces a very useful library of S4VP morphologies, using different compositions of the blocks, which served as templates for the incorporation of AuNP within S4VP domains with controllable orientation of BCP microdomains^[42,43,123,124]. Figure 2.13 shows a scheme of the FAHMI 's research diversity of S4VP/AuNP nanocomposites.

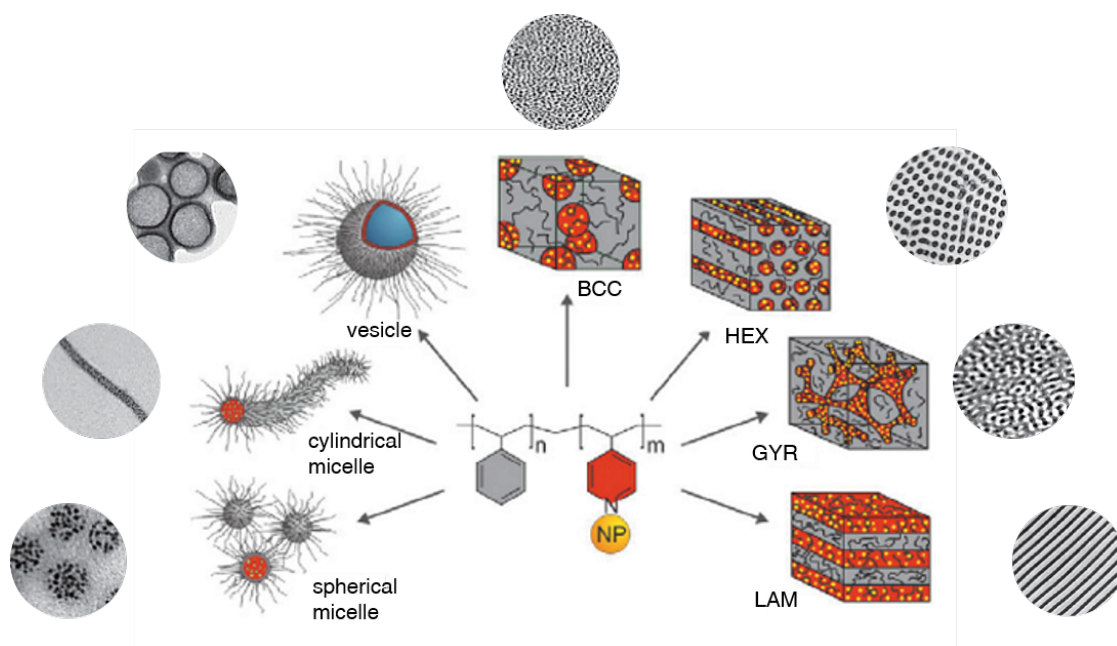


Figure 2.13: Schematic representation of different S4VP/AuNP nanocomposites, according to FAHMI^[43].

For the incorporation of AuNP into the 4VP domains FAHMI used the strategy of *in situ* synthesis. Subsequently this method can be itemized in several routes^[125] (Scheme 2.14): (i) known as the „dispersion route“, in which nanocomposites emerge as colloids, mixing a metal salt and the protecting polymer in solution, followed by addition of the reduction agent. (ii) The „immersion route“ is a reaction, in which the solid polymer material is placed in a solution of the metal salt. Once the metal salt diffuses within the polymer the solvent is evaporated and the reduction takes place. (iii) The third route describes the deposition of a metal salt solution as well as a polymer solution on a substrate. After drying and conversion to a thin-film, the reduction is performed. FAHMI 's research is concentrated on the second and third route.

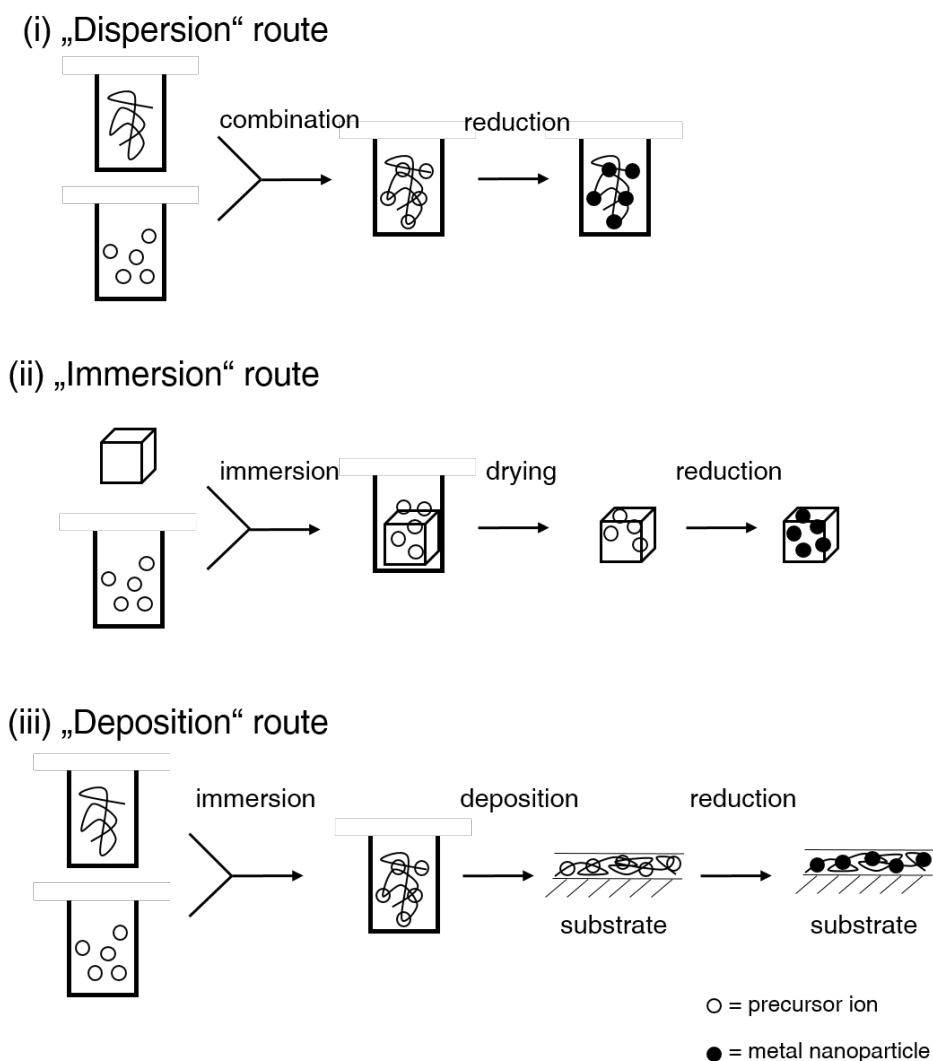


Figure 2.14: Schematic representation of different *in situ* routes for the preparation of S4VP/AuNP nanocomposites^[125].

Research on this topic reported by PINE, SHEN, ALIVISATOS and others employed the strategy of ligand exchange reactions by using preformed AuNP. This strategy implies the stabilization of AuNP with homopolymers, which are compatible to one of the blocks of the BCP to minimize the role of enthalpy between AuNP and the polymer domain^[126–131]. Using this procedure it is possible to fabricate precise designs of S4VP block copolymers loaded with AuNP.

3 Motivation, Aim, and Scope of the Thesis

S4VP/AuNP nanocomposites have already been well established as bulk materials. They showed a variety of morphologies, which were controlled by the nature and the volume fraction of block copolymers. The use of a selective or non-selective solvent for one of the blocks results in micellar nanostructures, such as spheres, cylinders, and vesicles. However, so far the resulting morphologies were mainly driven by self-organization of S4VP and is less extended by AuNP. Control over self-organization of AuNP could open new perspectives for strong plasmonic coupling properties, such as strong magnetic resonances and propagation of low-loss magnetic plasmons.

The present thesis is divided in four sections, containing three different projects, each addressing a different approach for the functionalization and self-assembly of AuNP with functional S4VP block copolymers. On the one hand the 4VP moiety is exploited to be used as monodentate and multidentate ligands for the functionalization of metal nanoparticles in solution and investigate their behavior on the AuNP surface by tuning the molar ratio of AuNP versus ligands. On the other hand the S4VP block copolymer is modified to attach a functional group to the polystyrene chain and use this as a template for further functionalizations with chromophores, while keeping the functionality of 4VP for the incorporation of metal nanoparticles. Control over self-assembly of AuNP and introducing another functionality to the S4VP is combined in order to broaden the optical properties of AuNP within S4VP/AuNP nanocomposites.

In the following, a short introduction into the motivation and aim of the chosen approaches is given. A detailed presentation of the concepts and strategies pursued in this thesis can be found in the respective sections (4). An overview of the already established S4VP/AuNP nanocomposites can be found in chapter 4, section 4.1.

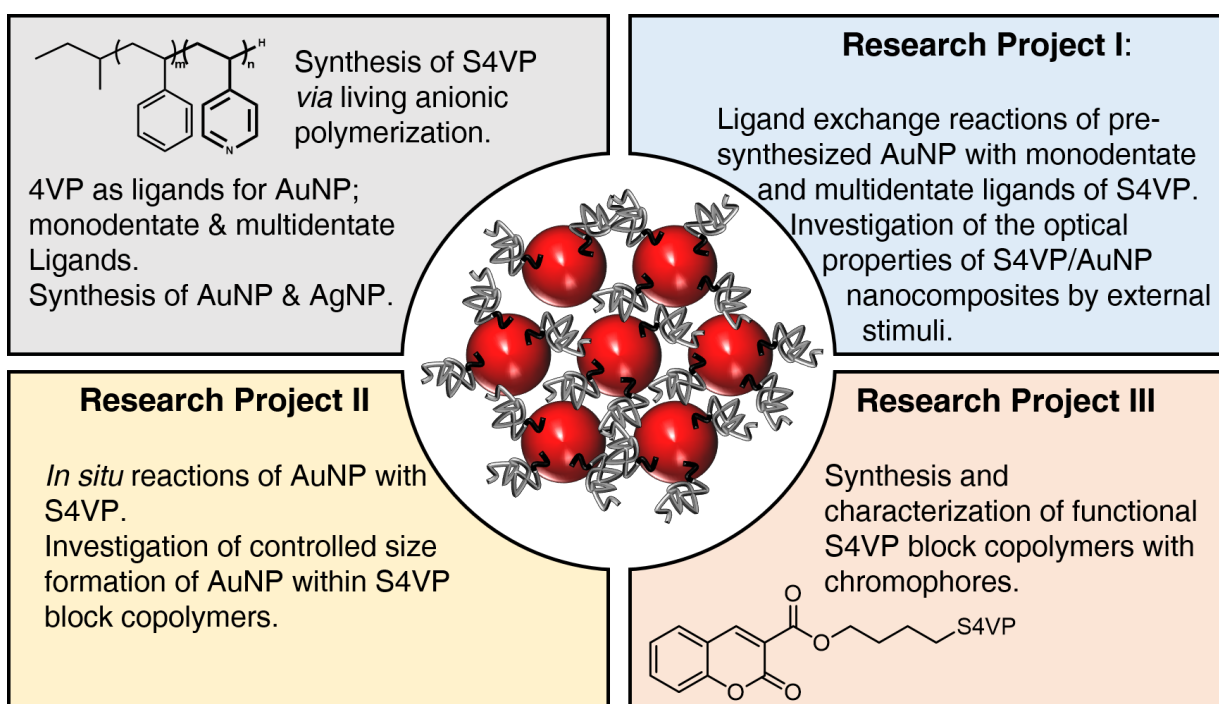


Figure 3.1: Overview of the different research projects conducted in this thesis.

The quintessence of this thesis begins with the synthesis and characterization of S4VP block copolymers. Five S4VP block copolymers are introduced in this work. By using the technique of sequential living anionic polymerization it was able to synthesized three different S4VP block copolymers with the same molar mass of polystyrene with different block lengths of 4VP. Subsequently two different S4VP polymers with one moiety group of 4VP and different molar mass of polystyrene were synthesized. Furthermore the synthesis and characterization of gold- and silver nanoparticles (AuNP and AgNP) are described.

The first research project embraces the ligand exchange reactions of citrate-stabilized gold nanoparticles (Citrate@AuNP) with monodentate and multidentate ligands of S4VP. A series of experiments is performed to explore the self-assembly of AuNP as well as the topology of S4VP/AuNP nanocomposites, which is influenced by the amount of monodentate and multidentate ligands relative to the amount of AuNP and viceversa. The S4VP/AuNP nanocomposites are analyzed by means of TEM, DLS and UV/Vis spectroscopy. The optical properties of the S4VP/AuNP nanocomposites are especially investigated by applying an external stimulus.

In the second research project the role of polymers with distinct 4VP moieties for the controlled preparation of AuNP by *in situ* reduction of HAuCl_4 with NaBH_4 in organic solvents is discussed. The „dispersion route“ is used to systematically screen the influence of the 4VP block length and 4VP molar ratio to gold precursor on the resulting S4VP/AuNP nanocomposites. With this approach is possible to identify proper conditions to synthesize *in situ* AuNP with small standard deviations in different sizes. The formation of AuNP with varying diameter shows distinct optical properties, which are carefully analyzed by means of TEM and UV/Vis spectroscopy. The reported approach demonstrates a facile and versatile method for the controlled *in situ* synthesis towards S4VP/AuNP nanocomposites.

The third research project comprises the synthesis and characterization of a functional telechelic α -OH-S4VP polymer *via* anionic polymerization. The synthesis of a bifunctional initiator is thoroughly investigated. Furthermore a functionalization with the chromophore coumarin as well as the stabilization of AuNP and AgNP by ligand exchange reactions in a biphasic system is presented.

4 Results and Discussion

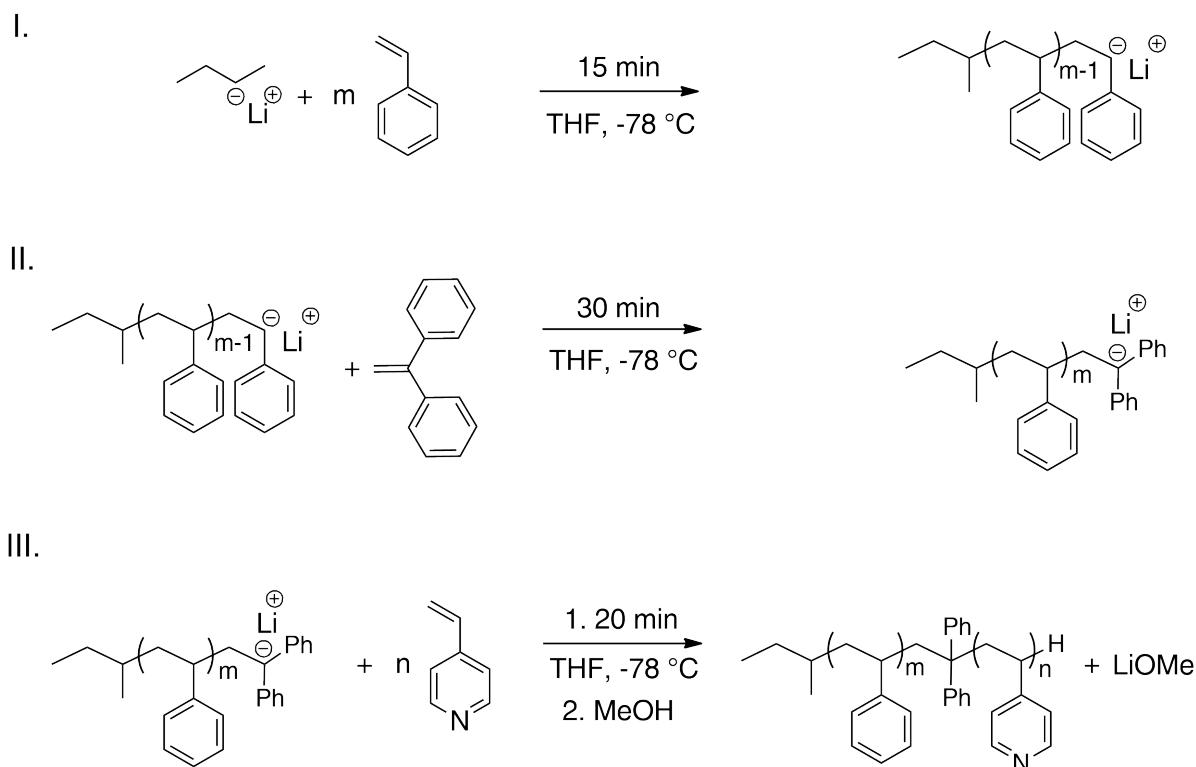
The principal part of this dissertation is subdivided into four sections. In the first section the synthesis of S4VP block copolymers and citrate-functionalized gold and silver nanoparticles (Citrate@AuNP and Citrate@AgNP) are reported. The next three sections describe the executed topics during the time of the thesis. Each section will be introduced by a short motivation, concept, hypothesis, and conclusion.

4.1 Synthesis of S4VP Block Copolymers

In the present work five different S4VP block copolymers were synthesized by sequential living anionic polymerization. Three pyridyl-terminated polystyrenes $S_{26}4VP_1$ **I**, $S_{43}4VP_1$ **II**, and $S_{77}4VP_1$ **III** with a different degree of polymerization (DP) of styrene as well as two block copolymers $S_{77}4VP_{17}$ **IV** and $S_{77}4VP_{34}$ **V** with different 4VP block lengths were synthesized.

The reaction was carried out in a temperature-controlled laboratory autoclave using THF_{abs.} as a solvent. To remove all impurities of the solvent, the THF was cooled down to -35 °C and sec-BuLi was added until a yellow color occurred. The THF solution was allowed to warm up to room temperature prior to reaction. After cooling to -78 °C, a given amount of sec-BuLi was added as Initiator. Styrene was transferred into the reactor over a glass ampoule under vigorous stirring and the typical orange color of the polystyryl anion was observed. After 10 min stirring an aliquot of the polystyrene (PS precursor) was withdrawn for Nuclear Magnetic Resonance Spectroscopy (NMR) and Gel Permeation Chromatography (GPC) analysis. Afterwards, 1,1-diphenylethylene (DPE) was added to end cap the polystyryl anion and stirred for 30 min. The color of the solution changed immediately from orange to deep red. Finally, a given amount of 4VP was added *via* a syringe to the reaction mixture. The color changed in a few minutes from

deep red to yellow. The reaction was terminated by adding a few drops of degassed methanol. The block copolymers (BCPs) S4VP I-V were precipitated from pentane and characterized by means of $^1\text{H-NMR}$ -spectroscopy and GPC. Scheme 3 shows the overall reaction scheme of the living anionic polymerization.



SCHEME: 3 Reaction scheme of sequential living anionic polymerization of S4VP block copolymers I-V.

The relative molar mass (M_n) and relative molecular mass (M_w) of polystyrene (PS-precursor) was determined by GPC-THF analysis, while the molar mass distributions of all S4VP BCPs I-V were calculated by GPC-DMF analysis. Figure 4.1 shows the elution volume of the PS-precursor with a degree of polymerization of styrene DP = 26, 43 and 77 and the elution volume of the polymers S₂₆4VP₁ I, S₄₃4VP₁ II, S₇₇4VP₁ III, S₇₇4VP₁₇ IV, and S₇₇4VP₃₄ V.

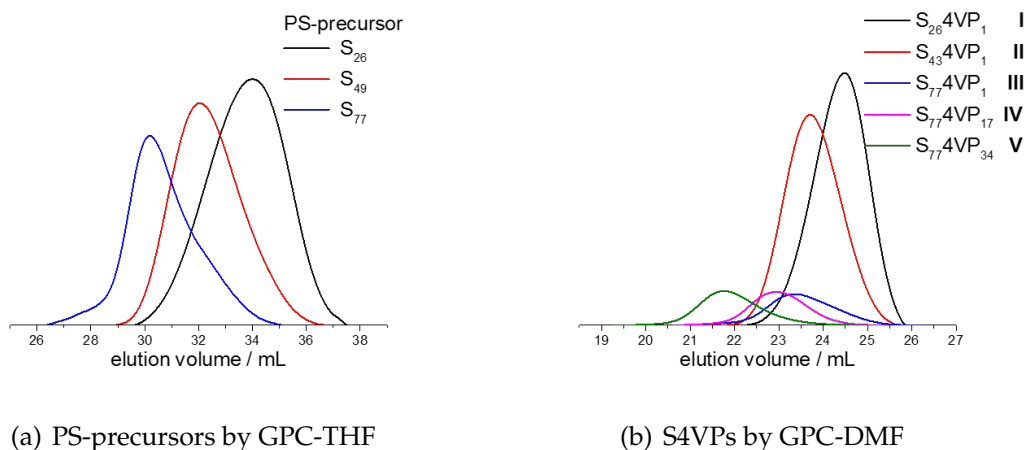


Figure 4.1: GPC chromatograms: (a) elution volume of PS-precursors S_{26} , S_{43} , and S_{77} by GPC-THF. (b) Elution volume of S4VPs I-V by GPC-DMF.

Table 4.1 and Table 4.2 show the relative molar mass (M_n), relative molecular mass (M_w), and molar mass dispersity (\mathcal{D}) of the polystyrene precursors and S4VP block copolymers evaluated by GPC-THF and GPC-DMF respectively.

Table 4.1: GPC-THF Data of PS-precursors S_{26} , S_{43} , and S_{77} .

Polymer	M_n (th.) $\text{kg} \cdot \text{mol}^{-1}$	M_n $\text{kg} \cdot \text{mol}^{-1}$	M_w $\text{kg} \cdot \text{mol}^{-1}$	\mathcal{D}
S_{26}	2.0	2.7	3.4	1.3
S_{43}	5.2	4.5	5.6	1.2
S_{77}	8.3	8.0	10.8	1.3

Table 4.2: GPC-DMF Data of S4VPs I-V.

Entry	Polymer	M_n (th.)	M_n	M_w	\mathcal{D}
I	$S_{26}4VP_1$	2.2	3.8	4.9	1.3
II	$S_{43}4VP_1$	5.3	6.4	8.1	1.2
III	$S_{77}4VP_1$	8.5	7.2	10.4	1.4
IV	$S_{77}4VP_{17}$	10.4	10.6	12.6	1.1
V	$S_{77}4VP_{34}$	12.5	19.8	24.7	1.1

The degree of polymerization of the 4VP blocks was calculated by $^1\text{H-NMR}$ -spectroscopy by integration of the methyl end-groups of the initiator to the protons of the pyridyl group of 4VP (Figure 4.2).

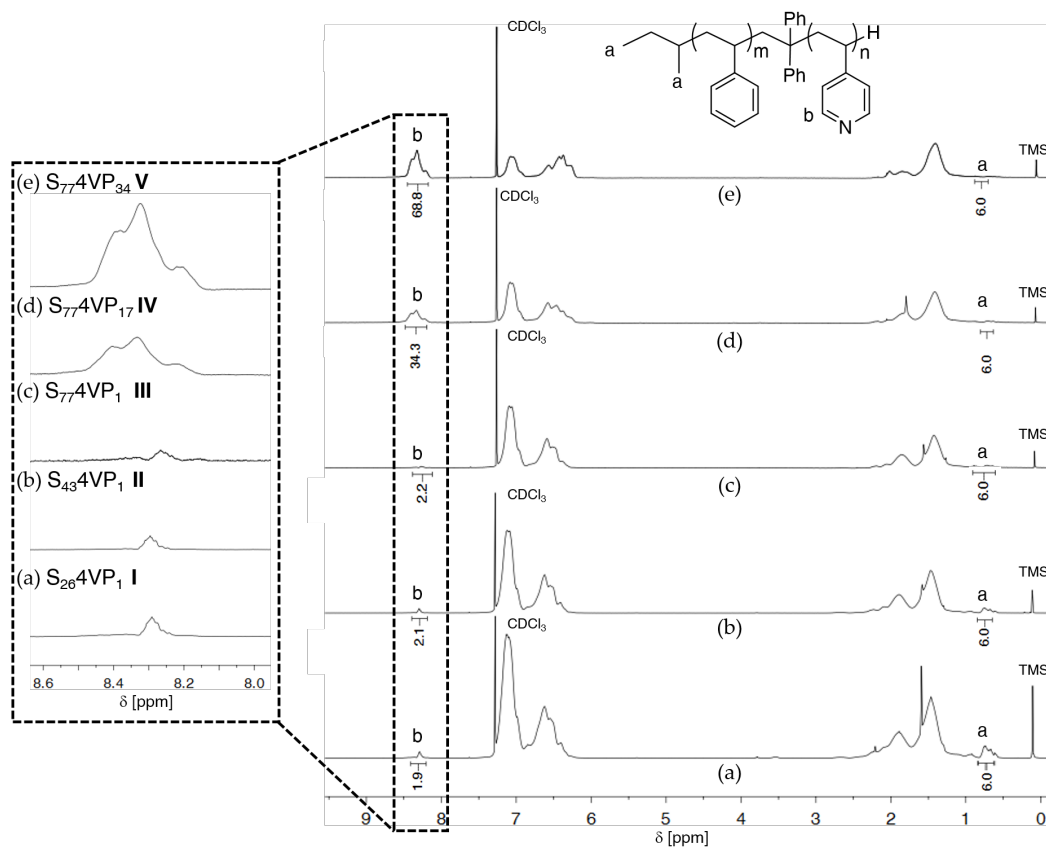


Figure 4.2: $^1\text{H-NMR}$ spectra of S4VPs I-V.

The thermal decomposition of all S4VPs I-V was determined by TGA as shown in Figure 4.3. Thermal analysis revealed one degradation transition for all S4VPs (I-V) with a small difference of molar loss due to the different composition of the blocks.

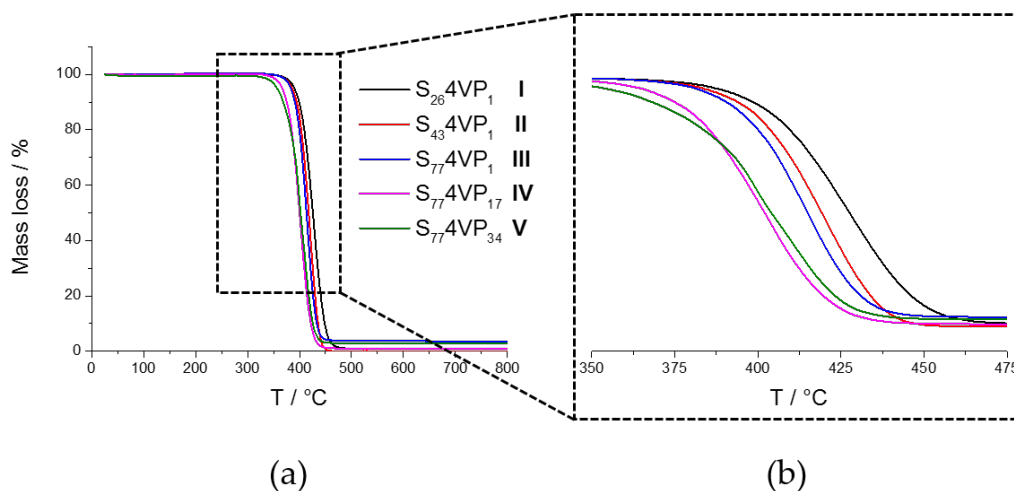
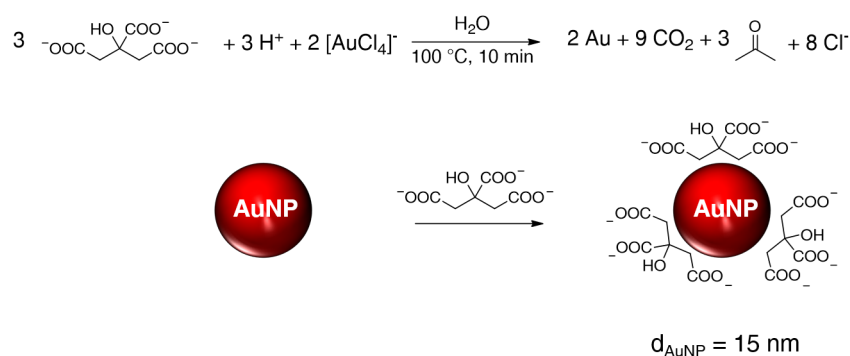


Figure 4.3: (a) Decomposition curves of S4VPs I-V. (b) Inset of S4VPs I-V. (c) Degradation temperatures at a maximum loss (T_{max}) and at 5% ($T_{5\%}$).

4.2 Synthesis of Citrate-stabilized Gold Nanoparticles Citrate@AuNP

Citrate-stabilized AuNP (Citrate@AuNP) with a diameter of $d = 15$ nm were synthesized following the procedure of TURKEVICH and FRENS^[78,79]. In general, AuNP are generated by reduction of tetrachloroauric acid with an excess of trisodium citrate in aqueous solution. Aggregation of AuNP is avoided due to the electrostatic repulsion of the citrate-anions, which are adsorbed on the nanoparticle surface. The reaction synthesis is schematically represented in Scheme 4.



SCHEME: 4 Schematic representation of Citrate@AuNP by the method of TURKEVICH and FRENS^[78,79].

The typical red-color dispersion of Citrate@AuNP was characterized by means of UV/Vis spectroscopy, Dynamic Light Scattering (DLS), and Transmission Electron Microscopy (TEM). During the PhD thesis several batches of AuNP were performed, in which the particle size distribution of AuNP was in accordance to similar results. Thus, an exemplified characterization of AuNP is shown in Figure 4.4. Citrate@AuNP showed surface plasmon resonance (SPR) at a wavelength of $\lambda_{max} = 520 \text{ nm}$. The hydrodynamic diameter D_H was determined by DLS, which displayed a $D_H = 22 \text{ nm}$. The hydrodynamic volume of AuNP corresponds to the citrate ligands. In contrast, TEM micrographs showed an average diameter size of $d = 14.6 \text{ nm} \pm 1.0 \text{ nm}$ calculated by counting 500 nanoparticles.

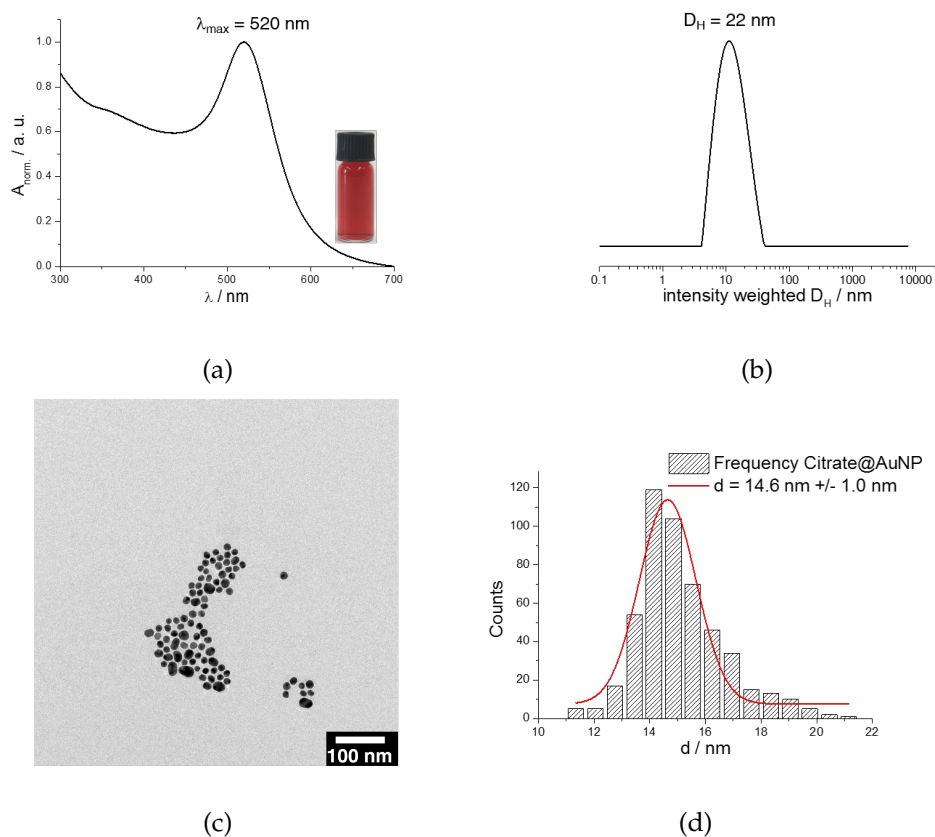


Figure 4.4: (a) UV/Vis spectrum of Citrate@AuNP with SPR at $\lambda_{max} = 520$ nm in water. (b) D_H (22 nm) of Citrate@AuNP in water. (c) TEM image of Citrate@AuNP with $d = 14.6$ nm \pm 1.0 nm and (d) their size distribution determined by counting 500 particles.

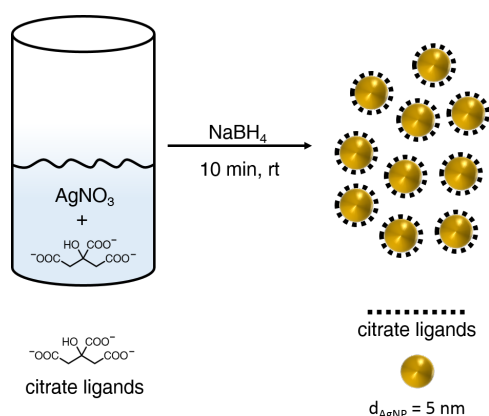
Table 4.3 compiles the resulted Data of Citrate@AuNP.

Table 4.3: Characterization of Citrate@AuNP by means of UV/Vis spectroscopy, DLS, and TEM.

Method	Dimension	Result
UV/Vis	wavelength	$\lambda_{max} = 520$ nm
DLS	hydrodynamic diameter	$D_H = 22$ nm
TEM	diameter	$d = 14.6$ nm \pm 1.0 nm

4.3 Synthesis of Citrate-stabilized Silver Nanoparticles Citrate@AgNP

Citrate-stabilized AgNP (Citrate@AgNP) with a diameter of $d = 5$ nm were synthesized following the protocol of PEREIRA^[132]. AgNP are generated by reduction of sodium borohydride (NaBH_4) using trisodium citrate dihydrate as stabilizing agent. The reaction is schematically represented in Scheme 5.



SCHEME: 5 Schematic representation of Citrate@AgNP described by PEREIRA^[132].

Citrate@AgNP were characterized by means of UV/Vis spectroscopy, DLS, and TEM. Figure 4.5 shows the results of Citrate@AgNP. AgNP with a diameter size of $d = 5$ nm showed SPR at a wavelength of $\lambda_{\text{max}} = 393$ nm (Figure 4.5a), which is in accordance to the literature^[133]. The hydrodynamic diameter was calculated to be $D_H = 20$ nm (Figure 4.5b). TEM analysis showed an average diameter size of $d = 4.0 \text{ nm} \pm 2.0 \text{ nm}$, calculated by counting 300 nanoparticles (Figure 4.5c).

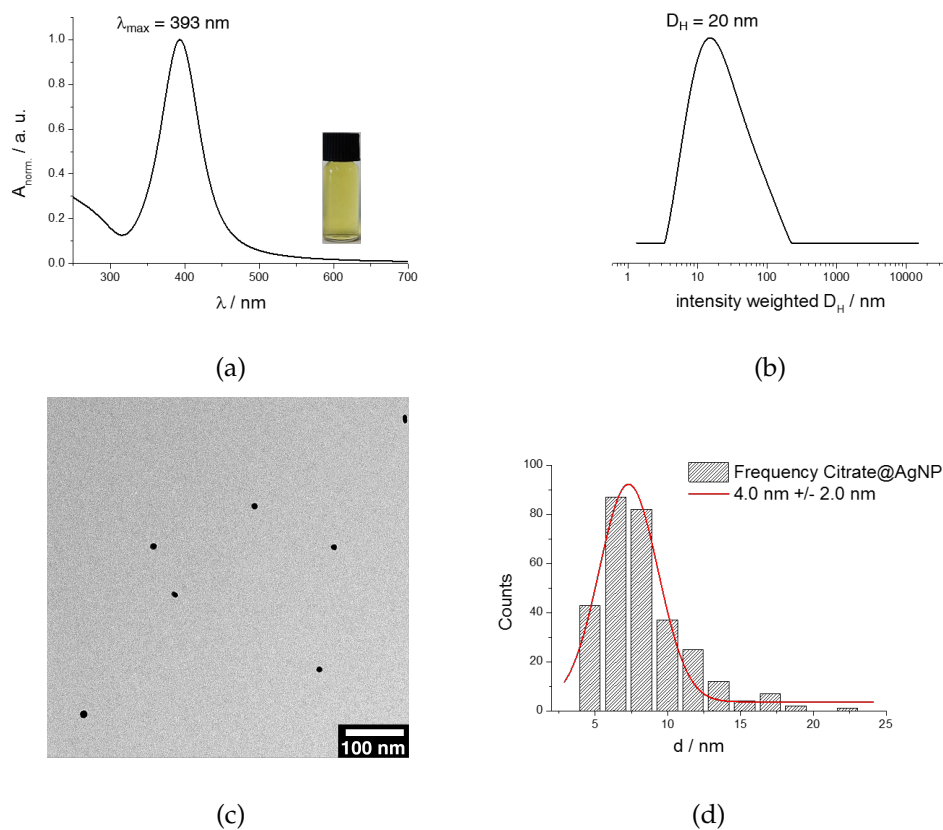


Figure 4.5: (a) UV/Vis spectrum of Citrate@AgNP with SPR at $\lambda_{max} = 393$ nm in water. (b) D_H (20 nm) of Citrate@AgNP in water. (c) TEM image of Citrate@AgNP with $d = 4.0$ nm \pm 2.0 nm and (d) their size distribution determined by counting 300 particles.

Table 4.4 compiles the resulted Data of Citrate@AgNP.

Table 4.4: Characterization of Citrate@AgNP by means of UV/Vis spectroscopy, DLS, and TEM.

Method	Dimension	Result
UV/Vis	maximal wavelength	$\lambda_{max} = 393$ nm
DLS	hydrodynamic diameter	$D_H = 20$ nm
TEM	diameter	$d = 4.0$ nm \pm 2.0 nm

4.4 Ligand Exchange Reactions of Citrate@AuNP with $S_{26}4VP_1$, $S_{77}4VP_1$, and $S_{77}4VP_{34}$ with Variation of AuNP/4VP Ratio

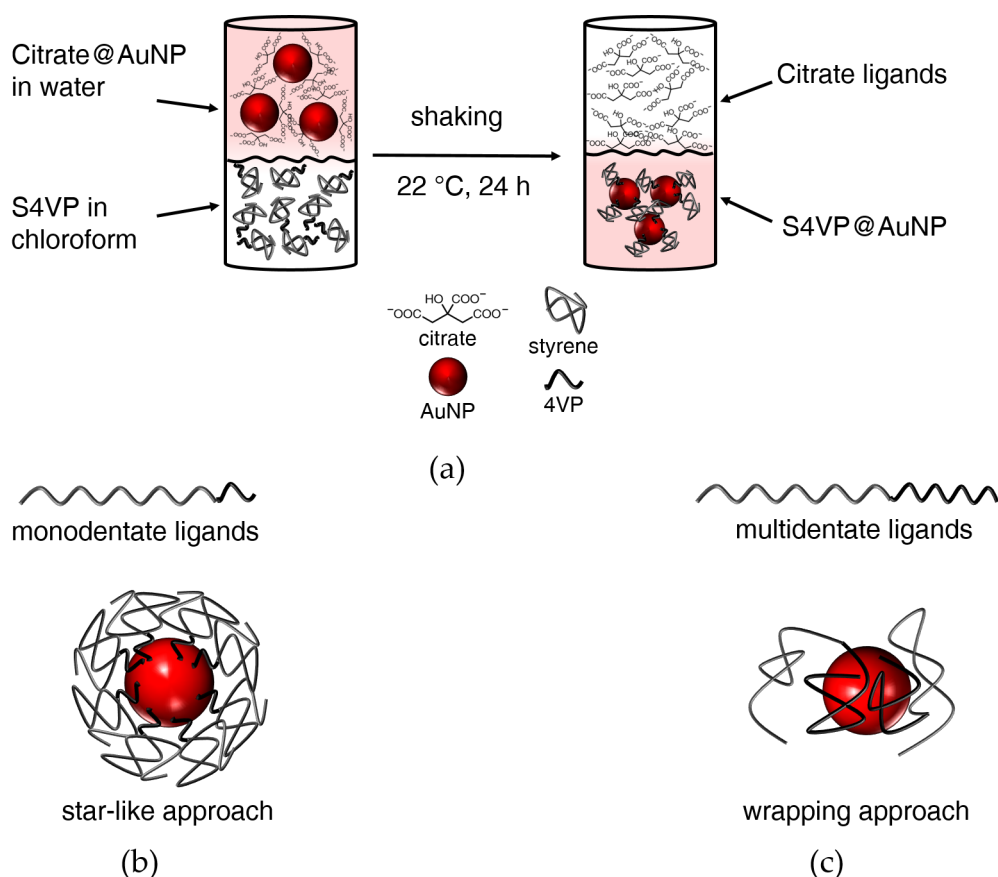
The major part of these results have been prepared in form of a manuscript and have already been submitted. The authors involved in this project were Melissa S. Köhn Serano, Tobias A. F. König, Johannes S. Haataja, Tina I. Löbling, Holger Schmalz, Seema Agarwal, Andreas Fery, and Andreas Greiner in corporation with the Department of Physical Chemistry of the University of Bayreuth and The Department of Applied Physics of the Aalto University, Espoo, Finland.

4.4.1 Hypothesis and Motivation

This section comprehends ligand exchange reactions of Citrate@AuNP with the pyridyl-terminated polystyrenes $S_{26}4VP_1$ **I**, $S_{77}4VP_1$ **III** as monodentate ligands and $S_{77}4VP_{34}$ **V** as multidentate ligands for AuNP. Since citrate ligands are weak and only ionic bound to the AuNP surface an exchange of ligands with stronger bonds, such as amines, thiols or phosphines is achievable. VANA 's work described different possible coordination motifs for AuNP by using mono- and multidentate ligands^[110]. Polymer with a functional end group for AuNP, or in this case a pyridyl-terminated polystyrene served as monodentate ligands, which led to S4VP/AuNP nanocomposites with a „star-like“ approach, while longer units of 4VP acted as multidentate ligands for AuNP, resulting in a „wrapping“ approach. Speculatively, the star-like structure implies more polystyrene chains per AuNP as compared to the wrapping like structure. Also a strong steric repulsion by the polystyrene chains was present, which prevented aggregation of AuNP. A specified amount of AuNP versus ligands showed also different structures of S4VP/AuNP nanocomposites.

Aim of this project was to investigate the resulting structures of S4VP/AuNP nanocomposites and their optical properties by variation of AuNP/4VP ratio. The influence of an external stimuli, such as temperature or additives on the S4VP/AuNP nanocomposites was further investigated.

Ligand exchange reactions of Citrate@AuNP were performed in a biphasic system water/chloroform. Scheme 6 shows schematically a ligand exchange reaction and the mechanism of possible structures of S4VP/AuNP nanocomposites with mono- and multidentate ligands.



SCHEME: 6 Schematic representation of (a) ligand exchange reactions of Citrate@AuNP with S4VP in a biphasic system water/chloroform. (b) Star-like approach; pyridyl-terminated polystyrene acting as a monodentate ligand for AuNP. (c) Wrapping approach; S4VP block copolymers acting as multidentate ligands for AuNP.

With this concept the importance of ligand design and its quantity for the preparation of S4VP/AuNP nanocomposites was reported. Based on the well-established literature for self-assembly of block copolymers we focused on the control over the self-assembly of AuNP, which showed highly ordered structures of AuNP within the S4VP block copolymers.

In this study the polymers S₂₆4VP₁ **I**, S₇₇4VP₁ **III**, and S₇₇4VP₃₄ **V** were used to performed ligand exchange reactions with Citrate@AuNP.

Within these experiments mathematical approximations were performed to calculate the surface area of gold nanoparticles and pyridyl-groups.

To estimate the number of pyridyl-terminated polystyrene ligands on the AuNP surface, following assumptions were set^[134]:

1. The volume of AuNP was set as an ideal spherical shape:

$$V = \frac{4}{3} \cdot \pi \cdot r^3 \quad (4.1)$$

2. AuNP are arranged in a close cubic packing with a density of 74 % gold.

3. Adsorption on the surface is comparable to one on flat single crystal model surface area of Au(111):

$$A = 4 \cdot \pi \cdot r^2 \quad (4.2)$$

4. Possible interaction of the 4-vinylpyridine group was assumed to be only perpendicular to the nanoparticle surface^[135].

5. The area of 4-vinylpyridine on the surface of the AuNP was assumed to be the area between the two vicinal protons of the nitrogen atom of 4VP.

6. The approximate size of the area of 4-vinylpyridine was obtained by a calculation of the distance of vicinal protons of the nitrogen atoms (254 pm) and the van der Waals radius of the nitrogen atom (155 pm).

Volume of AuNP with average particle diameter size $d = 14.6$ nm

$$V = \frac{4}{3} \cdot \pi \cdot r^3 = 1.63 \cdot 10^{-24} \text{ m}^3 \cdot 0.74 = 1.17 \cdot 10^{-24} \text{ m}^3$$

Surface area of AuNP sphere:

$$A = 4 \cdot \pi \cdot r^2 = 6.6 \cdot 10^{-16} \text{ m}^2$$

To calculate the number atoms of the gold surface, atoms are shown as two dimensional circles with an atomic radius of gold $r_{Au} = 144$ pm and a circle area of:

$$A_{Au(circle)} = \pi \cdot r^2 = 6.5 \cdot 10^{-20} \text{ m}^2$$

Volume of a gold atom:

$$V = \frac{4}{3} \cdot \pi \cdot r^3 = 1.25 \cdot 10^{-29} \text{ m}^3$$

Calculated number of atoms per AuNP:

$$\frac{1.17 \cdot 10^{-24} m^3}{1.25 \cdot 10^{-29} m^3} = 936000. N_{AuNP} = 93600 \text{ atoms}$$

Area of one molecule of 4VP on the surface of AuNP:

$$254 \text{ pm} \cdot (2 \cdot 155 \text{ pm}) = 7.8 \cdot 10^{-20} m^2$$

The surface area of AuNP was calculated to be $A_{Au}(\text{surface}) = 6.6 \cdot 10^{-16} m^2$, while the area of 4VP was $A_{4VP} = 7.8 \cdot 10^{-20} m^2$. This leads to a maximum number of around 8500 4VP molecules on the surface of AuNP with an average diameter of $d = 14.6$. Applying those assumptions to the experimental set up and the series of experiments with variation of AuNP the following ratios of molecules of 4VP to AuNP were obtained (Table 4.5).

Table 4.5: Excess amount of 4VP related to the amount of AuNP.

Molar ratio Au/4VP	0.5	1.0	2.0	5.0	8.0	10.0
Molar ratio 4VP/AuNP	187 200	93 600	46 800	18 720	11 700	9 360

While the 4VP content was kept constant, the amount of Citrate@AuNP was varied. The systematic variation of Citrate@AuNP ratio to 4VP is presented in Table 4.6 as well shown in Table 4.5, which are the calculated absolute amounts of 4VP ligands that are available for each gold nanoparticle.

Table 4.6: Parameters for ligand exchange reactions. Systematic variation of Citrate@AuNP/4VP ratio.

Entry	$S_{26}4VP_1$ I / $S_{77}4VP_1$ III / $S_{77}4VP_{34}$ V	Citrate@AuNP	Molar ratio
	n(4VP) [μmol]	n(Au) [μmol]	4VP/AuNP
1	1.0	0.5	187 200
2	1.0	1.0	93 600
3	1.0	2.0	46 800
4	1.0	5.0	18 720
5	1.0	8.0	11 700
6	1.0	10.0	9 360

Figure 4.6 shows the ligand exchange of $S_{77}4VP_1$ III before and after vigorously shaking over night at room temperature with complete phase transfer of AuNP.

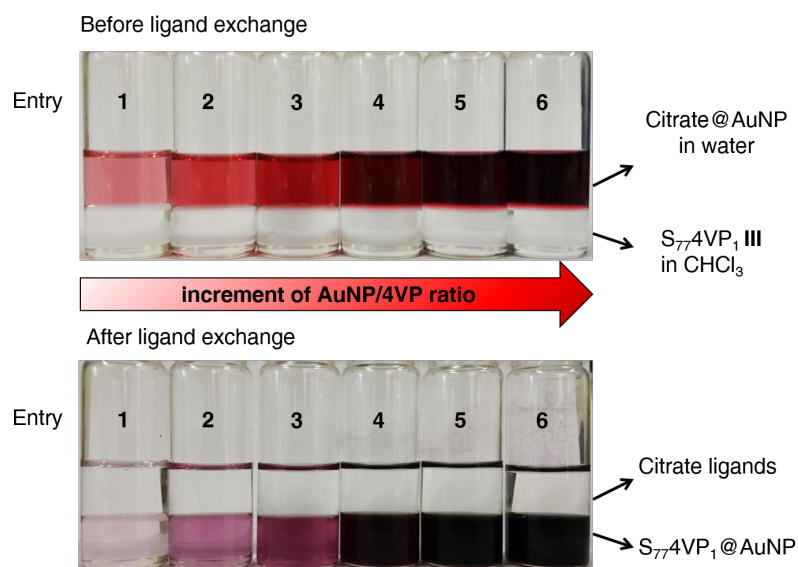


Figure 4.6: Ligand exchange reactions of Citrate@AuNP, exemplified with $S_{77}4VP_1$ III in a two phase system water/chloroform. The amount of AuNP ranged from 0.5 μmol to 10 μmol .

After completion of the ligand exchange the S4VP-functionalized AuNP ($S_{4VP}@AuNP$) were isolated and characterized by means of UV/Vis spectroscopy, electromagnetic simulations, Transmission Electron Microscopy (TEM), cryo-TEM, and dynamic light scat-

tering (DLS). In the following sections the results of S4VP@AuNP with mono- and multidentate ligands will be described separately.

4.4.2 Ligand Exchange Reactions of Citrate@AuNP with S₂₆4VP₁ and S₇₇4VP₁ with Variation of AuNP/4VP Ratio

This section describes ligand exchange reactions with monodentate ligands. Figure 4.7 shows the absorption spectra of S₂₆4VP₁@AuNP and S₇₇4VP₁@AuNP.

S₂₆4VP₁@AuNP showed a shift of the surface plasmon resonance (SPR) from $\lambda_{max} = 520$ nm to $\lambda_{max} = 534$ nm. This shift indicated an increase of the hydrodynamic diameter of the system by changing the surrounding media of AuNP and therefore a successful ligand exchange. S₇₇4VP₁@AuNP also showed SPR red shifted to $\lambda_{max} = 530$ nm. However, in both systems a bimodal SPR for different amounts of AuNP (5.0 μ mol, 8.0 μ mol, 10.0 μ mol) was observed (Figure 4.7a, b). This is related to the plasmonic interaction of AuNP due to their close interparticle distance (below 2 nm) in suspension.

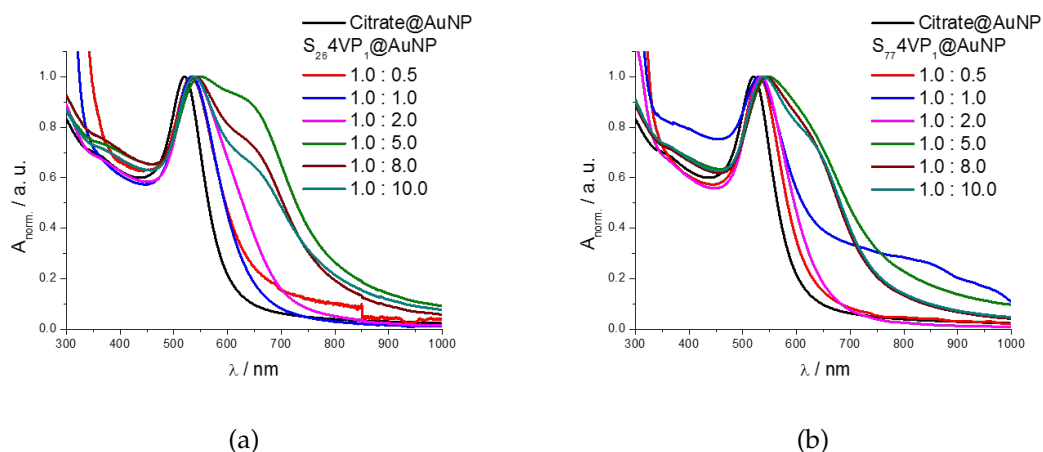


Figure 4.7: UV/Vis spectra of (a) S₂₆4VP₁@AuNP, (b) S₇₇4VP₁@AuNP with variation of AuNP/4VP ratio after ligand exchange of Citrate@AuNP.

To explain the plasmonic interaction in detail the optical response of AuNP was determined with finite difference time domain simulations (FDTD) in chloroform. The experiments were performed by Dr. Tobias A. F. König from the Department of Physical Chemistry II at the University of Bayreuth. This method has been used to predict the field enhancements in the vicinity of single metal nanoparticles of a variety of shapes^[136–138]. The electromagnetic simulations are shown in Figure 4.8

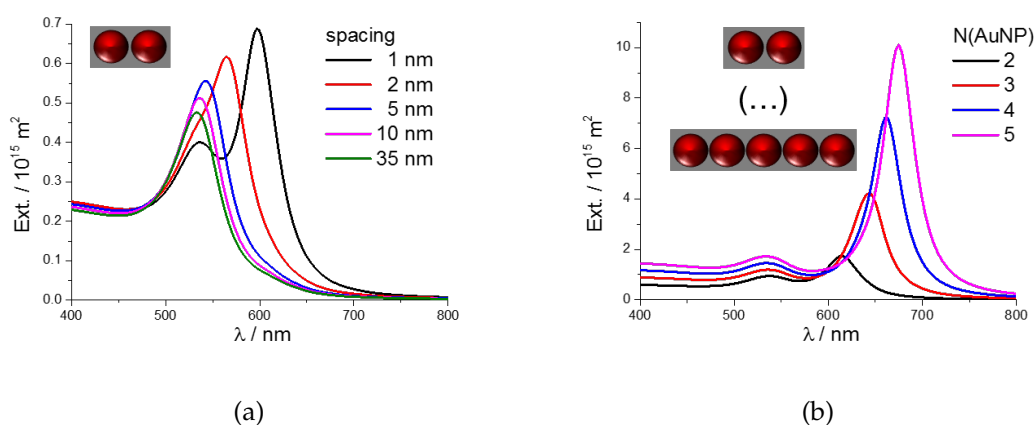


Figure 4.8: Optical response of different AuNP assemblies and inter particle spacing. (a) Extinction cross-section of AuNP dimer assembly between very close spacing (1 nm) and non-coupling condition (35 nm). (b) Optical response from dimer (2), trimer (3), tetramer (4), and pentamer (5) at 1 nm inter particle spacing.

Experimentally two plasmonic modes at $\lambda_{max} = 530$ nm and $\lambda_{max} = 650$ nm. The energetically higher plasmonic mode at 530 nm is attributed to the typical dipolar plasmonic mode of single AuNP in a homogenous surrounding media. With decreasing distance another plasmonic mode was excited, which is called the longitudinal mode. This longitudinal mode was only excited when the polarization vector is parallel to the geometric line of the assembly. The significant red shift of the plasmonic resonance at decreasing inter particle spacing is also known as the plasmon ruler^[139]. The energetically lowest mode, which could be obtain at a dimer AuNP configuration at 1 nm inter particle distance is 600 nm. From the experimental results in suspension more than two particles must be assembled to reach the experimental mode at 650 nm. Consequently, AuNP must be added to the particle chain to reach the experimental peak position. Figure 4.8b shows the addition up to five AuNP to the particle line with an equal inter particle dis-

tance fixed at 1 nm. This energetically lowest mode is called the super radiant mode, which converges with an increasing AuNP chain length to a specific wavelength^[140,141]. The linear chain model is a simplification of the experimental S4VP/AuNP assembly for a good reason. As HANSKE *et al.* have shown, the experimental assembly is basically a perturbed case of the ideal assembly modeled in Figure 4.8a, b. This perturbation in form of statistical distribution of the inter particle distance results in blue shift of the super radiant mode^[142]. This situation is also valid when a second particle line or a second plane of particles is added. For instance, the extinction cross-section of a dimer pair (four AuNP assembly) is a weighted superposition of extinction cross-section of one dimer^[143]. Consequently, the experimental measured optical response could be deconvoluted into a single particle dipolar mode and a super radiant mode due to closed inter particle coupling.

The systematic variation of AuNP/4VP ratio in the solid state was followed by TEM. Figure 4.9 shows images from the series of experiments starting with a low amount of AuNP (0.5 μmol), which showed single distributed AuNP with a dense coverage of the surface with S4VP up to high amounts of AuNP (10 μmol), where the AuNP showed self-assembly with a narrow interparticle distance and an hexagonal order of AuNP.

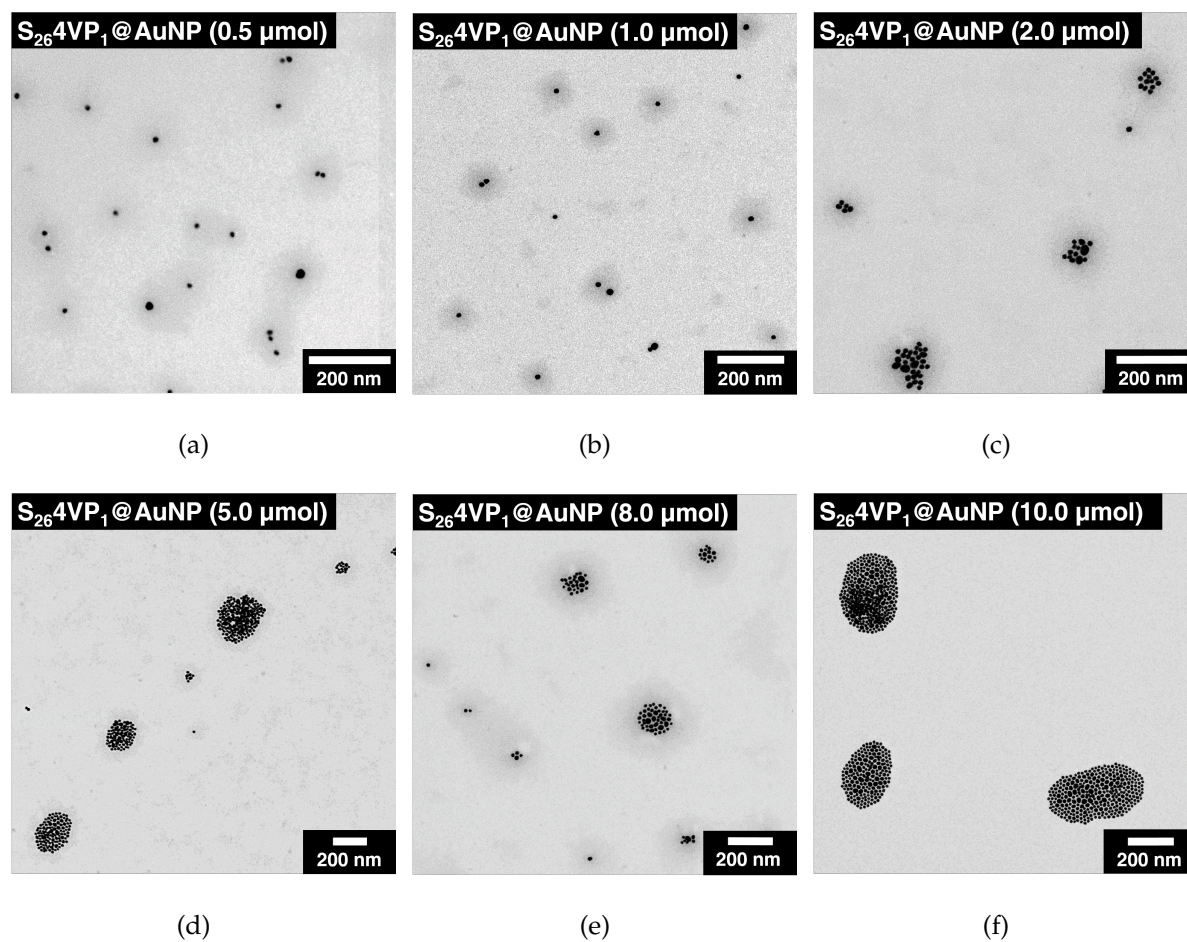


Figure 4.9: TEM-micrographs of $S_{26}4VP_1@AuNP$ with increase of AuNP/4VP ratio. Variation of AuNP: (a) 0.5 μmol , (b) 1.0 μmol 2.0 (c) μmol , (d) 5.0 μmol , (e) 8.0 μmol , (f) 10.0 μmol .

The samples of $S_{77}4VP_1@AuNP$ showed an analogous self-assembly of AuNP with increase of AuNP/4VP ratio, as displayed in Figure 4.10.

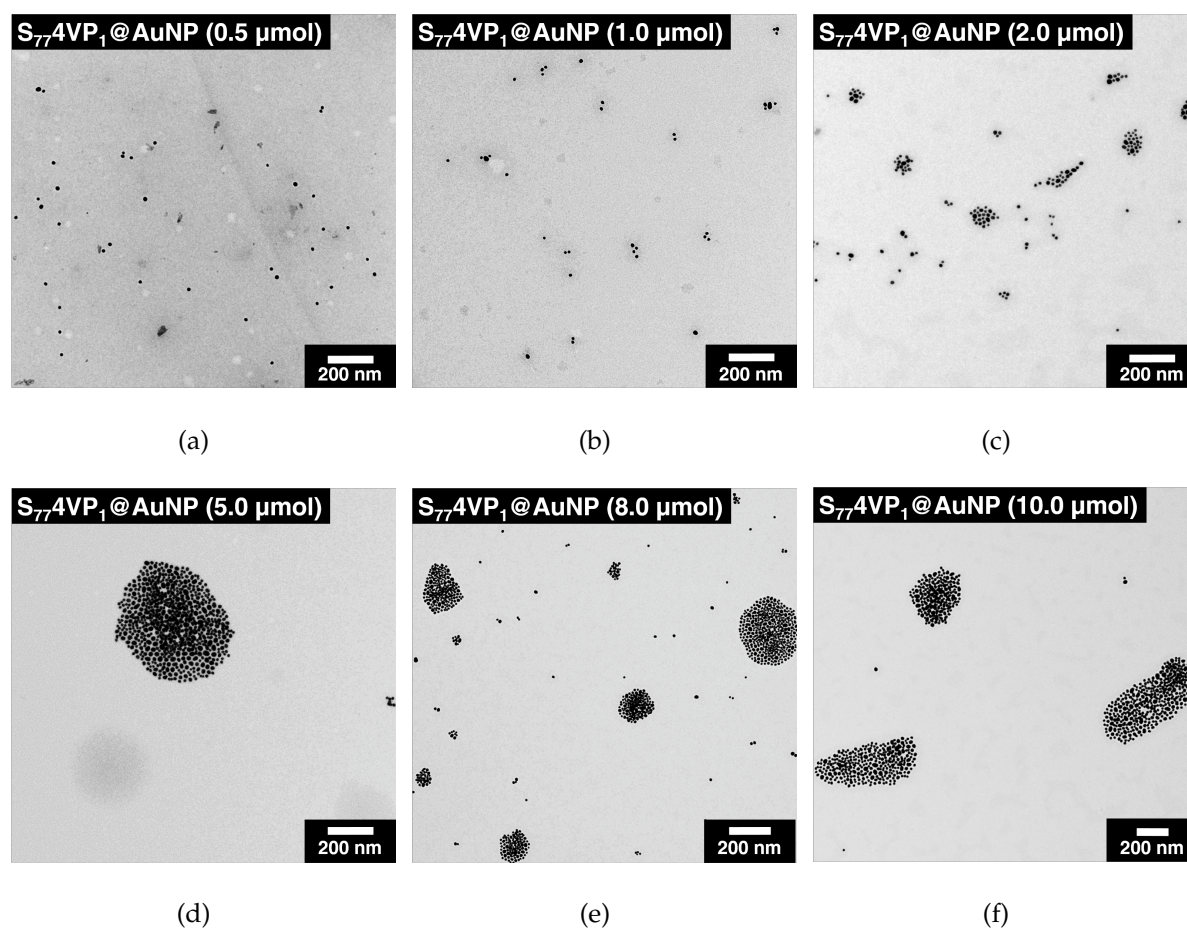


Figure 4.10: TEM-micrographs of $S_{77}4VP_1@AuNP$ with increase of AuNP/4VP ratio. Variation of AuNP: (a) 0.5 μmol , (b) 1.0 μmol , (c) 2.0 μmol , (d) 5.0 μmol , (e) 8.0 μmol , (f) 10.0 μmol .

$S_{26}4VP_1@AuNP$ and $S_{77}4VP_1@AuNP$ with amounts of AuNP 0.5 μmol and 1.0 μmol (Figure 4.9a, b and Figure 4.10a, b) showed similar structures of single distributed AuNP, which is in relation to the use of monodentate ligands and its excess to cover the whole nanoparticle surface.

The self-assembly of AuNP in suspension and in the solid state was investigated in detail by means of cryo-TEM and Electron Tomography (ET) respectively. For this measurement the sample $S_{26}4VP_1@AuNP$ with an amount of AuNP of 8 μmol was analyzed. Figure 4.11 shows a cryo-TEM image of the self-assembly of AuNP. In this cryo-TEM image a split of the frozen chloroform film is observed, thus it was possible to differentiate the organization of AuNP in suspension and in the solid state. Under certain conditions the formation of hexagonal ordered AuNP with a narrow interparticle distance

was observed in the solid state. This arrangement could explain the shoulder of the SPR observed in the UV/Vis spectrum at $\lambda_{max} = 650$ nm. In suspension AuNP tended to form agglomerates in an irregular shape most likely due to solvent present, which altered a precise arrangement of hexagonal ordered AuNP. Aggregation of AuNP was not observed due to the unbound polystyrene block around the AuNP surface that acted as a repulsion agent between the nanoparticles.

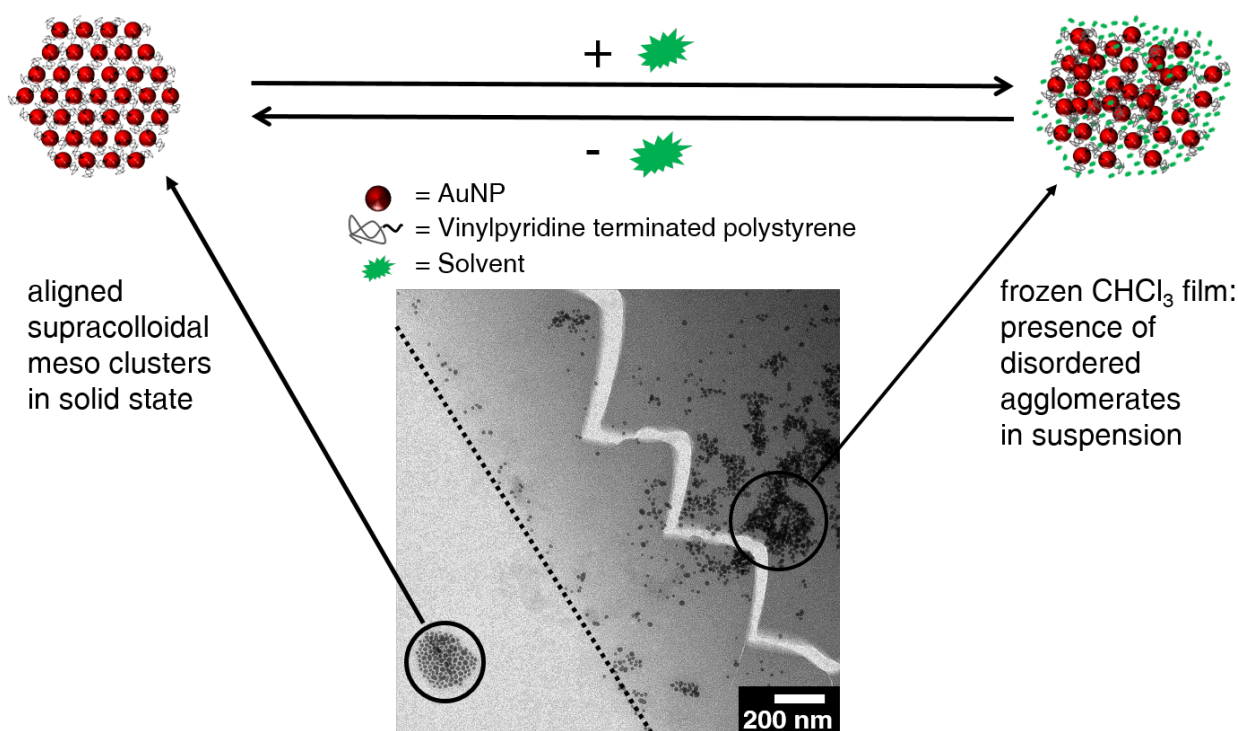


Figure 4.11: Cryo-TEM image of $\text{S}_{264}\text{VP}_1@AuNP$ (1:8). Representative scheme of self-assembly of AuNP in suspension and in the solid state.

By performing an Electron Tomography it was possible to explore the hexagonal order structure of AuNP in detail. A tilt sequence of the sample $\text{S}_{264}\text{VP}_1@AuNP$ (1:8) was recorded between $\pm 60^\circ$ in 2° increment steps. A recorded sequence is placed in Figure 4.12.

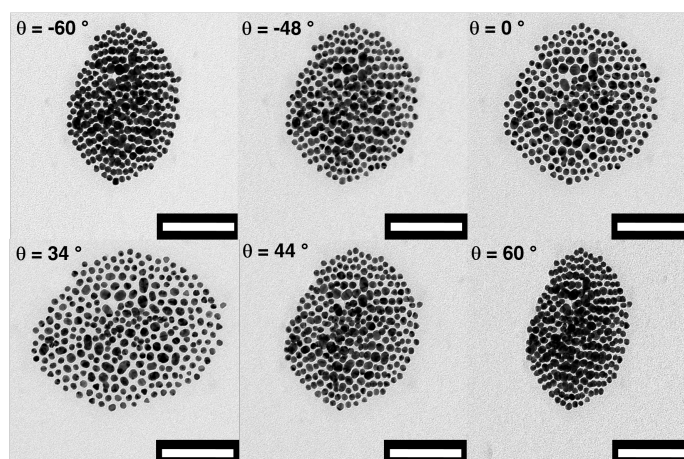


Figure 4.12: Tilt sequence of an ET image of $S_{26}4VP_1@AuNP$ (1:8) between angles $\pm 60^\circ$. Scale bar is 200 nm.

ET measurements were supported by theoretical 3D reconstructions. Herein it was possible to visualize an ellipsoid ordered three dimensional structure of AuNP in the solid state as shown in Figure 4.13.

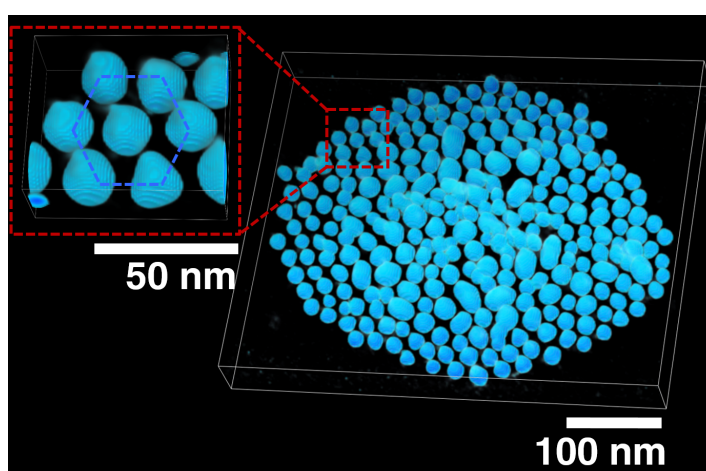


Figure 4.13: Computational 3D reconstruction of $S_{26}4VP_1@AuNP$. Self-assembly of $S_{26}4VP_1@AuNP$ (1:8) in solid state. Inset of hexagonal ordered AuNP.

As mentioned before, the polystyrene block plays an important role for the precise formation of $S_4VP/AuNP$ nanocomposites. Depending on the length of the polystyrene block it was possible to control the interparticle distance of AuNP. FÖRSTER *et al.* showed different interparticle distances of metal nanoparticles by variation of the polymer chain^[144].

To confirm the influence of the polystyrene block over the interparticle distance of S4VP/AuNP nanocomposites an auxiliary pyridyl-terminated polystyrene $S_{43}4VP_1$ II was used to fabricate the same structures of S4VP/AuNP nanocomposites as before. Figure 4.14 shows different interparticle distances of precise order of S4VP/AuNP nanocomposites by using three different block lengths of polystyrene.

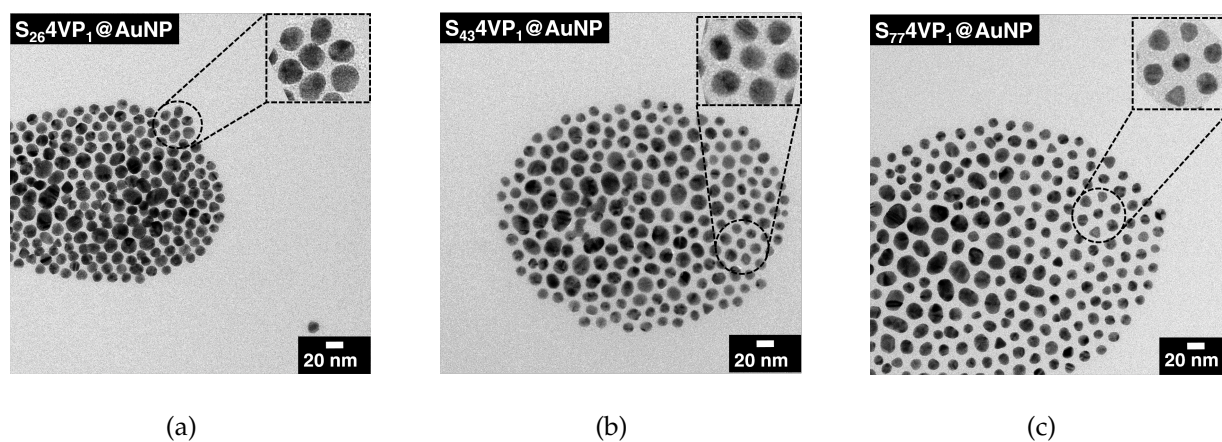


Figure 4.14: TEM micrographs of precise order of S4VP/AuNP nanocomposites with different block lengths of polystyrene. (a) $S_{26}4VP_1@AuNP$, mean interparticle distance $ds = 3.1 \text{ nm} \pm 1.5 \text{ nm}$ (138 particles measured). (b) $S_{43}4VP_1@AuNP$, $ds = 5.4 \text{ nm} \pm 1.3 \text{ nm}$ (510 particles measured). (c) $S_{77}4VP_1@AuNP$, $ds = 8.4 \text{ nm} \pm 2.1 \text{ nm}$ (544 particles measured).

All samples of $S_{26}4VP_1@AuNP$ and $S_{77}4VP_1@AuNP$ in suspension were characterized by means of DLS. A systematic increase of the hydrodynamic diameter D_H by the increment of AuNP was observed and is in accordance with the TEM images displayed in Figure 4.9 and 4.10.

Figure 4.15 and Table 4.7 show the particle size distributions D_H of $S_{26}4VP_1@AuNP$ and $S_{77}4VP_1@AuNP$ determined by DLS in $CHCl_3$.

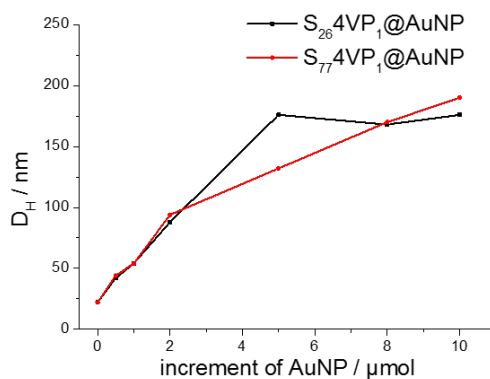


Figure 4.15: Particle size distributions D_H of $S_{26}4VP_1@AuNP$ and $S_{77}4VP_1@AuNP$ determined by DLS in $CHCl_3$.

Table 4.7: Particle size distributions determined by DLS in $CHCl_3$, for Citrate@AuNP, $S_{26}4VP_1@AuNP$, and $S_{77}4VP_1@AuNP$ with variation of AuNP/4VP ratio.

Entry	Molar ratio AuNP/4VP [μmol]	Hydrodynamic diameter	
		$S_{26}4VP_1@AuNP$ D_H [nm]	$S_{77}4VP_1@AuNP$ D_H [nm]
	Citrate@AuNP	22	22
1	0.5 : 1.0	42	44
2	1.0 : 1.0	54	54
3	2.0 : 1.0	82	94
4	5.0 : 1.0	176	132
5	8.0 : 1.0	168	170
6	10.0 : 1.0	176	190

Citrate@AuNP exhibited a hydrodynamic diameter of $D_H = 22$ nm. By changing the ligand and solvent for AuNP the hydrodynamic volume increased. The increment of AuNP ratio led to a systematically increase of D_H , which confirmed the formation of AuNP agglomerates and is also in accordance to the formation of self-assembly observed by TEM analysis displayed in Figure 4.9 and Figure 4.10.

To prove the presence of these agglomerates in suspension DLS measurements of $S_{26}4VP_1@AuNP$ with a molar ratio (1:5) were performed at 5°C and 55°C with different scattering angles starting from $\theta = 30^\circ$ to 150° in 20° steps. At 5°C a strong dependence

of the field autocorrelation functions with increase of scattering angles is observed. Also the unweighted hydrodynamic diameter decreases by increasing the scattering angle, which confirmed the large AuNP agglomerates in the suspension (4.16).

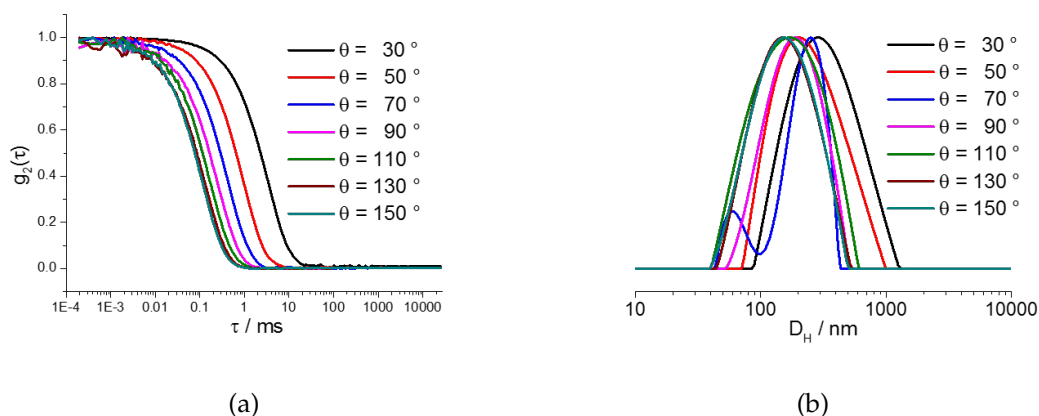


Figure 4.16: DLS data of $S_{26}4VP_1@AuNP$ (1:5) in suspension with different angles at 5 °C. (a) Normalized field autocorrelation functions and (b) their corresponding D_H .

After applying temperature at 55 °C for 30 min it was possible to disintegrate the AuNP agglomerates. Figure 4.17 shows consistent field autocorrelation functions and unweighted hydrodynamic diameter with different angles after the sample was cooled down at room temperature.

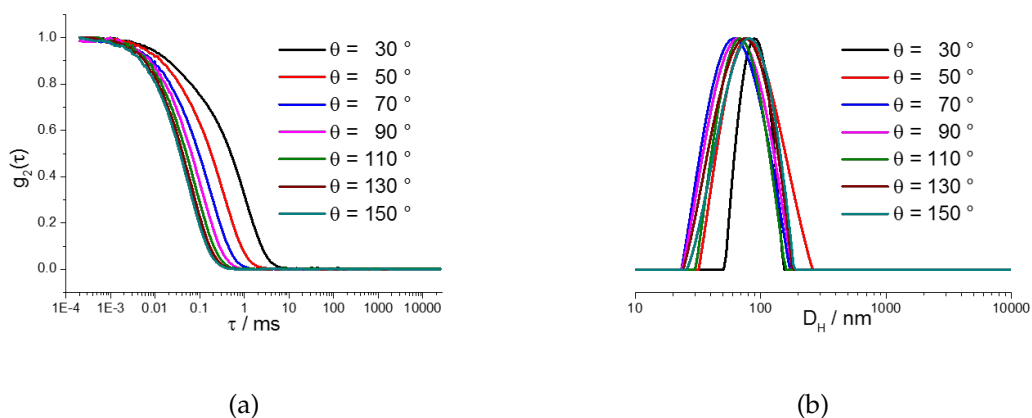


Figure 4.17: DLS data of $S_{26}4VP_1@AuNP$ (1:5) in suspension with different angles at 55 °C. (a) Normalized field autocorrelation functions and (b) their corresponding D_H .

Figure 4.18 summarizes the size distribution analysis of $S_{26}4VP_1@AuNP$ (1:5) evaluated by DLS before and after applying temperature with different angles. The disintegration

of AuNP agglomerates was distinctly observed after temperature treatment and cooling down the sample at 5 °C. T1 is starting temperature at 5 °C, D_H showed a strong dependence at different angles, which supported the presence of AuNP agglomerates in suspension. T2 is heating temperature at 55 °C, agglomerates started to disintegrate, this temperature was kept for 30 min. T3 is cooling down temperature at 5 °C, after two hours D_H remained constant at different angles, meaning a complete disintegration of the AuNP agglomerates

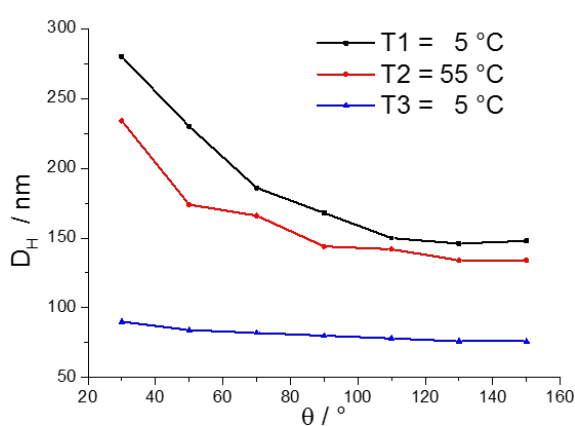


Figure 4.18: DLS data of $S_{264VP_1}@AuNP$ (1:5) for different angles at various temperatures.

Temperature dependent UV/Vis measurements were performed to support the disintegration of AuNP agglomerates in suspension. The sample $S_{264VP_1}@AuNP$ (1:5) was initially probed in a temperature range between 5 °C to 55 °C in 5 °C increment steps. By increasing the temperature a linear decrease of the plasmon band shoulder at 650 nm was observed, which confirmed the disintegration of AuNP agglomerates. This was also accompanied by a color change of the suspension from blue-violet to red-violet. Figure 4.19a shows the temperature dependent UV/Vis measurements of $S_{264VP_1}@AuNP$ (1:5) and the corresponding linear decrease of the plasmon absorption at 650 nm (Figure 4.19b).

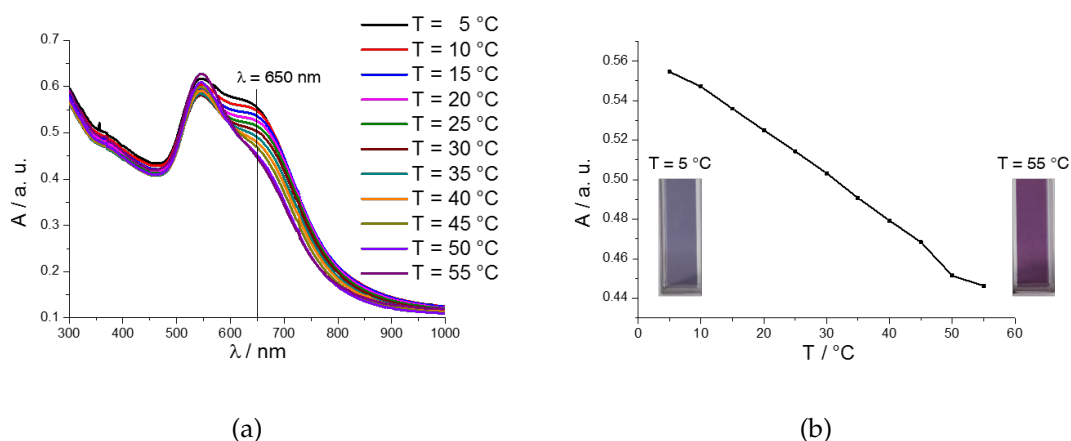


Figure 4.19: (a) UV/Vis spectra of $S_{26}4VP_1@AuNP$ (1:5) taken in a temperature range between 5 °C to 55 °C in 5 °C increment steps. (b) Plasmon absorbance at $\lambda = 650$ nm as a function of temperature.

The disintegration of AuNP agglomerates was also confirmed by TEM analysis, by preparing samples of $S_{26}4VP_1@AuNP$ (1:5) at 5 °C and 55 °C (Figure 4.20).

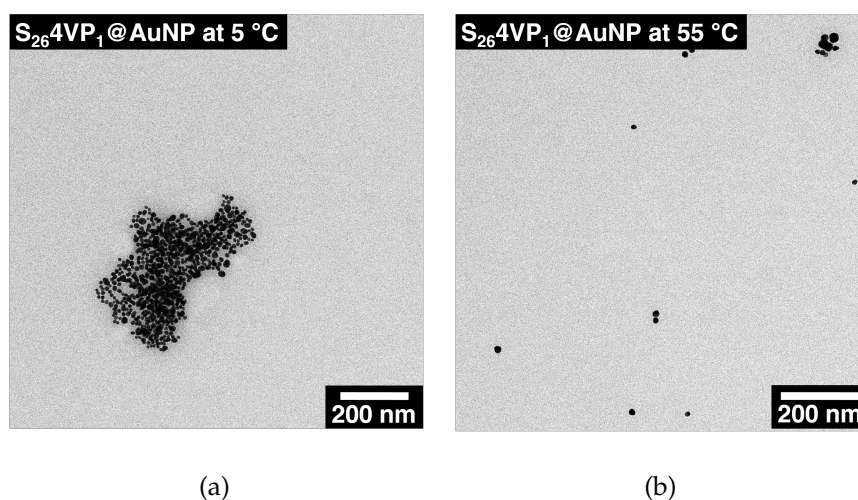


Figure 4.20: TEM images of $S_{26}4VP_1@AuNP$ (1:5) prepared at (a) 5 °C and (b) 55 °C.

After treating the sample at high temperatures, a second temperature ramp between 55 °C and 5 °C in 5 °C decrease steps was performed. Figure 4.21 shows the UV/Vis spectra of $S_{26}4VP_1@AuNP$ (1:5) and their corresponding plasmon absorption by decreasing temperature. The reappearance of the plasmon band shoulder at low temperatures was not observed, which indicated an irreversible self-assembly of the $S_{4VP}/AuNP$ nanocomposites.

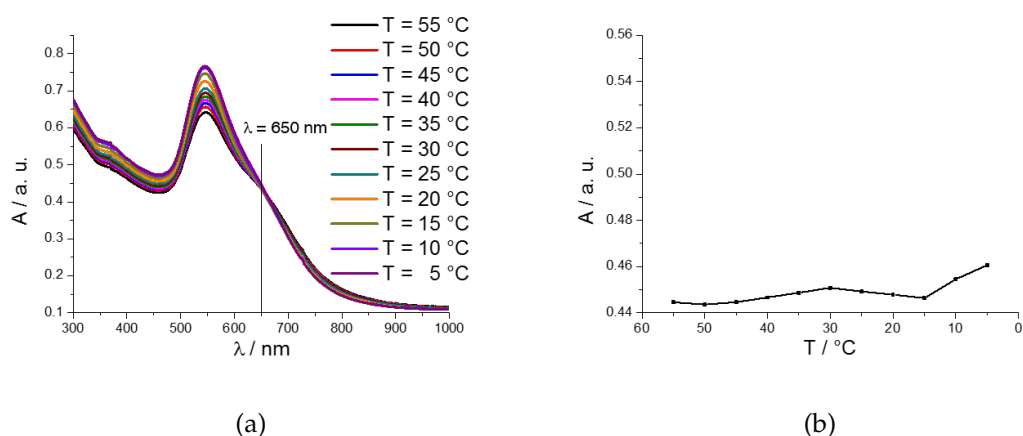


Figure 4.21: (a) UV/Vis spectra of $S_{26}4VP_1@AuNP$ (1:5) taken in a temperature range between 55 °C to 5 °C in 5 °C increment steps. (b) Plasmon absorbance at $\lambda = 650$ nm as a function of temperature.

Kinetic experiments were also performed to follow the disintegration of AuNP agglomerates. A sample of $S_{26}4VP_1@AuNP$ (1:5) was placed in the UV/Vis chamber at 55 °C and every ten minutes a UV/Vis spectrum was taken within 140 minutes. Figure 4.22 shows the UV/Vis spectra and their corresponding plasmon absorption by kinetics. By heating the sample after 20 minutes the extinction of the plasmon shoulder was observed, which means a rapid disintegration of the AuNP agglomerates.

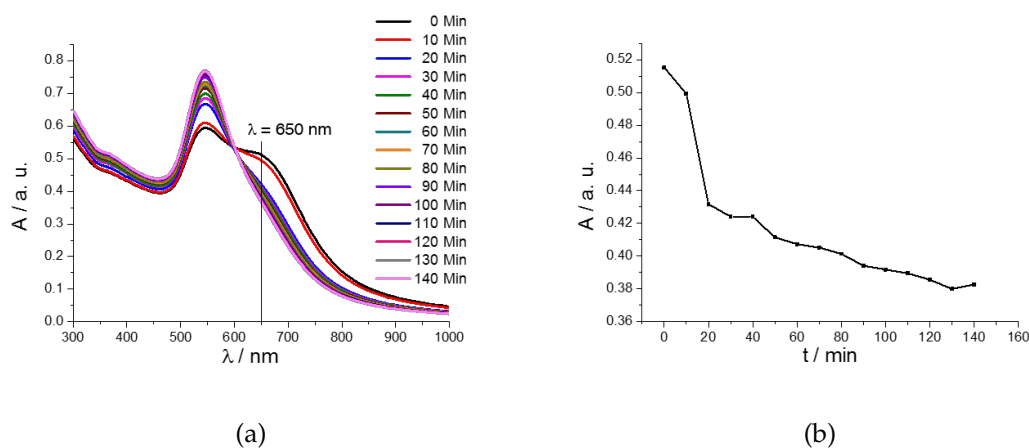


Figure 4.22: (a) UV/Vis spectra of $S_{26}4VP_1@AuNP$ (1:5) by kinetic experiments. (b) Plasmon absorbance at $\lambda = 650$ nm as a function of time.

Further addition of $S_{26}4VP_1$ to the suspension caused also a tendency to disintegrate the AuNP agglomerates. Figure 4.23 shows the UV/Vis spectra and the corresponding TEM images before and after addition of $S_{26}4VP_1$.

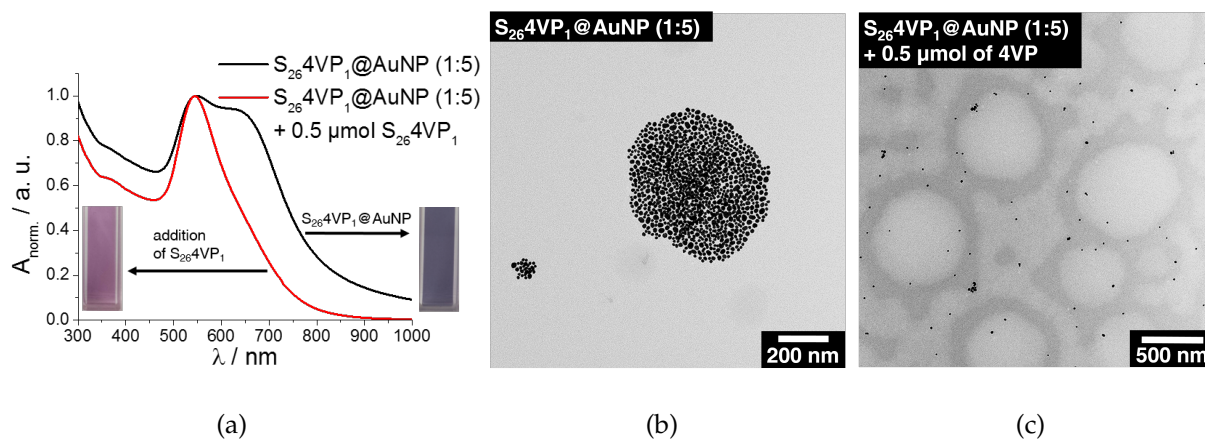
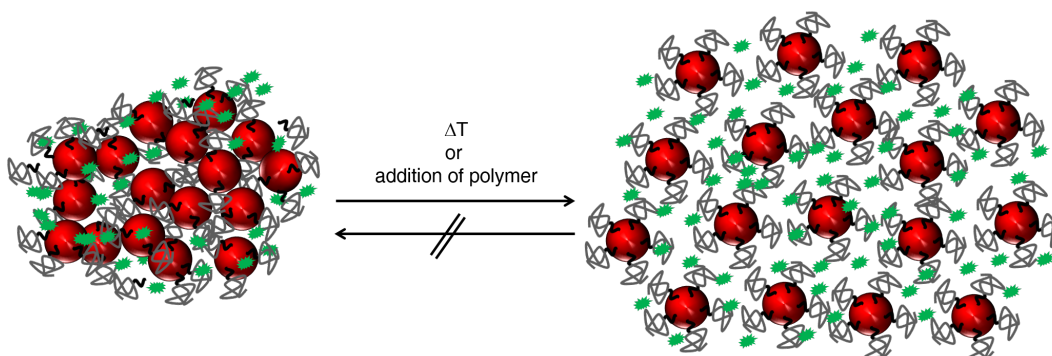


Figure 4.23: (a) UV/Vis spectra of $S_{26}4VP_1@AuNP (1:5)$ before and after addition of polymer, corresponding TEM images (b) before addition of polymer and (c) after addition of polymer.

According to the mathematical approximations (Table 4.5), it was shown, that the molar amount of ligands relative to the amount of AuNP is crucial for the formation of ordered $S4VP/AuNP$ nanocomposites.

Under strict quantitative consideration of the system, the sample with a molar ratio $Au/4VP = 10.0 \mu\text{mol}$ required an excess of 9360 monodentate ligands for the formation of ordered AuNP. Significant excess of ligands resulted in single nanoparticles in solid state, which can be explained by the presence of free ligands, which suppress the irreversibility of AuNP agglomerates.

Scheme 7 compiles schematically the disintegration of the AuNP agglomerates. Treating the $S4VP/AuNP$ nanocomposites by an external stimuli, such as temperature or additives showed an irreversible disintegration of the AuNP agglomerates, without observation of AuNP aggregation.



SCHEME: 7 Schematic representation of the disintegration of the AuNP agglomerates by external stimuli.

4.4.3 Ligand Exchange Reactions of Citrate@AuNP with $S_{77}4VP_{34}$ with Variation of AuNP/4VP Ratio

In contrast to the system with monodentate ligands described before, block copolymers with multidentate ligands, $S_{77}4VP_{34}$ @AuNP showed SPR shifted to $\lambda_{max} = 535$ nm (Figure 4.24). The sample with the amounts of AuNP 8.0 μmol and 10.0 μmol showed SPR shifted to $\lambda_{max} = 615$ nm, which might be due the formation of unstable AuNP aggregates.

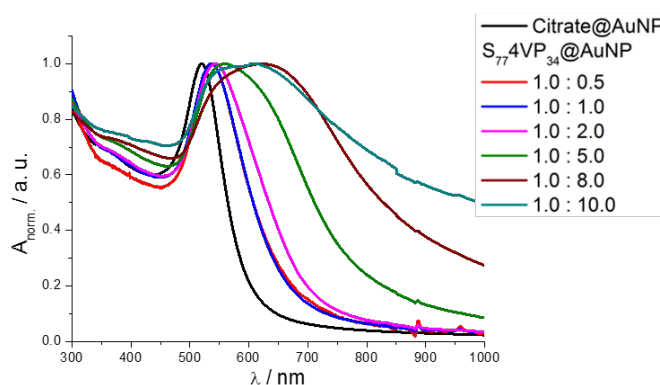


Figure 4.24: UV/Vis spectra of $S_{77}4VP_{34}$ @AuNP with variation of AuNP/4VP ratio after ligand exchange of Citrate@AuNP.

TEM-micrographs of $S_{77}4VP_{34}@AuNP$ are depicted in Figure 4.25. In comparison to monodentate ligands, $S_{77}4VP_{34}@AuNP$ showed even with low amounts of AuNP supramolecular self-assembly of AuNP with no precise formation of hexagonal ordered $S_{4VP}/AuNP$ nanocomposites. This deals with the fact, that long 4VP chains are able to wrap around one nanoparticle and fewer ligands are needed to cover the nanoparticle surface. Higher amounts of AuNP led to large agglomerates of AuNP, which are in accordance to the UV/Vis spectra described in Figure 4.24. At a certain amount of AuNP (5.0 μmol) the $S_{4VP}/AuNP$ nanocomposites started to lose stability, where AuNP collapsed and formed unstable aggregates. This phenomenon was confirmed by UV/Vis spectroscopy and TEM analysis.

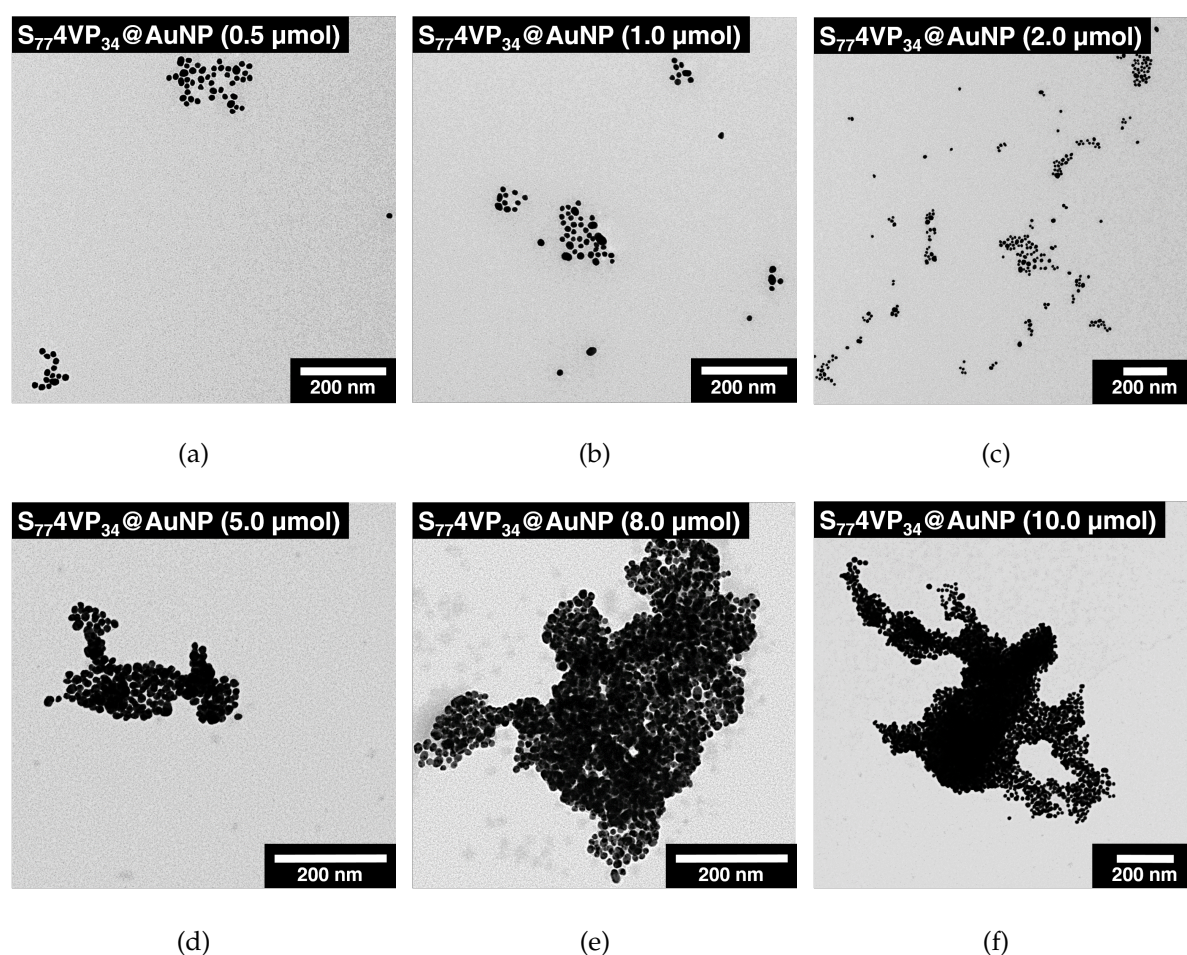


Figure 4.25: TEM-micrographs of $S_{77}4VP_{34}@AuNP$ with increase of AuNP/4VP ratio. Variation of AuNP: (a) 0.5 μmol , (b) 1.0 μmol , (c) 2.0 μmol , (d) 5.0 μmol , (e) 8.0 μmol , (f) 10.0 μmol .

Also DLS data showed a strong increase of D_H of $S_{77}4VP_{34}@AuNP$ with low concentrations due to the wrapping approach. Figure 4.26 and Table 4.8 shows the particle size distributions D_H of $S_{77}4VP_{34}@AuNP$ in suspension. For a better appreciation and comparison of the increase of D_H , the DLS Data of monodentate ligands were also plotted.

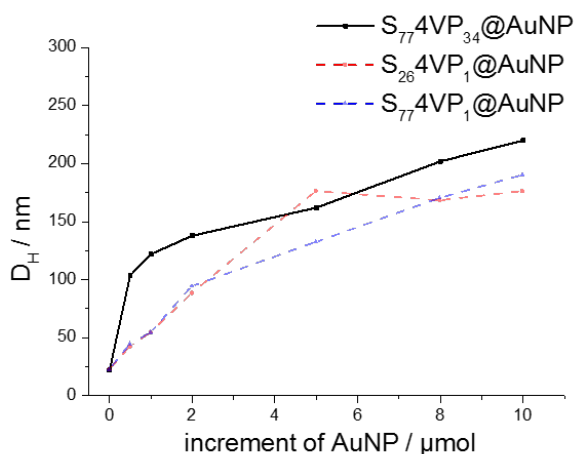


Figure 4.26: Particle size distributions D_H of $S_{77}4VP_{34}@AuNP$ in comparison to $S_{26}4VP_1@AuNP$ and $S_{77}4VP_1@AuNP$ determined by DLS in CHCl_3 .

Table 4.8: Particle size distributions determined by DLS in CHCl_3 , for Citrate@AuNP and $S_{77}4VP_{34}@AuNP$ with variation the AuNP/4VP ratio.

Entry	Molar ratio AuNP/4VP [μmol]	Hydrodynamic diameter $S_{77}4VP_{34}@AuNP$ D_H [nm]
	Citrate@AuNP	22
1	0.5 : 1.0	104
2	1.0 : 1.0	122
3	2.0 : 1.0	138
4	5.0 : 1.0	162
5	8.0 : 1.0	202
6	10.0 : 1.0	220

The addition of polymer as well as the appliance of temperature was also executed for $S_{77}4VP_{34}@AuNP$. In contrast, $S_{77}4VP_{34}$ (1:5) showed only modest alterations of the struc-

tures of S4VP/AuNP nanocomposites in the solid state. For this reason further temperature experiments were not performed. Figure 4.27 shows the UV/Vis spectra by variation of temperature and addition of polymer, as well as TEM images by addition of polymer.

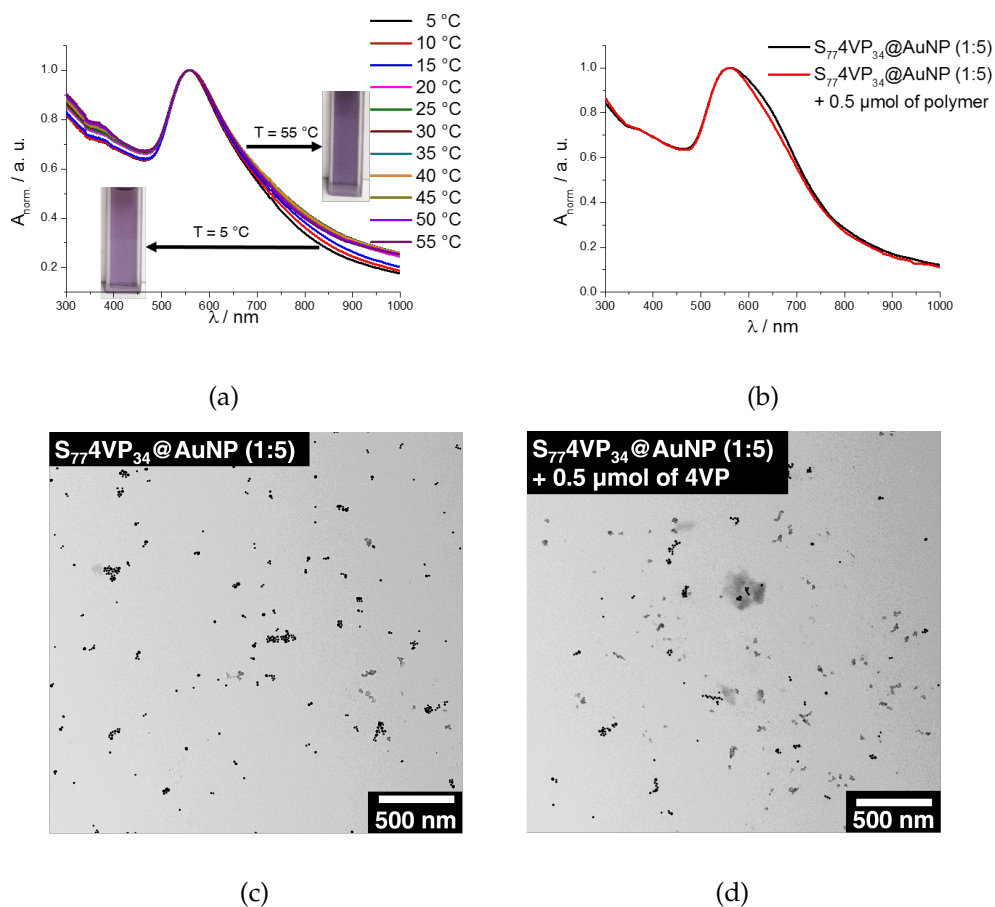


Figure 4.27: UV/Vis spectra at (a) different temperatures for S₇₇4VP₃₄ (1:5) at 5 °C and 55 °C, (b) UV/Vis spectra of S₇₇4VP₃₄ before and after addition of polymer, (c) TEM image of S₇₇4VP₃₄ before addition of polymer, (d) TEM image of S₇₇4VP₃₄ after addition of polymer.

4.4.4 Reverse Experiment: Ligand Exchange Reactions of Citrate@AuNP with S₂₆4VP₁ and S₇₇4VP₁, and S₇₇4VP₃₄ with Variation of 4VP/AuNP Ratio

The reverse experiment with a systematic variation of 4VP ratio was additionally performed, providing analogous results but in reverse order for precise formation of S4VP/AuNP nanocomposites. For ligand exchange reactions, the concentration of Citrate@AuNP was diluted to $c = 0.2$ mM. Table 4.9 shows the characteristics for variation of 4VP ratio to Citrate@AuNP.

Table 4.9: Parameters for ligand exchange reactions. Systematic variation of the molar ratio of 4VP to Citrate@AuNP.

Entry	S ₂₆ 4VP ₁ / S ₇₇ 4VP _{1/34} n(4VP) [μ mol]	Citrate@AuNP n(AuNP) [μ mol]
1	0.5	1.0
2	1.0	1.0
3	2.0	1.0
4	5.0	1.0
5	8.0	1.0
6	10.0	1.0

4.4.5 Ligand Exchange Reactions of Citrate@AuNP with S₂₆4VP₁ and S₇₇4VP₁ with Variation of 4VP/AuNP Ratio

Figure 4.28 shows the absorption spectra of S₂₆4VP₁@AuNP and S₇₇4VP₁@AuNP. A shift of the SPR in the absorption spectra from $\lambda_{max} = 521$ nm to $\lambda_{max} = 530$ nm was observed. Both S4VP₁@AuNP showed an asymmetrical SPR by a molar ratio 4VP/AuNP of 0.5 μ mol to 1.0 μ mol, which indicated plasmonic interactions of AuNP. This asymmetrical SPR is similar to the asymmetrical SPR of S4VP₁@AuNP with a molar ratio of 1.0 μ mol to 5.0 μ mol, described in Figure 4.7, section 4.4.2.

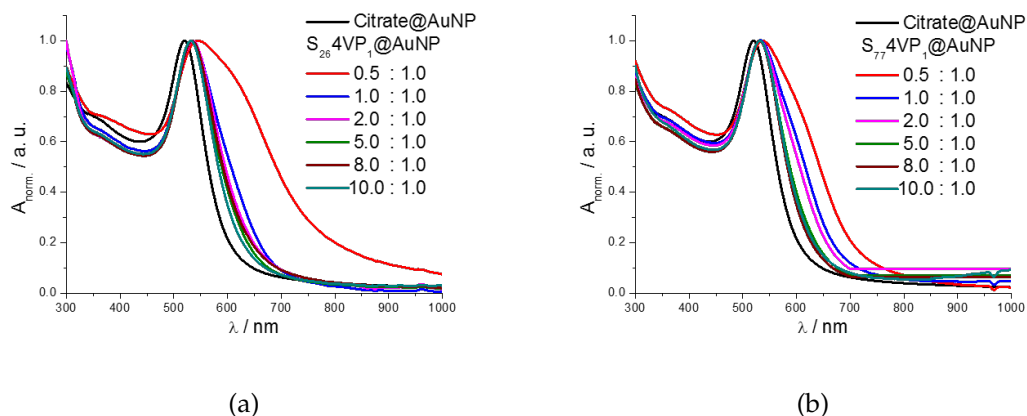


Figure 4.28: UV/Vis spectra of (a) $S_{26}4VP_1$, (b) $S_{77}4VP_1$ with different amounts of 4VP after ligand exchange of Citrate@AuNP.

Figure 4.29 and Figure 4.30 show TEM images of $S_{26}4VP_1$, $S_{77}4VP_1$, and $S_{77}4VP_{34}$ with increment of 4VP. $S_{26}4VP_1@AuNP$ and $S_{77}4VP_1@AuNP$ with an amount of 0.5 μmol 4VP showed formation of ordered $S4VP/AuNP$ nanocomposites in the solid state, which supported the asymmetrical SPR in Figure 4.28a, b. A high 4VP/AuNP ratio led to a dense coverage of AuNP with monodentate ligands, as shown in Figure 4.29 and Figure 4.30. Yet $S_{77}4VP_1@AuNP$ (1:10) showed the formation of self Assembly of AuNP (Figure 4.30f), which might be caused by the excess of polymer, that could led to a merging of free polymer with the already $S4VP$ -functionalized AuNP.

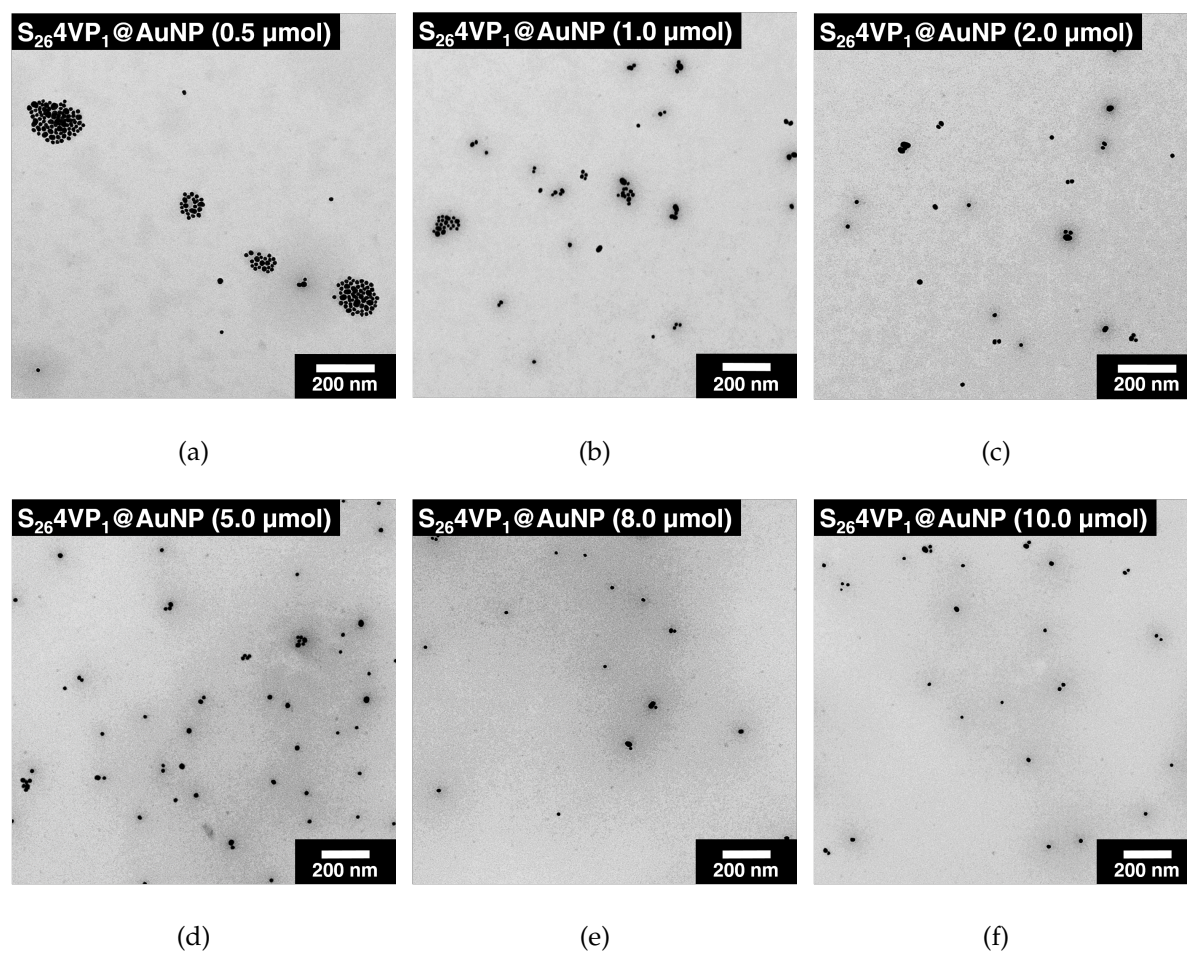


Figure 4.29: TEM-micrographs of $S_{26}4VP_1@AuNP$ with increase of 4VP/AuNP ratio. Variation of 4VP: (a) 0.5 μmol , (b) 1.0 μmol , (c) 2.0 μmol , (d) 5.0 μmol , (e) 8.0 μmol , (f) 10.0 μmol .

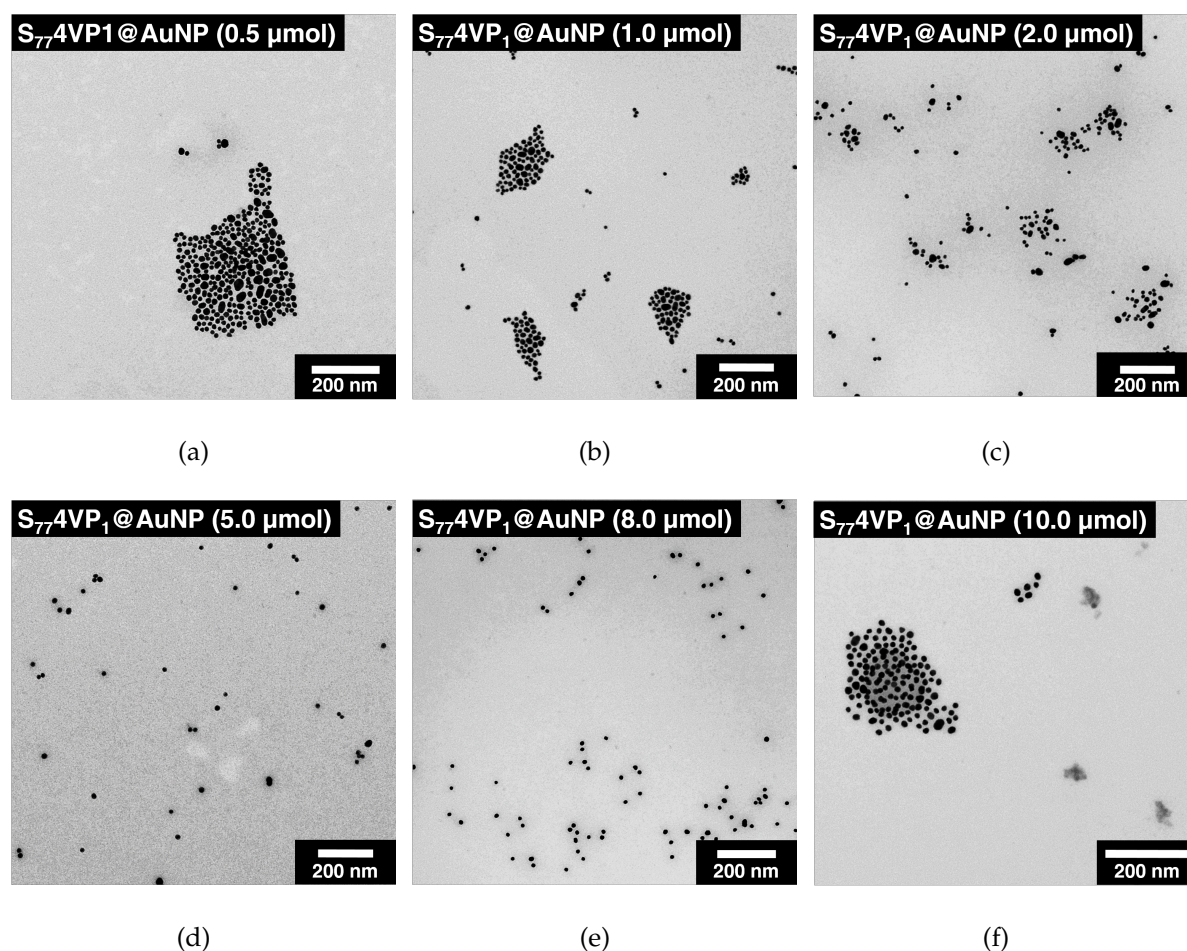


Figure 4.30: TEM-micrographs of $S_{77}4VP_1@AuNP$ with increase of 4VP/AuNP ratio. Variation of 4VP: (a) 0.5 μmol , (b) 1.0 μmol , (c) 2.0 μmol , (d) 5.0 μmol , (e) 8.0 μmol , (f) 10.0 μmol .

The DLS analysis shown in Figure 4.31 exhibited a decrease of D_H of $S_{26}4VP_1@AuNP$ and $S_{77}4VP_1@AuNP$ for low amounts of 4VP, which supported the formation of AuNP agglomerates in suspension, also confirmed by UV/Vis and TEM analysis. However, an increase in particle size distribution was observed for both systems. This might be caused by the entropic influence of polymer excess in the solution, which also can be detected by DLS analysis. Higher amounts of polymer should lead to a full coverage of the AuNP surface and a decrease of D_H respectively, which can be observed for molar ratios of 5.0 μmol for $S_{26}4VP_1@AuNP$ and 2.0 μmol for $S_{77}4VP_1@AuNP$. At this point a dense coverage of AuNP might be reached, leading to free polymer in the solution. Table 4.11 shows the size distributions evaluated by DLS.

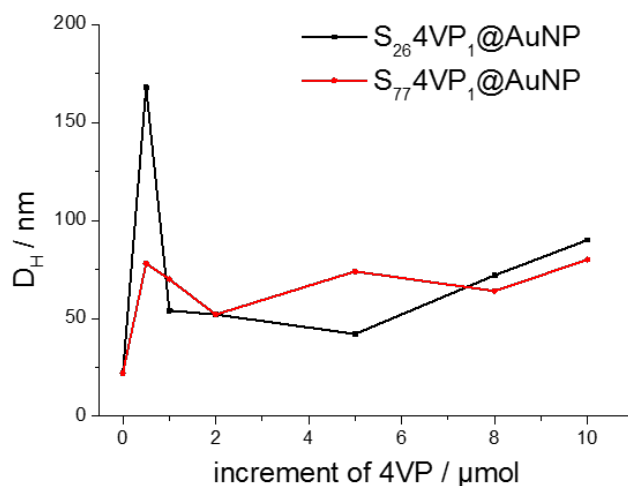


Figure 4.31: Particle size distributions D_H of $S_{26}4VP_1@AuNP$ and $S_{77}4VP_1@AuNP$ determined by DLS in $CHCl_3$.

Table 4.10: Particle size distributions determined by DLS in $CHCl_3$, for Citrate@AuNP, $S_{26}4VP_1@AuNP$ and $S_{77}4VP_1@AuNP$ with different amounts of 4VP.

Entry	Molar ratio 4VP/AuNP [μmol]	Hydrodynamic diameter	
		$S_{26}4VP_1@AuNP$ D_H [nm]	$S_{77}4VP_1@AuNP$ D_H [nm]
	Citrate@AuNP	22	22
1	0.5 : 1.0	168	78
2	1.0 : 1.0	54	70
3	2.0 : 1.0	52	52
4	5.0 : 1.0	42	74
5	8.0 : 1.0	72	64
6	10.0 : 1.0	90	80

4.4.6 Ligand Exchange Reactions of Citrate@AuNP with $S_{77}4VP_{34}$ with Variation of 4VP/AuNP Ratio

Figure 4.32 shows the UV/Vis spectra of $S_{77}4VP_{34}@AuNP$. A shift of SPR from $\lambda_{max} = 521$ nm to $\lambda_{max} = 545$ nm was observed. All samples displayed a strong ab-

sorbance with no shoulder formation, which corroborated the formation of S4VP/AuNP nanocomposites with no interplasmonic interactions. Also a broad SPR was not observed, hence the formation of larger agglomerates.

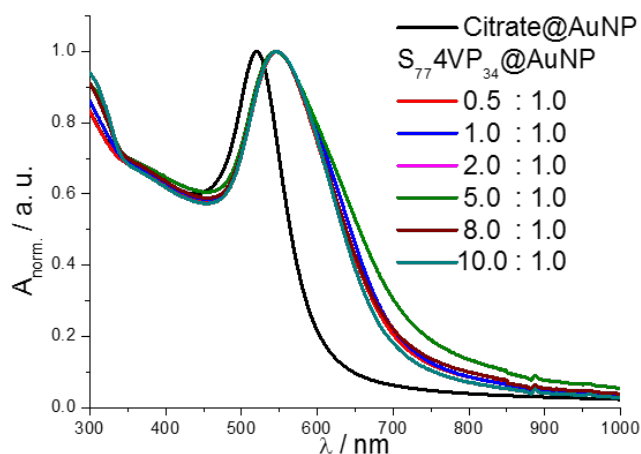


Figure 4.32: UV/Vis spectra of S₇₇4VP₃₄@AuP with increment of 4VP after ligand exchange of Citrate@AuNP.

TEM analysis showed the formation of supramolecular self-assembly of AuNP, but no formation of ordered S4VP/AuNP nanocomposites in solid state, Figure 4.33. Even at low ratios of 4VP it was not possible to observe single distributed AuNP due to the multidentate ligands wrapped around the AuNP, diminishing the entropic forces between the nanoparticles. This was also the case described in section 4.4.3.

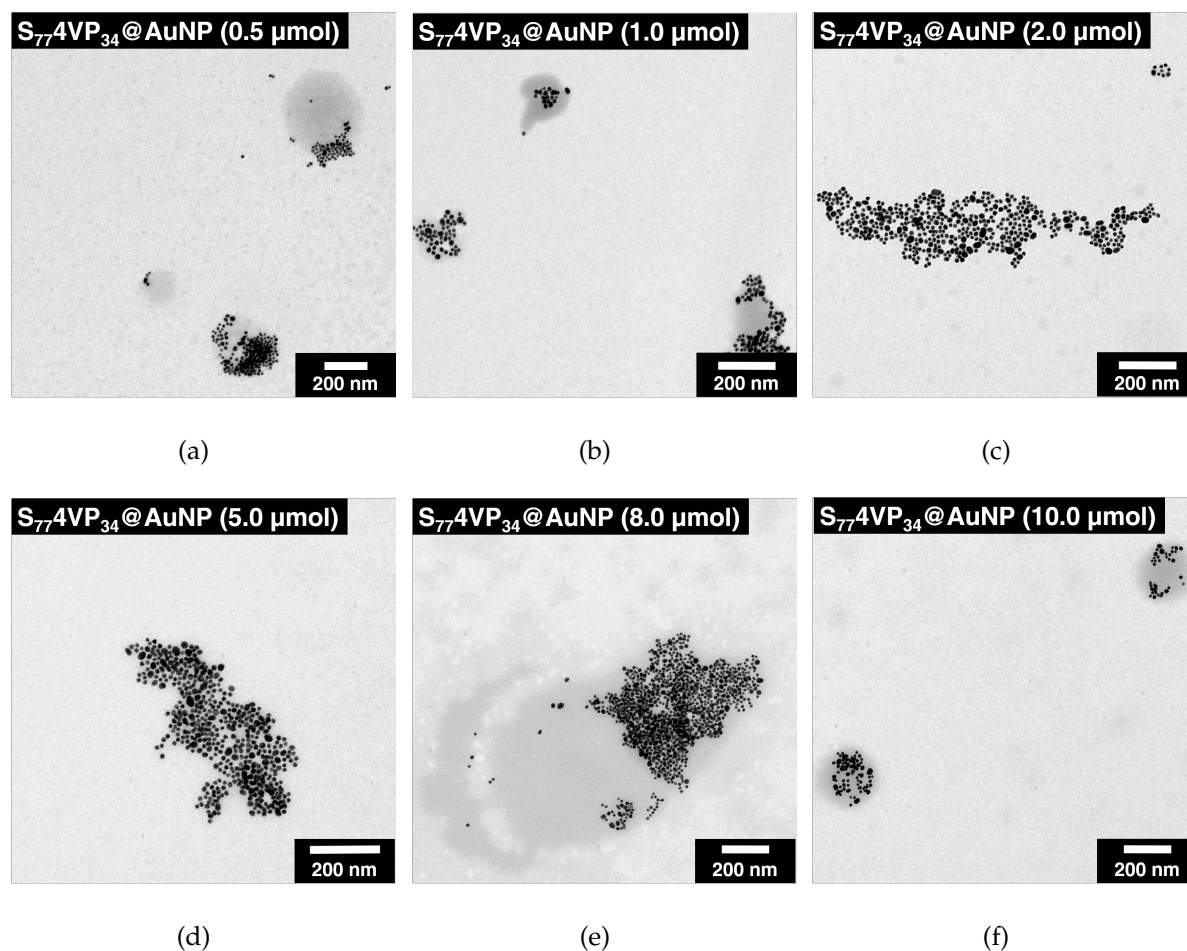


Figure 4.33: TEM-micrographs of $S_{77}4VP_{34}@AuNP$ with increase of 4VP/AuNP ratio. Variation of 4VP: (a) 0.5 μmol , (b) 1.0 μmol , (c) 2.0 μmol , (d) 5.0 μmol , (e) 8.0 μmol , (f) 10.0 μmol .

Figure 4.34 and Table 4.34 show the particle size distributions determined by DLS. In contrast to monodentate ligands, showed multidentate ligands no systematic increase of D_H by increment of 4VP. At a molar ratio of 4VP of 5.0 μmol the D_H reached a plateau, which speculated a maximum formation of $S_{77}4VP_{34}@AuNP$ nanocomposites in suspension, which is also in accordance to the UV/Vis and TEM Data.

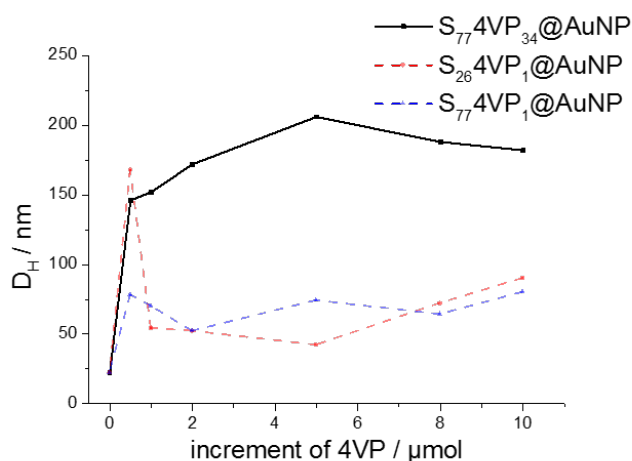


Figure 4.34: Particle size distributions D_H of $S_{77}4VP_{34}@AuNP$ in comparison to $S_{26}4VP_1@AuNP$ and $S_{77}4VP_1@AuNP$ determined by DLS in $CHCl_3$.

Table 4.11: Particle size distributions determined by DLS in $CHCl_3$, for Citrate@AuNP and $S_{77}4VP_{34}@AuNP$ with increment of 4VP.

Entry	Molar ratio 4VP/AuNP [μmol]	Hydrodynamic diameter $S_{77}4VP_{34}@AuNP$ D_H [nm]
	Citrate@AuNP	22
1	0.5 : 1.0	146
2	1.0 : 1.0	152
3	2.0 : 1.0	172
4	5.0 : 1.0	206
5	8.0 : 1.0	188
6	10.0 : 1.0	182

4.4.7 Conclusion

To conclude this section, interesting supramolecular structures of S4VP/AuNP nanocomposites were found. Polymers composed of styrene and 4VP were used. The 4VP block was used as monodentate and multidentate ligands for AuNP. Ligand exchange reactions of Citrate@AuNP with variation of AuNP ratio, as well as the variation of the

4VP ratio were performed. The formation of hexagonal ordered S4VP/AuNP nanocomposites was observed depending on the quantity of monodentate ligands. By the employment of external stimuli, such as temperature or addition of extra polymer, it was possible to disintegrate these high ordered S4VP/AuNP agglomerates in suspension into single distributed AuNP with irreversible formation into S4VP/AuNP agglomerates. The optical properties of these system was affected by external stimuli. In contrast, multidentate ligands did not show either high ordered S4VP/AuNP nanocomposites by increment of AuNP/4VP nor alterations of the structure and optical properties by influence of an external stimulus.

4.5 *In situ* Reactions of AuNP with S₇₇4VP₁, S₇₇4VP₁₇, and S₇₇4VP₃₄

The results of this section have been also prepared in form of a manuscript and have already been submitted.

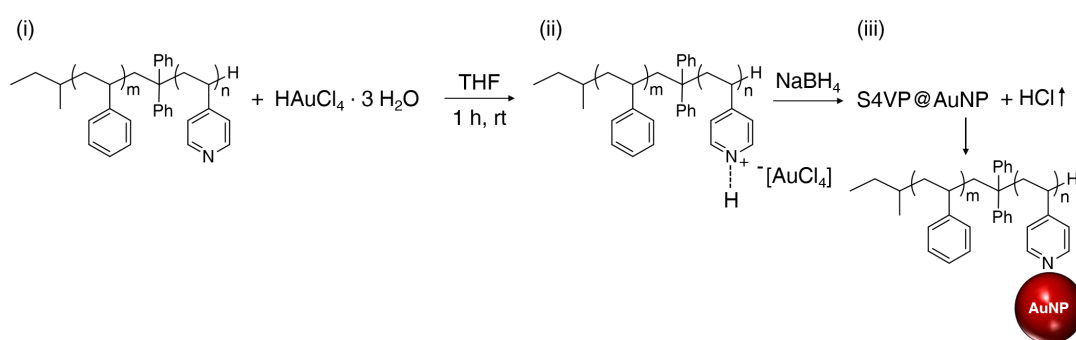
4.5.1 Hypothesis and Motivation

Within this section, the role of polymers with 4VP moieties of different lengths for the controlled size of AuNP was investigated. AuNP were generated by *in situ* reduction of HAuCl₄ with NaBH₄ in THF. Using the method known as the „dispersion route“, a systematic screen of the influence of 4VP block lengths and 4VP ratio to gold precursor on the resulting S4VP/AuNP nanocomposites was performed. With this systematic approach it was possible to identify proper conditions for the synthesis of *in situ* AuNP with small standard deviations. The formation of AuNP with varying diameter showed distinctive optical properties, which were carefully analyzed by means of Transmission Electron Microscopy (TEM) and UV/Vis spectroscopy. The reported approach demonstrates a facile and versatile method for the controlled *in situ* synthesis towards S4VP/AuNP nanocomposites. The polymers with 4VP moieties S₇₇4VP₁ **III**, S₇₇4VP₁₇ **IV**, and S₇₇4VP₃₄ **V** were synthesized *via* sequential living anionic polymerization of the corresponding monomers, according to scheme 3 in section 4.1. S₇₇4VP₁ **III** is considered to be a homopolymer of styrene with an end-group of 4VP, which served as a monodentate ligand for AuNP. 4VP coordinates to AuNP, surrounding and stabilizing the whole nanoparticle surface. Longer 4VP blocks (S₇₇4VP₁₇ **IV** and S₇₇4VP₃₄ **V**) were contemplated to function as multidentate ligands for AuNP, in which the pyridyl groups of 4VP are able to wrap around one nanoparticle.

4.5.2 *In situ* Formation of AuNP

S4VP/AuNP nanocomposites were synthesized by the „dispersion route“ according to the literature^[43] (Scheme 8). AuNP were prepared *in situ* in the presence of S4VPs **III-V** with a direct coordination of the 4VP block as a stabilizing ligand for AuNP using NaBH₄ as reducing agent. First, tetrachloroauric acid trihydrate (HAuCl₄ · 3H₂O)

and S4VPs, respectively were mixed in a desired ratio (i). As a result, the gold acid protonated the pyridyl-groups and a complex of polyionic blocks was formed (ii). After the gold ions were selectively incorporated into the 4VP domains of the S4VPs, NaBH_4 was used to reduce the gold acid into AuNP to form $\text{S}_{77}4\text{VP}_1@AuNP$, $\text{S}_{77}4\text{VP}_{17}@AuNP$, and $\text{S}_{77}4\text{VP}_{34}@AuNP$ (iii). Reactions were performed at room temperature with an end concentration of HAuCl_4 $c = 0.2 \text{ g} \cdot \text{L}^{-1}$ and THF as a solvent. Tetrachloroauric acid was reduced to AuNP with 2.5 eq. of NaBH_4 , which acted as a fast reducing agent and provided a fast, homogenous nucleation of AuNP.



SCHEME: 8 (i) Mechanism of *in situ* synthesis of AuNP in the presence of S4VPs **III-V**. (ii) Protonation of pyridyl groups with HAuCl_4 to form a complex of polyionic-blocks. (iii) Reduction of HAuCl_4 with NaBH_4 to generate $\text{S}_{77}4\text{VP}_1@AuNP$, $\text{S}_{77}4\text{VP}_{17}@AuNP$, and $\text{S}_{77}4\text{VP}_{34}@AuNP$.

To investigate the role of employed S4VPs **III-V** for the stabilization and size distribution of AuNP during the *in situ* process, different molar ratios of 4VP/ HAuCl_4 were tested. The chosen parameters for the preparation of S4VP@AuNP are listed in Table 4.12.

Table 4.12: Parameters for the *in situ* synthesis of $S_{77}4VP_1@AuNP$, $S_{77}4VP_{17}@AuNP$, and $S_{77}4VP_{34}@AuNP$.

Entry	$S_{77}4VP_1$ n(S4VP) [μmol]	$S_{77}4VP_{17}$ n(S4VP) [μmol]	$S_{77}4VP_{34}$ n(S4VP) [μmol]	$HAuCl_4$ [μmol]	Molar ratio 4VP/ $HAuCl_4$
1	1.3	0.051	0.028	10.0	0.1 : 1.0
2	6.5	0.25	0.14	10.0	0.5 : 1.0
3	12	0.51	0.28	10.0	1.0 : 1.0
4	26	1.0	0.55	10.0	2.0 : 1.0
5	65	2.5	1.4	10.0	5.0 : 1.0
6	130	51	2.8	10.0	10.0 : 1.0

After completion of the *in situ* reactions, the samples were dialyzed against water to remove salt impurities ($NaB(OH)_3$, $NaCl$) formed during the reaction. By replacing THF with water, the $S4VP@AuNP$ collapsed due to the fact that the stabilizing PS shell is insoluble in water, but dissolved again upon changing the solvent back to THF. The reactions with mono- and multidentate ligands will be discussed separately in the next sections.

4.5.3 Characterization of Monodentate Ligands: $S_{77}4VP_1@AuNP$

Figure 4.35 shows the absorption spectra of $S_{77}4VP_1@AuNP$. A strong SPR of AuNP at a wavelength of $\lambda_{max} = 533$ nm for all molar ratios was observed. This peak confirmed the formation of AuNP, and a maximum peak at a wavelength of $\lambda = 290$ nm, which originated from the aromatic ring of the polystyrene block, acting as stabilizing corona for AuNP (Figure 4.35a). All samples showed a red-violet color, which is typical for spherical AuNP in the size range of 10-20 nm^[72] (Figure 4.35b).

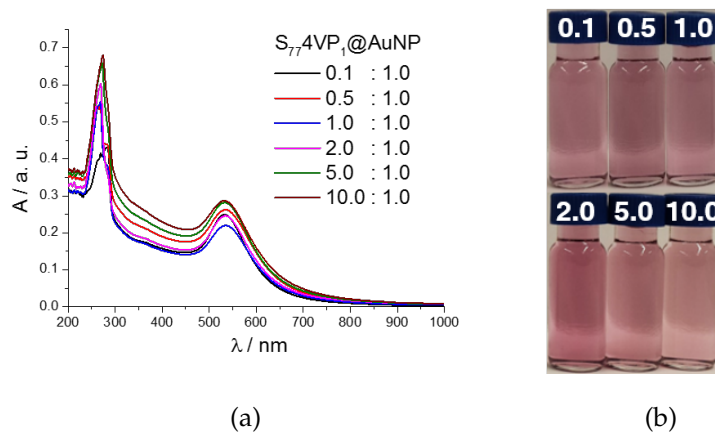


Figure 4.35: UV/Vis spectra of AuNP with monodentate ligands. a) Absorption spectra of $S_{77}4VP_1@AuNP$ with variation of 4VP/ $HAuCl_4$ ratio, according to Table 4.12, b) corresponding photograph of $S_{77}4VP_1@AuNP$ after dialysis, according to Table 4.12.

$S_{77}4VP_1$ acting as monodentate ligands for AuNP provided sufficient stabilization to avoid aggregation of AuNP, which is supported by TEM analysis. Figure 4.36 shows TEM images for all molar ratios.

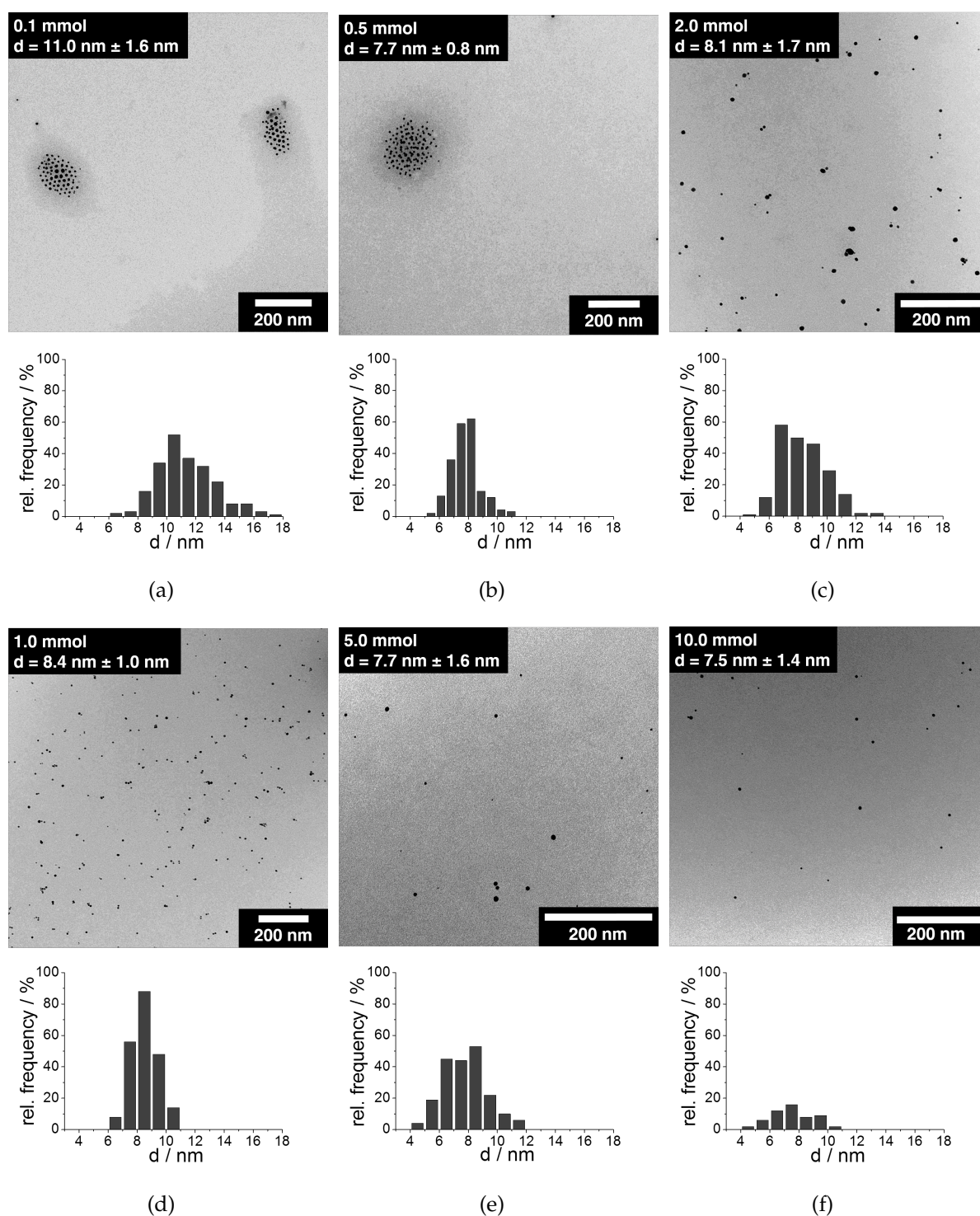
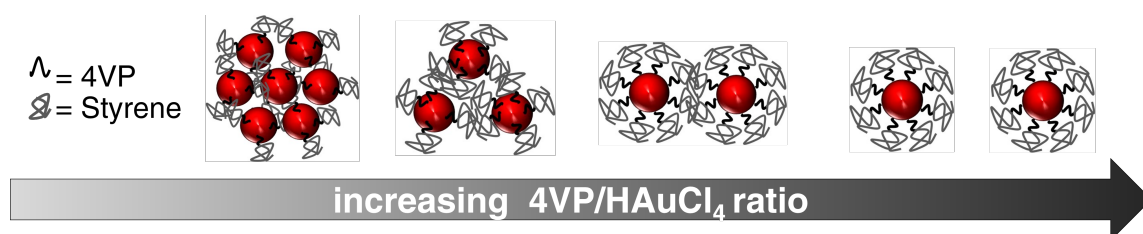


Figure 4.36: TEM-micrographs of $S_{774VP1}@AuNP$ with their corresponding particle size distributions with increase of 4VP/H $AuCl_4$ ratio. Variation of 4VP: (a) 0.1 μmol , (b) 0.5 μmol , (c) 1.0 μmol , (d) 2.0 μmol , (e) 5.0 μmol , (f) 10.0 μmol .

With a low ratio of 4VP/HAuCl₄ of 0.1 μmol and 0.5 μmol the density of monodentate ligands was depressed and merging of the AuNP into ordered AuNP/S4VP nanocomposites (Figure 4.36a, b). However, the tethered PS chains encapsulated the formed AuNP acting as sufficient repulsion agent to prevent aggregation of AuNP. Upon increasing the 4VP/HAuCl₄ ratio, single distributed AuNP were achieved (Figure 4.36c-f). This is attributed to a high grafting density of 4VP moieties on the AuNP surface and the high chain density of PS chains covalently bound to the 4VP head group, reminiscent of a star-like approach. Different grafting motifs, according to quantity of 4VP ligands is schematically represented in Scheme 9.



SCHEME: 9 Schematic representation of S4VP/AuNP nanocomposites with a 4VP moiety as monodentate ligands with increasing 4VP/HAuCl₄ ratio.

The behavior of 4VP as a monodentate ligand is similar to thiol-end capped polystyrenes (PS-SH) for AuNP. As described in the literature, PS-SH functionalized AuNP are well synthesized in a diameter range of $d = 5$ nm by using lithium triethylborohydride (Superhydride) as the reducing agent^[145,146]. In this case using 4VP as stabilizing ligand for gold and NaBH₄ as reducing agent resulted in stable, narrowly distributed AuNP almost absent of aggregates with diameters around $d = 8$ nm.

From TEM analysis it could be concluded, that the monodentate S4VP ligand showed two approaches for the surface stabilization of AuNP while using different ratios of 4VP. A low concentration of the polymer led to an arrangement of AuNP into ordered S4VP/AuNP nanocomposites due to less polymer on the AuNP surface. However, agglomerates are avoided by steric repulsion of tethered polystyrene chains on the AuNP surface. An excess of polymer in the solution induced a full coverage of the AuNP surface displaying a star-like approach, as described by VANA *et al.*^[110].

4.5.4 Characterization of Multidentate Ligands: $S_{77}4VP_{17}@AuNP$ and $S_{77}4VP_{34}@AuNP$

Compared to the as described $S_{77}4VP_1$, which acted as monodentate ligands for AuNP, $S_{77}4VP_{17}@AuNP$ and $S_{77}4VP_{34}@AuNP$ showed a change of the SPR due to different AuNP sizes.

Figure 4.37 shows the UV/Vis spectra of $S_{77}4VP_{17}@AuNP$ and $S_{77}4VP_{34}@AuNP$. By increasing the polymer concentration a blue shift of the SPR was detected. A weak and broad SPR for amounts of 4VP with 0.1 - 2.0 μmol was observed, which indicated the formation of larger particles, also observed in the violet color of the $S_{4VP}/AuNP$ nanocomposites (Figure 4.37b, d). Samples with amounts of 4VP of 5.0 μmol and 10.0 μmol showed no active SPR at a wavelength of $\lambda_{max} = 530 \text{ nm}$ (Figure 4.37a, Figure 4.38a), which advised the formation of ultra-small AuNP or elemental gold. This scenario was also demonstrated by the brown color of the $S_{4VP}/AuNP$ and the absence of microscopic precipitation.

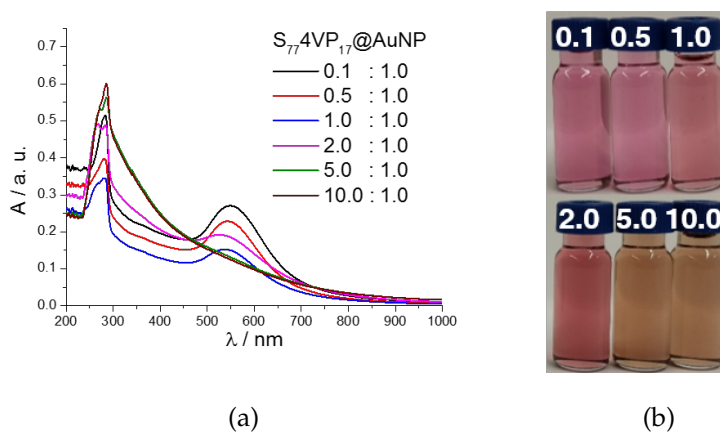


Figure 4.37: UV/Vis spectra of AuNP with multidentate ligands. (a) Absorption spectra of $S_{77}4VP_{17}@AuNP$ with variation of 4VP/ $HAuCl_4$ ratio, (b) corresponding photograph of $S_{77}4VP_{17}@AuNP$ after dialysis, according to Table 4.12.

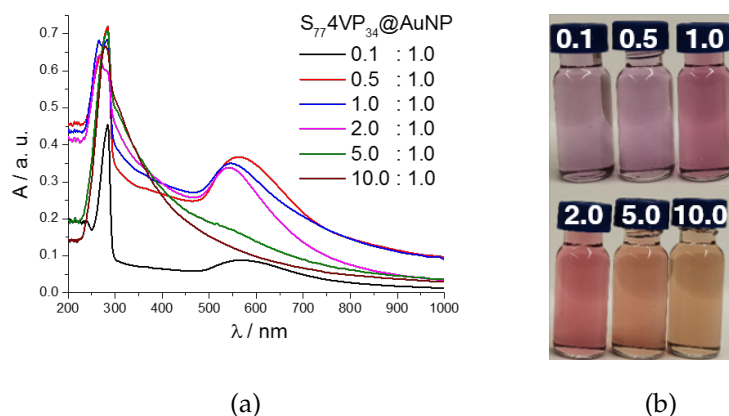


Figure 4.38: UV/Vis spectra of AuNP with multidentate ligands. (a) Absorption spectra of $S_{77}4VP_{34}@AuNP$ with variation of 4VP/HAuCl₄ ratio, (b) corresponding photograph of $S_{77}4VP_{34}@AuNP$ after dialysis, according to Table 4.12.

TEM images, depicted in Figure 4.39 and Figure 4.40 supported the statement on the formation of different sizes of AuNP. Using low concentrations of $S_{77}4VP_{17}$ (0.1 μmol and 0.5 μmol), it was possible to generate AuNP in diameter size around $d = 8$ nm. Samples with $S_{77}4VP_{17}@AuNP$ showed supramolecular self-assembly of AuNP (Figure 4.39a - c). Increasing the amount of 4VP up to 5.0 μmol led to the formation of spherical micelles of S4VP with AuNP diameter of around $d = 2.5$ nm (Figure 4.39e, f). These particles narrowed the formation of very small AuNP (Table 2 entries 5, 6), which also showed no SPR activity, as seen in Figure 4.37a.

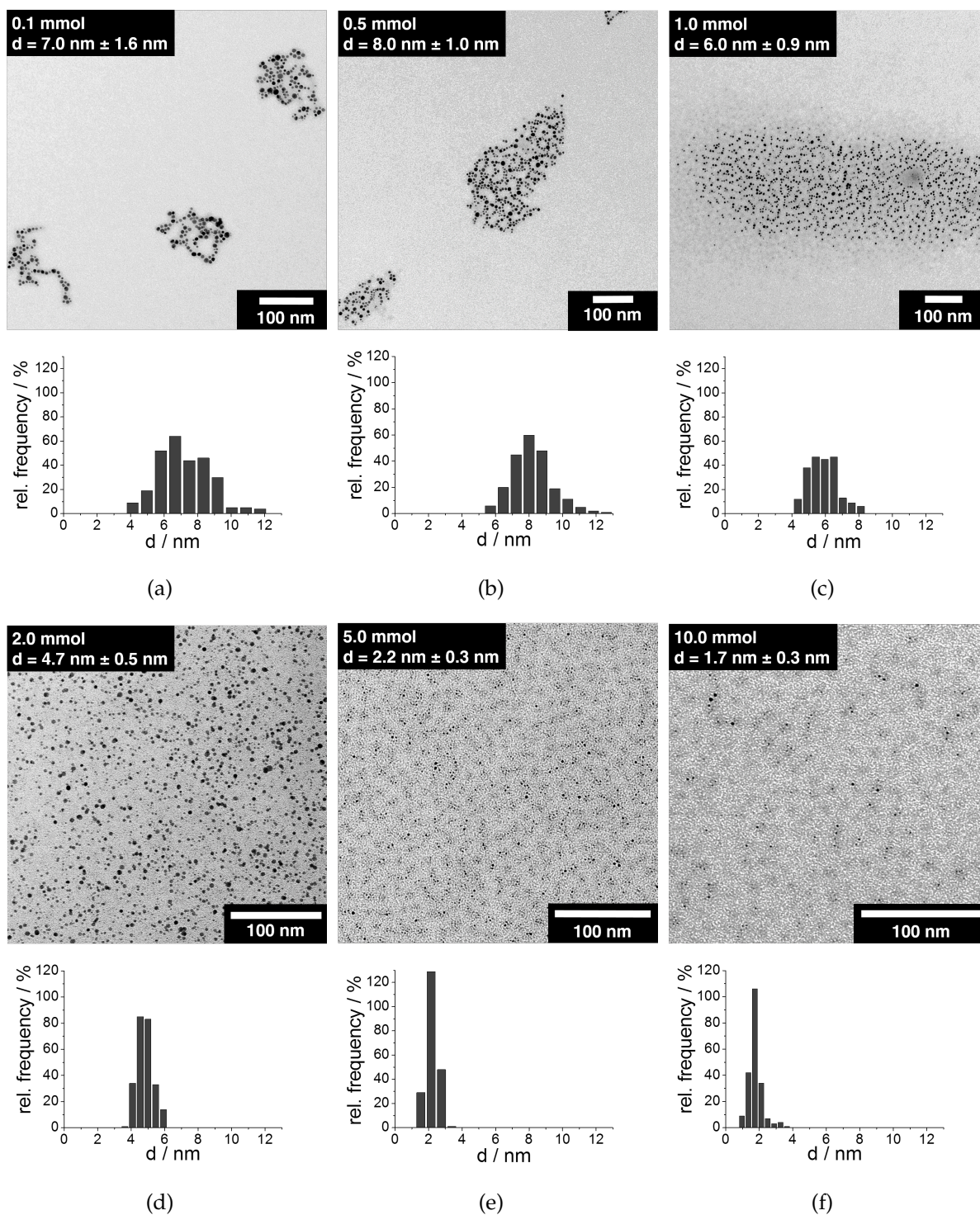


Figure 4.39: TEM-micrographs of $S_{774VP_{17}}@AuNP$ with their corresponding particle size distributions with increase of 4VP/HAuCl₄ ratio. Variation of 4VP: (a) 0.1 μmol , (b) 0.5 μmol , (c) 1.0 μmol , (d) 2.0 μmol , (e) 5.0 μmol , (f) 10.0 μmol .

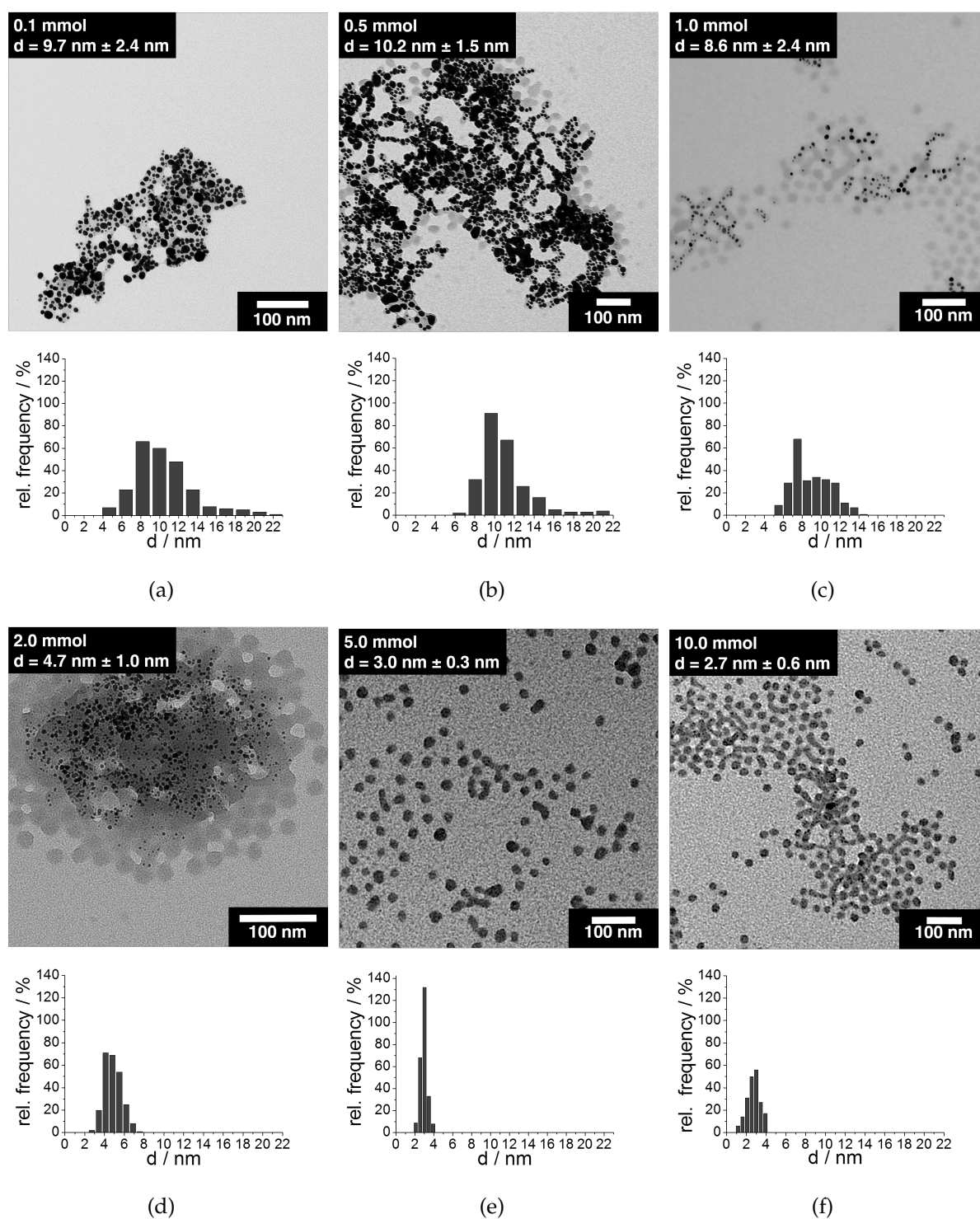
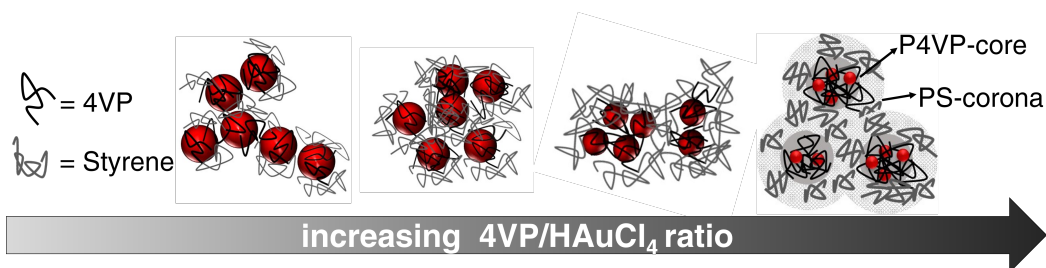


Figure 4.40: TEM-micrographs of $S_{774VP_{34}}@AuNP$ with their corresponding particle size distributions with increase of 4VP/HAuCl₄ ratio. Variation of 4VP: (a) 0.1 μmol , (b) 0.5 μmol , (c) 1.0 μmol , (d) 2.0 μmol , (e) 5.0 μmol , (f) 10.0 μmol .

Also the samples with $S_{77}4VP_{34}@AuNP$ showed an analogous size formation of AuNP. TEM images of $S_{77}4VP_{34}@AuNP$ are displayed in Figure 4.40. However, $S_{77}4VP_{34}$ led to an irregular size formation of AuNP with a broader distribution and large agglomerates in diameter of around $d = 10$ nm (Figure 4.40a), in comparison to $S_{77}4VP_{17}@AuNP$. This was also supported by the UV/Vis spectra, which showed no activity of SPR (Figure 4.37c).

Long 4VP chains acted as multidentate ligands for AuNP and resulted in a different coordination behavior towards the AuNP surface. In contrast to the monodentate ligand, multiple 4VP groups of a single polymer chain were able to wrap around the AuNP surface and less ligand was needed to cover the AuNP surface to reach sufficient stabilization of one single AuNP. Even at low $S_{4VP}/AuNP$ ratios, single AuNPs could be stabilized by wrapping of a multidentate 4VP ligand, yet the covalently linked polystyrene acted as a spacer to prevent aggregation of single nanoparticles, as also confirmed by VANA^[110]. High concentration of S_{4VP} led to a micelle formation with a saturation of 4VP chains, where gold ions were intercalated within the pyridyl groups prior to reduction, which restricted the nucleation growth of AuNP, as described by VALETSKY^[124]. Scheme 10 illustrates the distinctive size formation of AuNP by use of 4VP moieties as multidentate ligands.



SCHEME: 10 Schematic representation of $S_{4VP}/AuNP$ nanocomposites with 4VP moieties as multidentate ligands with increase of $4VP/HAuCl_4$ ratio.

According to the literature it was shown, that S_{4VP} block copolymers with volume fractions of 4VP $\phi_{4VP} = 0.19$, and $\phi_{4VP} = 0.3$ showed the formation of spherical micelles in THF^[107,147,148]. $S_{77}4VP_{17}$ and $S_{77}4VP_{34}$ with volume fractions of $\phi_{4VP} = 0.18$ and $\phi_{4VP} = 0.30$ respectively, showed the formation of spherical micelles once the critical micelle concentration (cmc) was reached. Figure 4.41 shows TEM micrographs of $S_{4VP}/AuNP$

nanocomposites with a molar ratio of 4VP of 10 μmol in a higher magnification, for a better appreciation of the micelles formation.

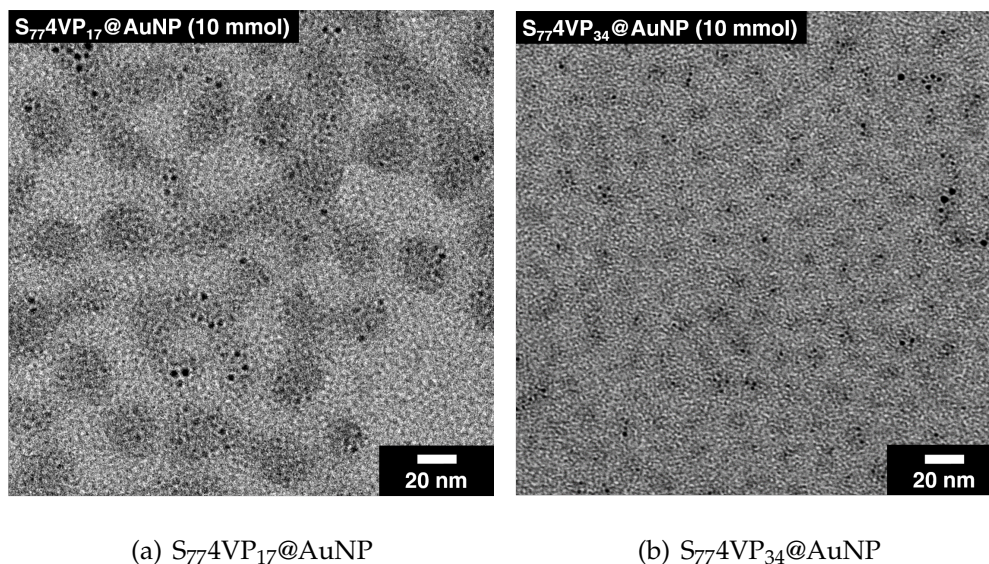


Figure 4.41: High magnification TEM-micrographs of (a) $S_{77}4VP_{17}@AuNP$ and (b) $S_{77}4VP_{34}@AuNP$ with a molar ratio of 4VP/ $H AuCl_4$ of 10 μmol .

In both systems it was possible to observe the encapsulation of AuNP within the 4VP domains and empty micelles as well. MÖLLER reported a similar effect of empty micelles, which are expected due to the stabilization of gold nanoparticles by significantly fewer block copolymer chains^[44].

As described in early articles AuNP exhibit a small diameter size around $d = 2$ nm within the micelles, which is in good accordance to our results^[43,44,149,150]. In our system we obtained different sizes of AuNP which could be controlled by varying the ratio of 4VP in $S_{77}4VP_{17}$ and $S_{77}4VP_{34}$. Below the critical micelle concentration AuNP showed diameters of around $d = 8$ nm. Moreover, longer units of 4VP ($DP = 34$) demanded an unfavorable formation of agglomerates, if the polymer concentration was too low.

The stabilization of AuNP with monodentate ligands showed a size formation of AuNP with a proportional size for all molar ratios of 4VP/ $H AuCl_4$. In the case of multidentate ligands a decrease in size of AuNP by variation of the 4VP/ $H AuCl_4$ ratio was clearly observed. Figure 4.42 and Table 4.13 compiles the size formation of AuNP with different 4VP moieties and different molar ratios of 4VP/ $H AuCl_4$.

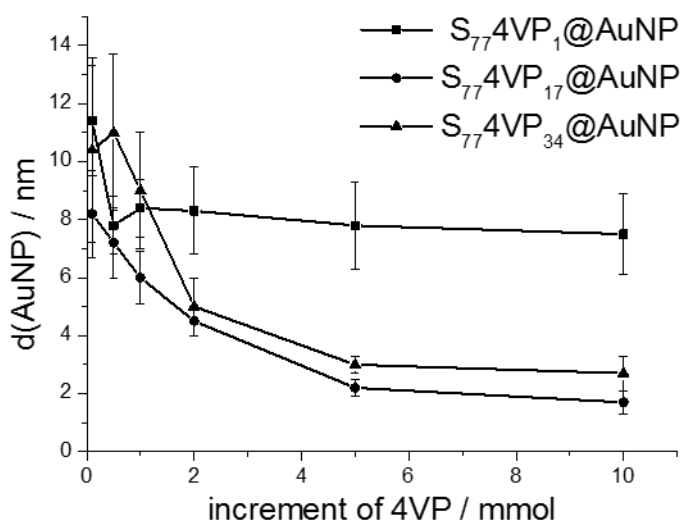


Figure 4.42: Distinctive AuNP diameter sizes. Influence of volume fraction of 4VP ϕ_{4VP} and variation of 4VP/HAuCl₄ ratio over AuNP size with S₇₇4VP₁, S₇₇4VP₁₇, and S₇₇4VP₃₄.

Table 4.13: Distinctive AuNP diameter sizes of S₇₇4VP₁@AuNP, S₇₇4VP₁₇@AuNP, and S₇₇4VP₃₄@AuNP with variation of 4VP/HAuCl₄ ratio.

4VP/HAuCl ₄	S ₇₇ 4VP ₁ @AuNP d(AuNP) [nm]	S ₇₇ 4VP ₁₇ @AuNP d(AuNP) [nm]	S ₇₇ 4VP ₃₄ @AuNP d(AuNP) [nm]
0.1	11.0 ± 1.6	7.0 ± 1.6	9.7 ± 2.4
0.5	7.7 ± 0.8	8.0 ± 1.0	10.2 ± 1.5
1.0	8.4 ± 1.0	6.0 ± 0.9	8.6 ± 2.4
2.0	8.1 ± 1.7	4.7 ± 0.5	4.7 ± 1.0
5.0	7.7 ± 1.6	2.2 ± 0.3	3.0 ± 0.3
10.0	7.5 ± 1.4	1.7 ± 0.3	2.7 ± 0.3

4.5.5 Conclusion

In this section the stabilization and particle size distribution of AuNP in solution generated *in situ* by using S4VPs III-V as monodentate and multidentate ligands was investigated. It was shown, that the particle size distribution as well as the particle diameter

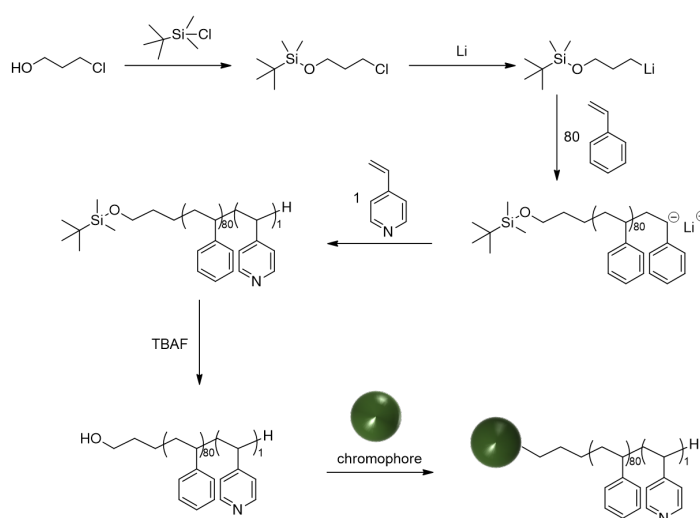
is crucially influenced by the length of the 4VP moiety, the polymer concentration, and the reducing agent. While the size distribution of $S_{77}4VP_1@AuNP$ is almost constant ($d = 8$ nm) over all molar ratios, either ordered $S_4VP/AuNP$ nanocomposites were formed at low polymer concentrations, while single distributed AuNP were formed at sufficient high amounts of 4VP compared to $HAuCl_4$.

Multidentate ligands of $S_{77}4VP_{17}@AuNP$ and $S_{77}4VP_{34}@AuNP$ showed a distinctive different formation mechanism. Increasing the 4VP/ $HAuCl_4$ ratio resulted in the formation of micelles at high polymer concentrations and small AuNP ($d = 2.5$ nm) with no signs of SPR activity. Low polymer concentrations showed the formation of narrowly distributed AuNP with diameters of around $d = 8$ nm with SPR activity. It was demonstrated that carefully chosen block copolymers can lead to narrowly distributed AuNP by *in situ* formation. The size control by synthetic protocols may have impact on the fields of optoelectronics and catalysis where small AuNP with controllable size and high surface area are required.

4.6 Synthesis, Characterization, and Application of α -Hydroxypolystyrene-*b*-poly-4(vinylpyridine) (α -HO-S4VP)

This section comprises the synthesis and characterization of a S4VP block copolymer with a hydroxyl group in α position of the polystyrene chain, which acts as telechelic polymer. While keeping the functionality of the 4VP block to coordinate metal nanoparticles, introducing the hydroxylic function will give access to the introduction of different end-groups. One possible path to achieve that, would be by using click-chemistry with carboxylic acids, azides, and epoxides. The aim of this project was to attach a chromophore to the α -hydroxyl group, followed by a functionalization of gold nanoparticles within the 4VP domains and investigate the interaction of both functionalities. Coumarin-3-carboxylic acid was chosen as the chromophore because of the easy accessibility and the low price.

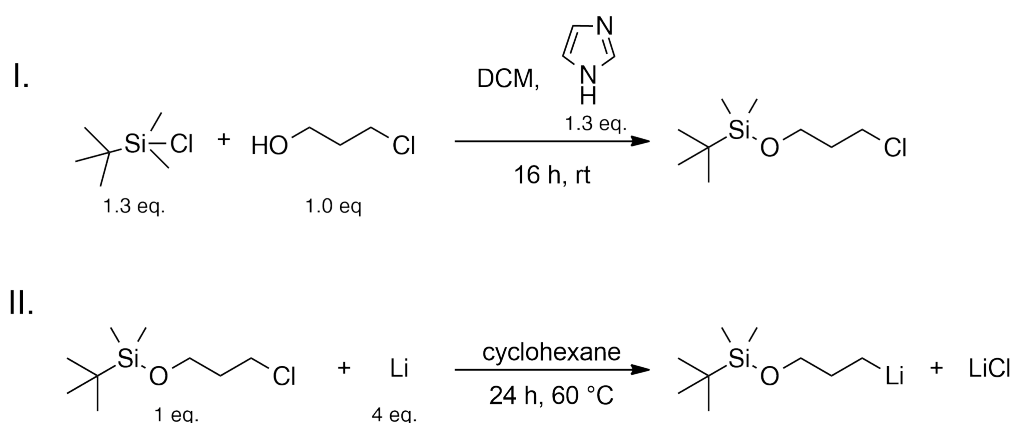
As initiator for the polymerization, the organolithium compound 3-*tert*-butyldimethylsilyloxy-1-propyllithium (*t*BDMSOPrLi) was selected. It has already been widely used to prepare functionalized polymers. This protected anionic polymerization initiator enables a facile synthesis of nearly monodisperse α -functionalized telechelic polystyrenes in nonpolar as well as in polar media^[52,53,57]. The planned synthetic route is presented in Scheme 11.



SCHEME: 11 Synthetic plan of a chromophore-functionalized α -OH-S4VP.

4.6.1 Synthesis of 3-*tert*-butyldimethylsilyloxy-1-propyllithium (*t*BDMSOPrLi)

The synthesis of the protected anionic polymerization initiator involves two reaction steps. First, the oxy-alkyl chloride is protected with a silyl-group (3-*tert*-butyldimethylsilyloxy-1-propylchloride), followed by a lithiation (Scheme 12).



SCHEME: 12 Synthesis of *t*BDMSOPrLi.

The synthesis of *t*BDMSOPrLi is a labile reaction due to the sensitivity of the organolithium compound to air, moisture and water, and its fast decomposition. During this procedure it was very important to keep the reaction conditions, as well as the reactants clean and constantly in an argon atmosphere. Another pitfall in the lithiation process was the sensitivity of the reaction to the condition of the lithium surface and the reaction temperatures. Different Lithium metals from different sources and in different appearances were tested. The best results were obtained using granular Lithium with 4-10 mesh particle size and 0.5% sodium. To ensure a reliable lithiation, prior to the reaction the lithium grains were vigorously stirred with the least possible amount of dry cyclohexane over night at room temperature to activate the metal surface by mechanical abrasion. Afterwards an additional amount of cyclohexane was added and the reaction was allowed to stir at 40 °C. Finally, the reaction was warmed up to 60 °C and the reactant was slowly added drop wise into the reaction. The lithiation was followed by GC analysis. During the reaction process aliquots were withdrawn and quenched with water to analyze the reactants and hydrolyzed products. Figure 4.43 shows a GC

chromatogram of the first aliquot and the corresponding GC chromatograms within 24 h.

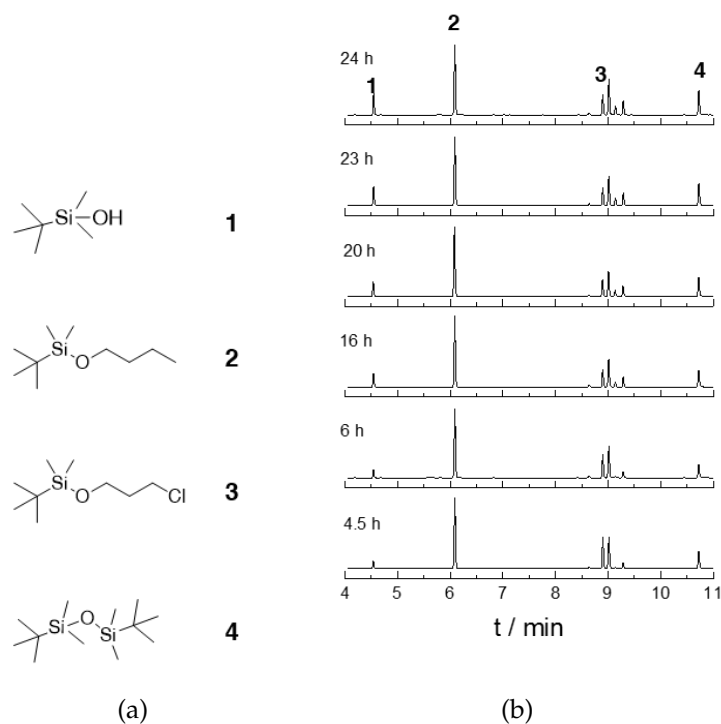


Figure 4.43: (a) Hydrolyzed products of *t*BDMSOPrLi after quenching with water, (b) GC chromatograms of the lithiation within 24 h.

To determine the amount of *t*BDMSOPrLi in the reaction mixture, a calibration curve of its hydrolyzed product 3-*tert*-butyldimethylsilyloxy-1-propane (*t*BDMSOPr) was carried out. Figure 4.44 shows the calibration curve of *t*BDMSOPr and the corresponding GC chromatogram with retention time of *t*BDMSOPr at 6.1 min.

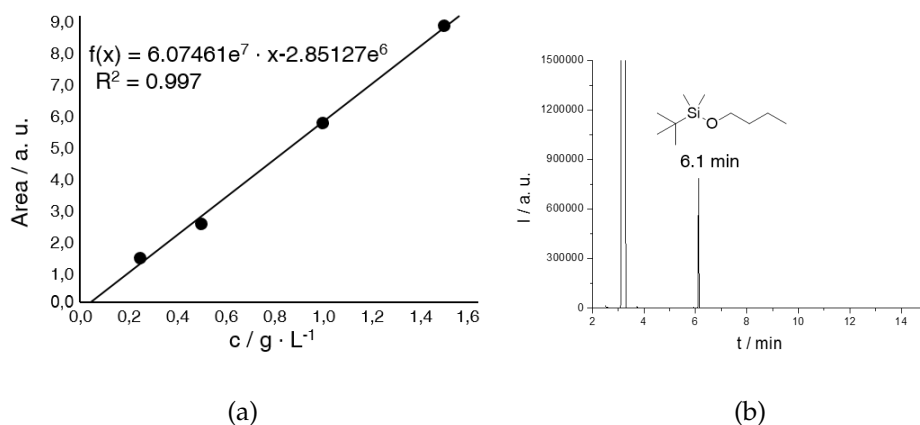


Figure 4.44: (a) Calibration curve of *t*BDMSOPr, (b) GC chromatogram of *t*BDMSOPr.

Table 4.14 shows the ratio of the area of the reactant **1** and the hydrolyzed product **2** of the lithiation in dependence of the reaction time.

Table 4.14: GC-Data of reactant and hydrolyzed products of the lithiation.

Time / h	1	2	3	4
4.5	5.7 %	56 %	24 %	15 %
6	7 %	60 %	19 %	14 %
16	10 %	58 %	14 %	16 %
20	11 %	56 %	14 %	17 %
21	13 %	54 %	13 %	19 %
22	12 %	53 %	13 %	20 %
23	13 %	53 %	13 %	18 %
24	14 %	51 %	14 %	19 %

After 6 h, the reaction yielded 60% of the product. However, the lithiation showed side products, that were not possible to prevent during the reaction process. In addition, a 100 % conversion of the educt was not possible due to the increased formation of side products and consequently a decrease of the product. Although the isolated product was filtered through a celite pad after the reaction, the side products remained in the solution, which affected the activity of the initiator for the further living anionic polymerization. The reaction was repeated several times with different time intervals between 20 and 36 hours to determine the bulk of impurities. After testing the initiator

for the living anionic polymerization of S4VP it was established, that the initiator with 20 % of remaining *t*BDMSOPrCl and side products possessed enough activity to initiate the polymerization of styrene. After 24 hours the reaction showed a conversion of 14 % with 51 % yield of the product. For this reason it was decided to terminate the reaction after 24 hours, to avoid the further increase of side products and further loss of product. Figures 4.45 and 4.46 show the H-NMR spectrum and GC chromatogram of *t*BDMSOPrCl.

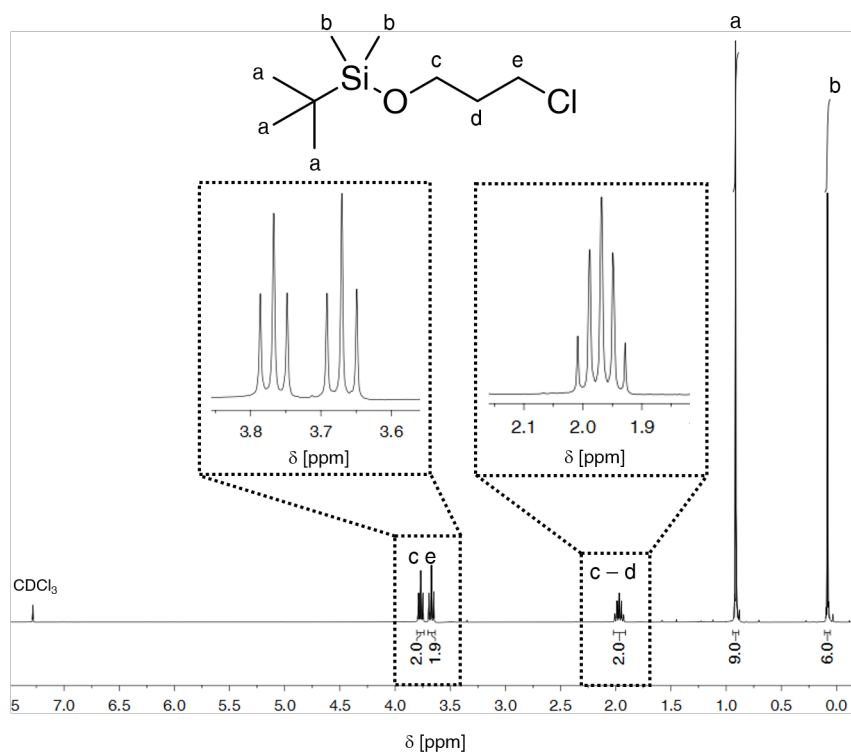


Figure 4.45: H-NMR spectrum of *t*BDMSOPrCl.

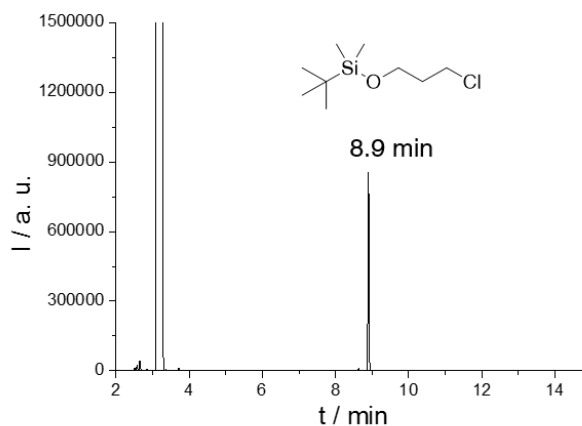


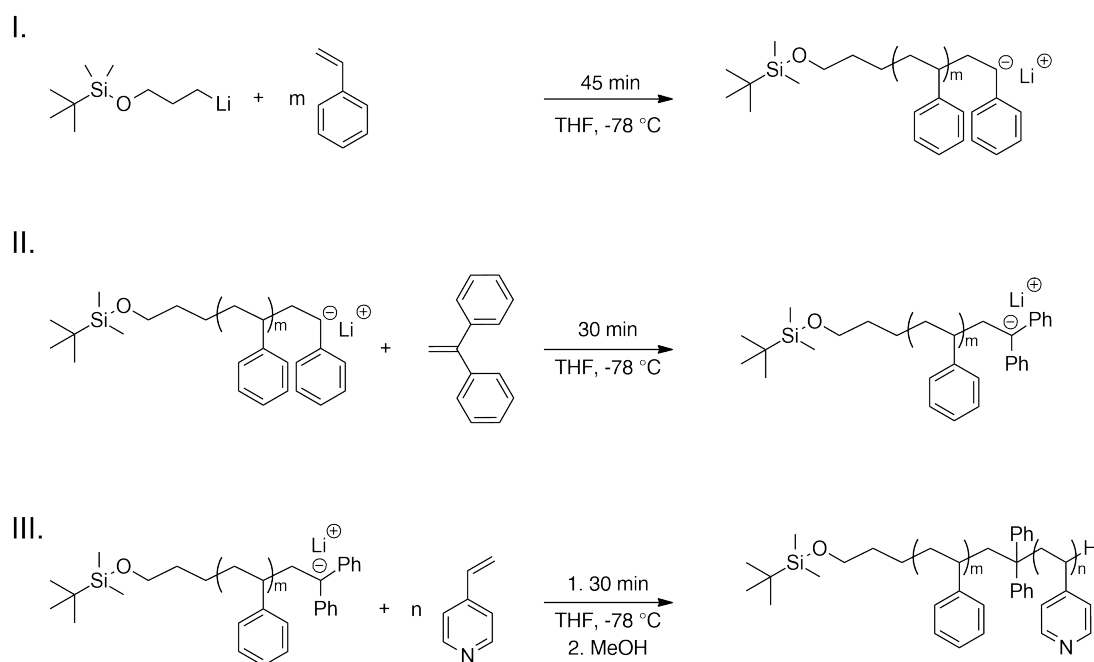
Figure 4.46: GC chromatogram of tBDMSOPrCl.

To determine the final concentration of the initiator two methods were utilized. The first method used was the titration of the initiator with a 0.1 N HCl solution. This method led to an initiator concentration of $c = 0.7$ M. However, performing the polymerization using this concentration in the calculation of the reaction stoichiometry, it showed an uncontrolled molecular weight of the polymer. For this reason it was decided to perform a calibration curve of tBDMSOPr and determine the initiator concentration by GC analysis. This method showed a concentration of $c = 0.07$ M, which is 10 times lower than that from the first method. Yet this concentration showed a better control of the anionic polymerization. In both cases the disadvantage to determine an exact concentration of the initiator was due to the presence of side products, that distorted the calculation process. In the next section the use of both concentrations for the anionic polymerization will be shown and explained in detail.

4.6.2 Synthesis and Characterization of α -Hydroxypolystyrene-*b*-poly-4-vinylpyridine (α -HO-S4VP) Block Copolymer *via* Living Anionic Polymerization

The living anionic polymerization of α -OH-S4VP was performed using standard Schlenk techniques. The reaction was carried out in THF at -78 °C. The desired molecular weight was around $8500 \text{ g} \cdot \text{mol}^{-1}$ with 80 repeat units of styrene and one unit of 4 VP. Three different α -OH-S4VP with different molecular weights were synthesized. Scheme 13 shows

the reaction scheme of *t*BDMSOPr-S4VP. The first two polymers were synthesized using a concentration of the initiator of $c(I) = 0.7$ M obtained by titration. The third polymer was synthesized by using a concentration of the initiator of $c(I) = 0.07$ M, determined by GC analysis. All anionic polymerization reactions were performed with a freshly synthesized initiator due to its high sensitivity and fast decomposition. As described in section 4.1, a sample of the living polystyryl-anion (*t*BDMSOPr-PS-precursor) was withdrawn for GPC and NMR analysis. The molar mass distribution of the *t*BDMSOPr-PS-precursor and the *t*BDMSOPr-S4VP was analyzed by GPC analysis, while the molar mass of the polymers were calculated by NMR spectroscopy.



SCHEME: 13 Synthesis of *t*BDMSOPr-S4VP.

Even by repeating the synthesis several times we experienced unsuccessful anionic polymerization reactions, which led to a bimodal distribution of the block copolymer, as seen in Figure 4.47a, b. The fast decomposition and lack of activity of the initiator was clearly observed by exposure of time. To achieve a successful anionic polymerization the initiator was freshly synthesized and immediately used.

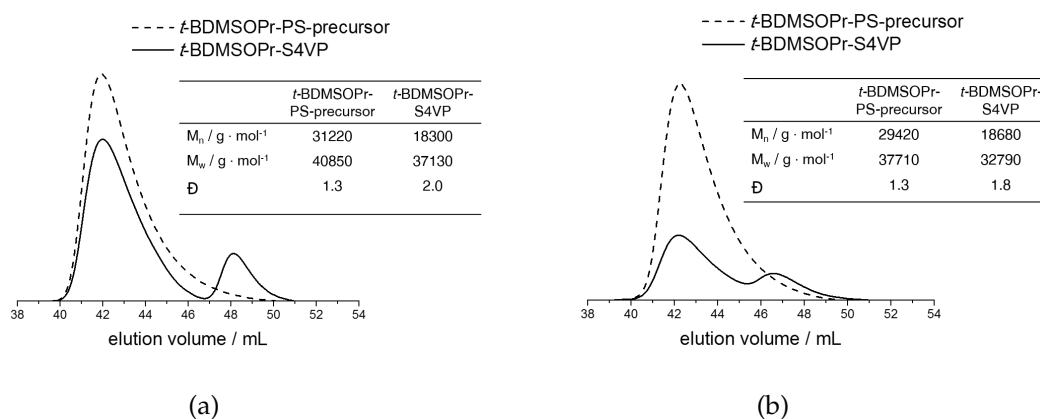


Figure 4.47: Elution volume of two unsuccessful syntheses of *t*BDMSOPr-S4VP in DMF-LiBr, calibrated with PMMA standards.

Synthesis of *t*BDMSOPr-S₁₈₅4VP₃ and *t*BDMSOPr-S₃₆₀4VP₇

The polymers *t*BDMSOPr-S₁₈₅4VP₃ and *t*BDMSOPr-S₃₆₀4VP₇ were successfully synthesized by using a concentration of the initiator of $c(\text{I}) = 0.7 \text{ M}$, which should have led to 80 repeating units of styrene. However, the reactions led to higher molecular weights than expected. Figure 4.48 shows the GPC chromatogram of *t*BDMSOPr-S₁₈₅4VP₃. The elution volume showed a monomodal distribution of the polymer. Since the internal standard of the GPC instrument deviated from the analyzed polymer, it was not possible to determine the exact molecular weight of the polymer by means of GPC analysis. For this reason the molecular weight of the polymer was calculated using NMR spectroscopy by calculating the ratio of the methyl groups of the silyl group to the protons of the aromatic group of polystyrene and the protons of 4VP, respectively. Figure 4.49 shows the NMR spectra of the synthesized *t*BDMSOPr-S₁₈₅4VP₃. The Polystyrene block was calculated with 185 units and the 4VP block with 3 units. The molecular weight deriving of the NMR spectrum was $17.500 \text{ g} \cdot \text{mol}^{-1}$.

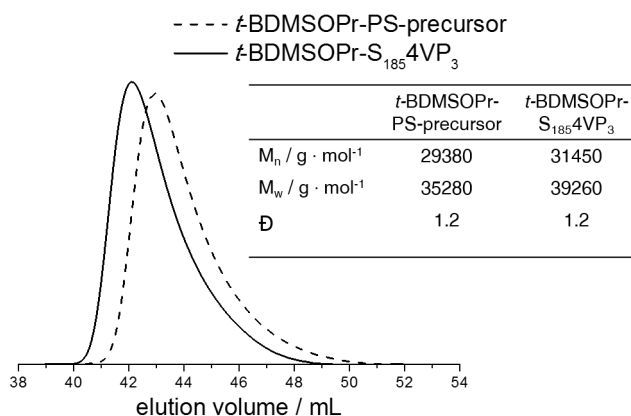


Figure 4.48: Elution volume of *t*BDMSOPr-PS precursor and *t*BDMSOPr-S₁₈₅4VP₃ in DMF-LiBr, calibrated with PMMA-standards.

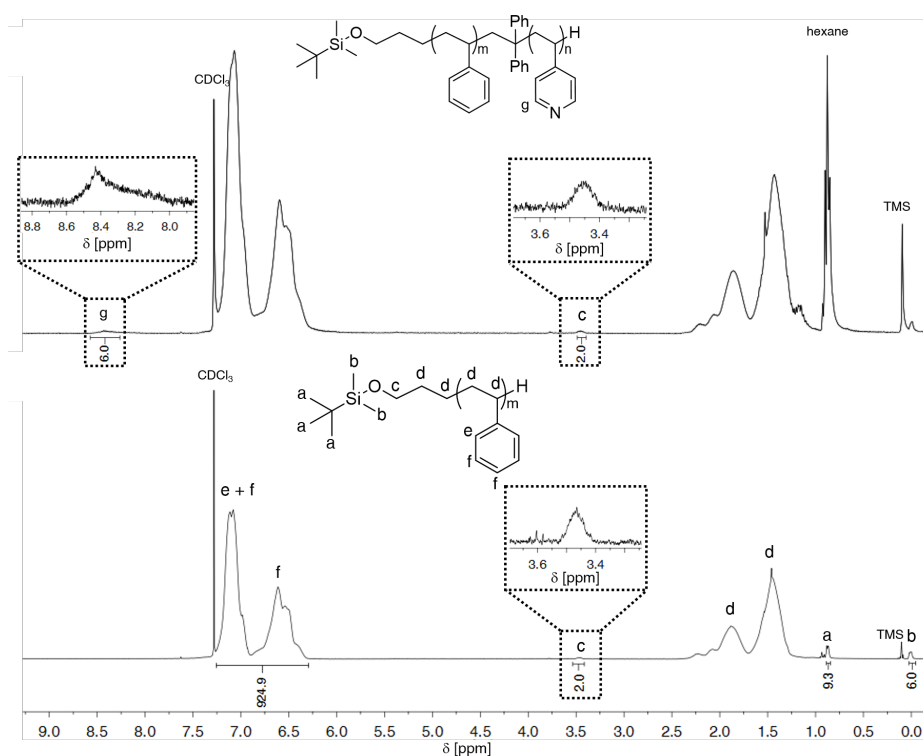


Figure 4.49: H-NMR spectra of *t*BDMSOPr-PS precursor and *t*BDMSOPr-S₁₈₅4VP₃ in CDCl₃.

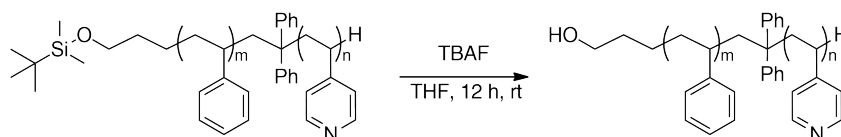
Figure 4.50 and Figure 4.51 show the GPC chromatogram and NMR spectra of *t*BDMSOPr-S₃₆₀4VP₇. The GPC chromatogram showed a monomodal distribution of the polymer, though with a two times higher molecular weight than *t*BDMSOPr-S₁₈₅4VP₃. From the NMR analysis the polymer was calculated with 360 units of styrene and 7 units of 4VP

From these results it was established that the titration method did not lead to reliable initiator concentrations.

Despite the high molecular weight the polymer $t\text{BDMSOPr-S}_{185}\text{4VP}_3$ was tested for further experiments to functionalize the hydroxyl group in α position.

Functionalization of the hydroxyl group of $\alpha\text{-OH-S}_{185}\text{4VP}_3$

Prior to any functionalization the polymer was treated with TBAF to cleave the silyl ether group protecting the hydroxyl functionality to get $\alpha\text{-OH-S}_{185}\text{4VP}_3$ ^[151]. The reaction was performed under mild conditions and is shown in scheme 14.



SCHEME: 14 Deprotection of the hydroxyl group of $t\text{BDMSOPr-S}_{185}\text{4VP}_3$ with TBAF under mild conditions.

The resulting $t\text{BDMSOPr-S}_{185}\text{4VP}_3$ was purified by dialysis and analyzed by NMR spectroscopy. The absence of the protons of the CH_3 groups of the silyl group at 0.01 ppm after treatment with TBAF indicated a complete deprotection to $\alpha\text{-OH-S}_{185}\text{4VP}_3$. Figure 4.52 shows the NMR spectrum of $\alpha\text{-OH-S}_{185}\text{4VP}_3$.

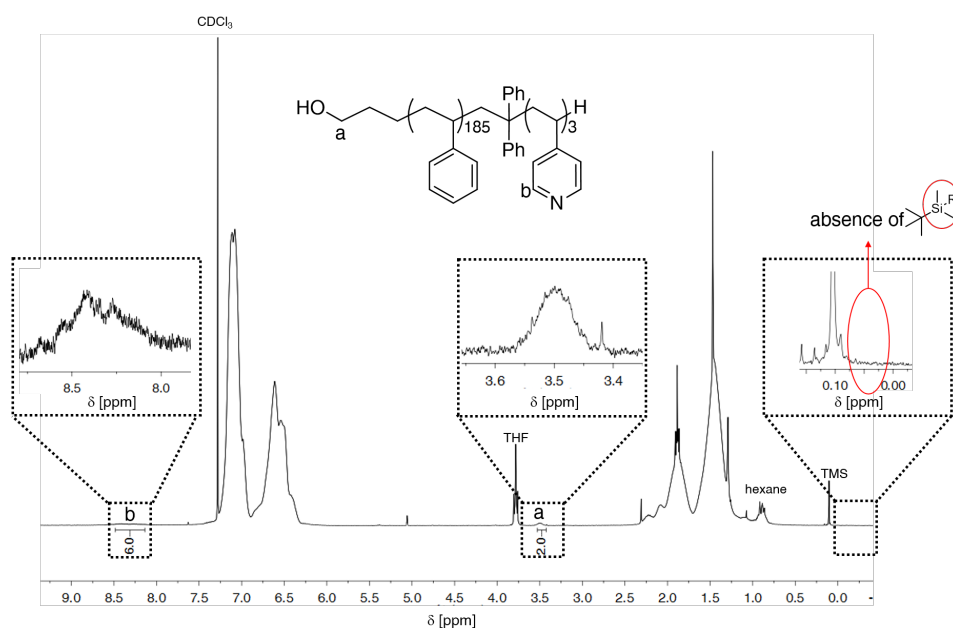
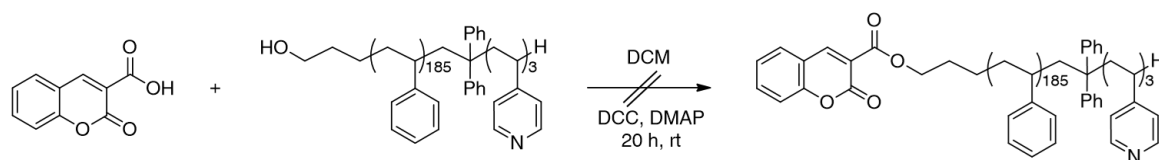


Figure 4.52: H-NMR spectrum of α -OH-S₁₈₅4VP₃ in CDCl₃ after treatment *t*BDMSOPr-S₁₈₅4VP₃ with TBAF and dialysis.

The next section comprehends the different experiments with α -OH-S₁₈₅4VP₃ and chromophores.

Steglich esterification of coumarin-carboxylic acid with α -OH-S₁₈₅4VP₃

Coumarin-carboxylic acid was chosen as a chromophore to be attached to the hydroxyl group in α position. A Steglich esterification between the carboxylic acid and the hydroxyl group was performed. Scheme 15 shows the reaction of the esterification^[152].

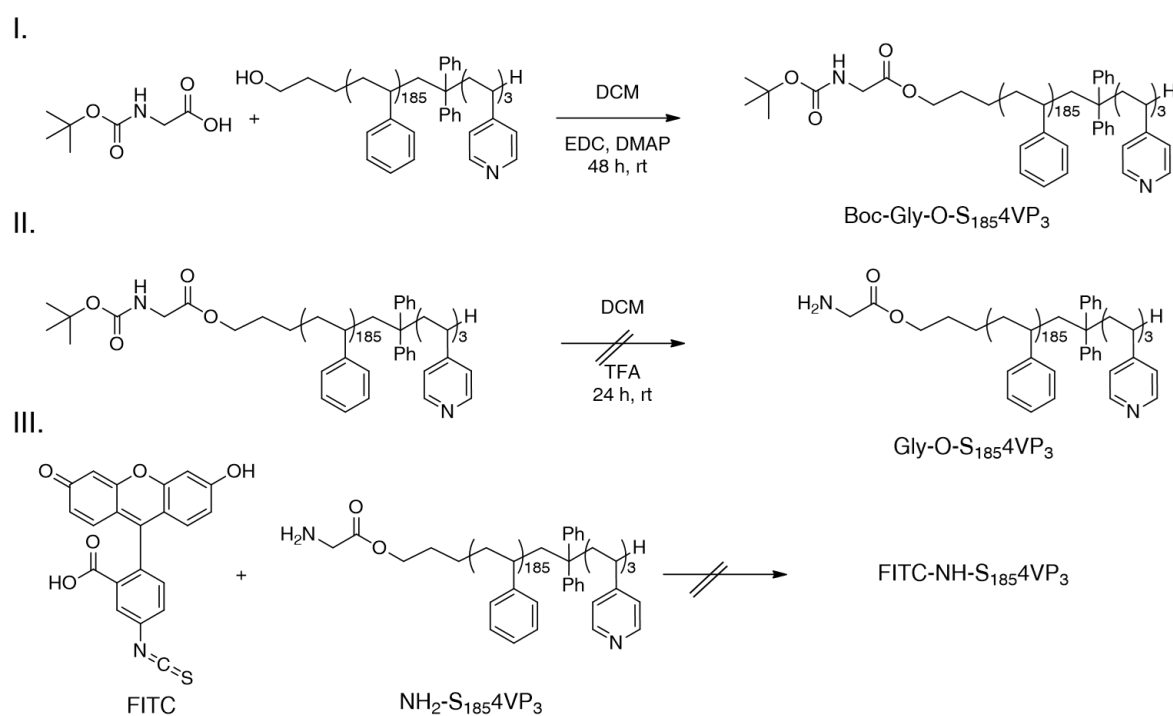


SCHEME: 15 Steglich esterification of coumarin hydroxylic acid with α -OH-S₁₈₅4VP₃.

This reaction did not show the formation of an ester product and was not further characterized.

Click-reactions between fluorescein isothiocyanate (FITC) and α -OH-S₁₈₅4VP₃

The commercially available fluorophore fluorescein isothiocyanate (FITC) was used for testing click reactions with α -OH-S₁₈₅4VP₃. Since it is hard to react a isothiocyanate group with the hydroxyl group of the polymer it was necessary to convert the hydroxyl group into an amine group to obtain a thio-urea-functionalized polymer. Scheme 16 shows the reactions steps for the synthesis of FITC-O-S₁₈₅4VP₃. In the first step the hydroxyl group was converted into an urethane via a Steglich esterification with the amino acid *tert*-butoxycarbonyl Glycine (Boc-Glycine) to get a urethane functional polymer. In step two the Boc group was unmasked by treating the polymer with TFA. The reaction of FITC and the primary amine of the polymer should lead to the thiourethane-functionalized polymer FITC-NH-S₁₈₅4VP₃.



SCHEME: 16 Synthesis of α -OH-S₁₈₅4VP₃ with FITC.

The Steglich esterification was characterized by means of IR spectroscopy. Figure 4.53 shows a strong band of the CO-ester group at a wave number 1714 cm⁻¹ and a strong band of the NCO group at a wave number 2130 cm⁻¹. These two bands prove a success-

ful esterification between α -OH-S₁₈₅4VP₃ and Boc-Glycine to get a protected butoxycarbonyl urethane-functional block copolymer (Boc-Gly-S₁₈₅4VP₃). However after deprotection of the Boc group with TFA, the IR-Spectrum of Gly-S₁₈₅4VP₃ did not show a strong Band of the CO-ester group (blue IR-spectrum). This might be caused by using TFA as deprotection agent, since TFA is able to protonate the pyridyl group of the block copolymer or to hydrolyze the ester.

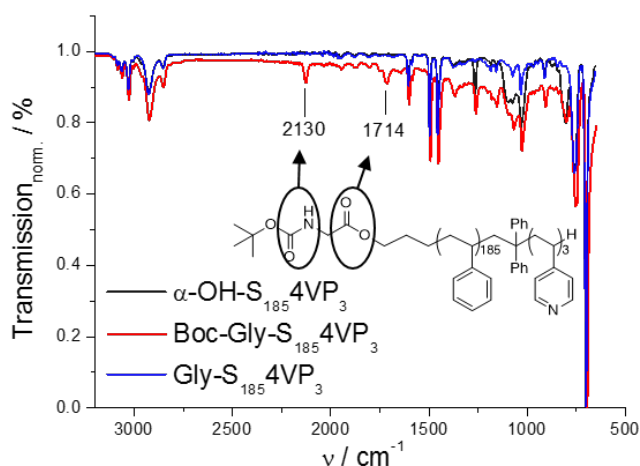


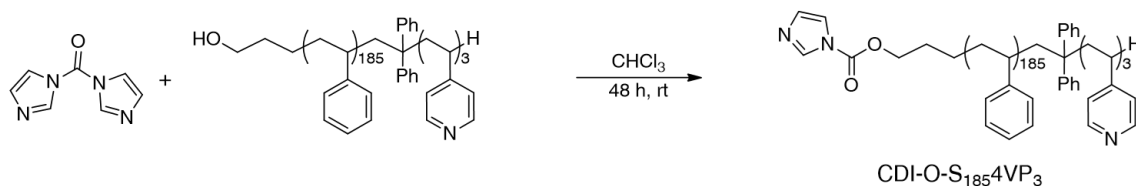
Figure 4.53: IR spectrum of Boc-Gly-S₁₈₅4VP₃ in comparison to α -OH-S₁₈₅4VP₃ and Gly-S₁₈₅4VP₃.

Using this route it was not possible to obtain a fluorophore-functionalized S4VP block copolymer. An alternative to convert the hydroxyl group into an amine group without using an acidic agent could be achieved by using CDI (Carbonyldiimidazole) as activating agent for the hydroxyl group *via* an esterification. Afterwards an amine, such as ethylene diamine (EDA) could be used to synthesize an urethane-functionalized S4VP block copolymer.

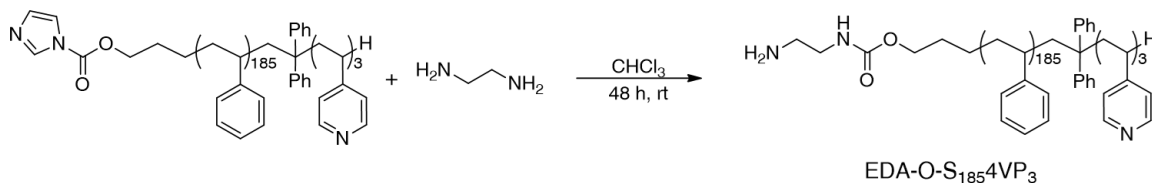
Activation of the α -OH-S₁₈₅4VP₃ with CDI

The first step of this reaction implies an esterification of α -OH-S₁₈₅4VP₃ with CDI (Scheme 17). The reaction mixture was allowed to stir at room temperature for 48 h.

I.



II.



SCHEME: 17 Esterification of α -OH-S₁₈₅4VP₃ with CDI, followed by an amination with EDA.

This reaction was characterized by means of NMR spectroscopy and IR spectroscopy. Figure 4.54 shows the NMR spectrum with a shift of the protons of the CH₂ group from 3.5 ppm to 4.2 ppm after after esterification. This is characteristic for a CH₂ group next to a carbonyl group. The IR spectrum in Figure 4.55 showed the typical ester band at a wave number of 1743 cm⁻¹.

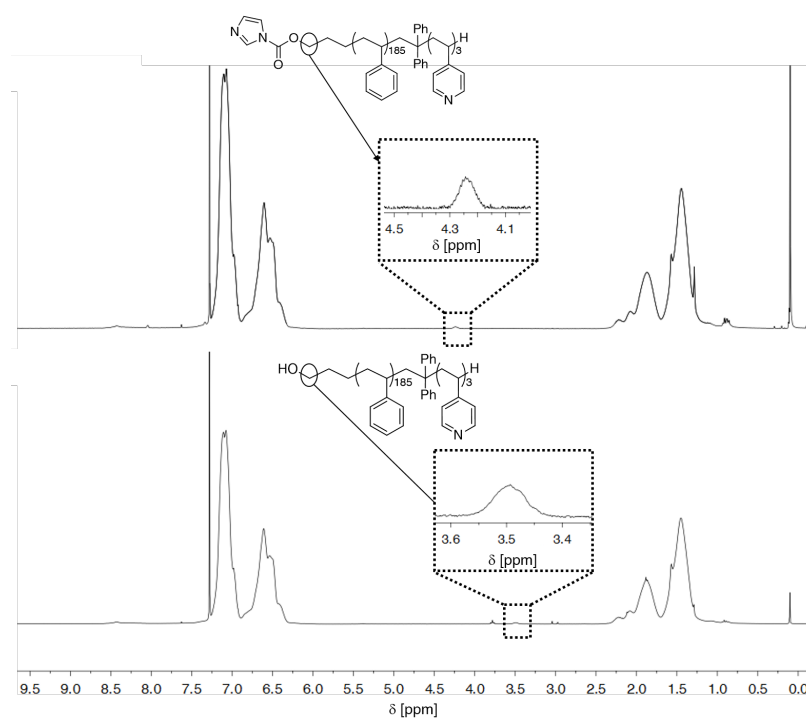


Figure 4.54: H-NMR spectrum of CDI-O-S₁₈₅4VP₃ in CDCl₃ in comparison to α-OH-S₁₈₅4VP₃.

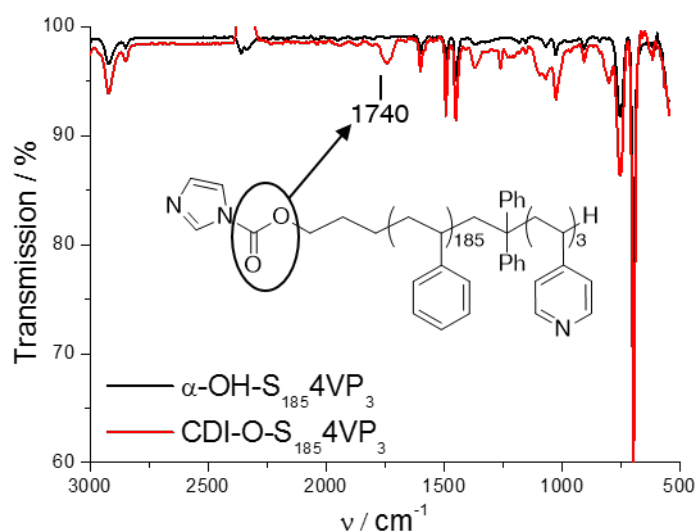


Figure 4.55: IR spectrum of CDI-O-S₁₈₅4VP₃ in comparison to α-OH-S₁₈₅4VP₃.

In the second step ethylene diamine (EDA) was used to performed a modification of the ester group. EDA was added to a solution of the previously synthesized polymer

and stirred at room temperature for 48 h. Figures 4.56 and 4.57 show the NMR- and IR spectra of the obtained product.

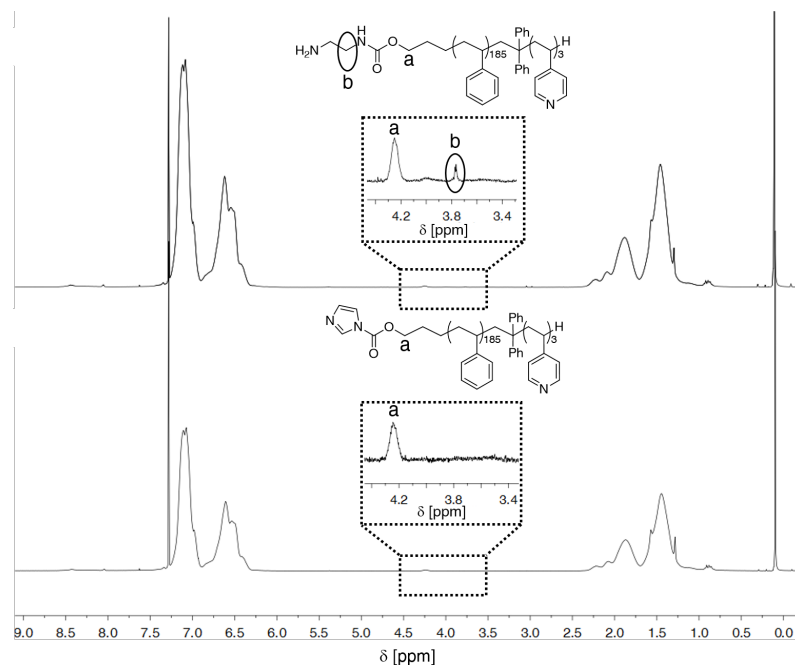


Figure 4.56: H-NMR spectrum of EDA-O-S₁₈₅4VP₃ in CDCl₃ in comparison to CDI-O-S₁₈₅4VP₃.

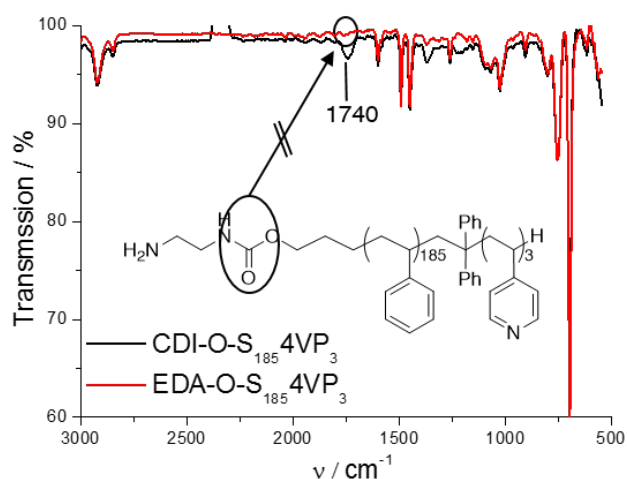


Figure 4.57: IR spectrum of EDA-O-S₁₈₅4VP₃ in comparison to CDI-O-S₁₈₅4VP₃.

The NMR spectrum did not show a shift of the CH₂ group next to the carbonyl group. In the IR spectrum no band of the carbonyl function could be observed. This might be due

to the strong absorbance of the amine group attached to the polymer. Since the polymer has a high molecular weight, it was not possible to perform an end group analysis by means of NMR. Another attempt to react the polymer with FITC, but no conversion to FITC-NH-S₁₈₅4VP₃ could be observed.

Synthesis of α -OH-S₈₅4VP₂

A third functional block copolymer α -OH-S₈₅4VP₂ was synthesized *via* anionic polymerization by using a calculated concentration of the initiator of $c(I) = 0.07$ M determined by GC analysis.

In contrast to the previous reactions, a polymer with 85 units of the polystyrene block and 2 units of the 4VP block with an overall molecular weight of $8600 \text{ g} \cdot \text{mol}^{-1}$ was successfully synthesized. Figure 4.58 and Figure 4.59 show the NMR spectra and GPC chromatograms of *t*BDSMOPr-PS-precursor, *t*BDSMOPr-S₈₅4VP₂, and α -OH-S₈₅4VP₂.

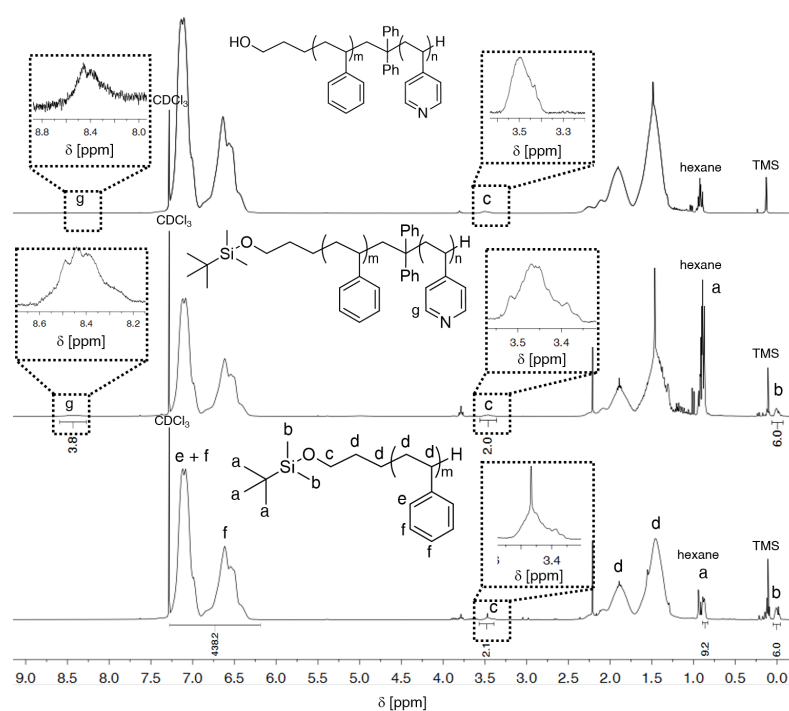


Figure 4.58: H-NMR spectra of *t*BDSMOPr-PS precursor, *t*BDSMOPr-S₈₅4VP₂, and α -OH-S₈₅4VP₂ in CDCl₃.

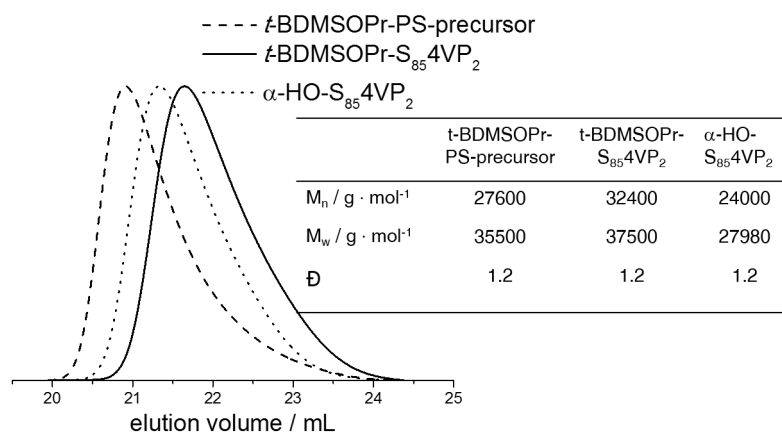
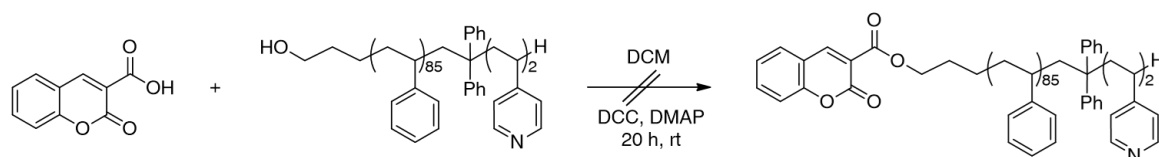


Figure 4.59: Elution volume of *t*BDMSOPr-PS precursor and *t*BDMSOPr-S₈₅4VP₂ in DMF-LiBr, calibrated with PMMA standards.

The α-OH-S₈₅4VP₂ polymer was used for further click reactions with chromophores.

4.6.3 Click Reactions of α-OH-S₈₅4VP₂ with Coumarin

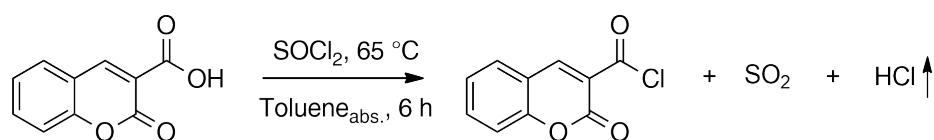
For a further functionalization of the hydroxyl group of the functional block copolymer α-OH-S₈₅4VP₂ the chromophore Coumarin-3-carboxylic acid was chosen. For this synthesis a Steglich esterification was performed. Scheme 18 shows the reaction scheme of the Steglich esterification.



SCHEME: 18 Steglich esterification of coumarin hydroxylic acid with α-OH-S₈₅4VP₂.

This reaction did not show the formation of an ester product and was not further characterized.

An alternative route towards the esterification with coumarin-3-carboxylic acid was a preceding conversion of the carboxylic acid into an acid chloride. The synthesis of coumarin-3-carboxylic chloride was performed by refluxing the carboxylic acid in thionyl dichloride in the presence of dried toluene as shown in Scheme 19.



SCHEME: 19 Synthesis of coumarin-3 carboxylic chloride.

The product was purified by recrystallization in toluene and characterized by means of IR-spectroscopy (Figure 4.60), which shows the extinction of the characteristic vibration frequency of the aryl-COOH group at a wave number around 3000 cm^{-1} .

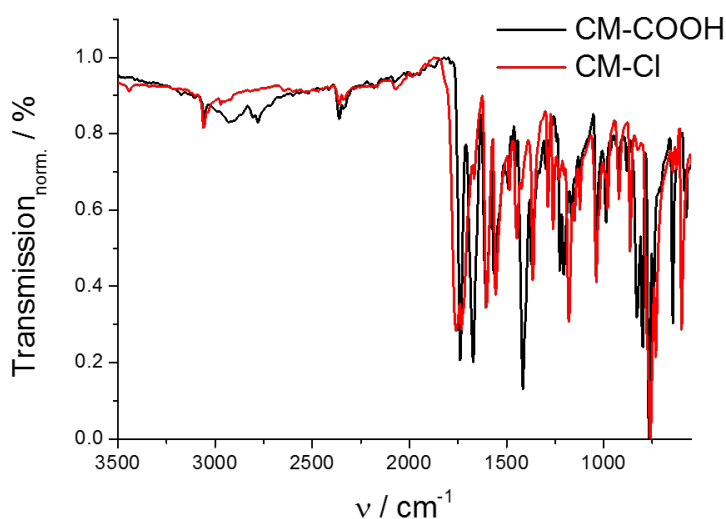


Figure 4.60: IR spectrum of coumarin-3-carboxylic chloride (CM-Cl) in comparison to coumarin-3-carboxylic (CM-COOH).

Afterwards an esterification of α -OH-S₈₅4VP₂ with coumarin-3-carboxylic chloride was carried out in dried DCM for 24 h at room temperature (Scheme 20).



SCHEME: 20 Synthesis of CM-O-S₈₅4VP₂.

The IR spectrum shown in Figure 4.61 shows the characteristic vibration frequency of the ester band at a wave number of 1735 cm^{-1} , which indicated the formation of the ester CM-O-S₈₅4VP₂.

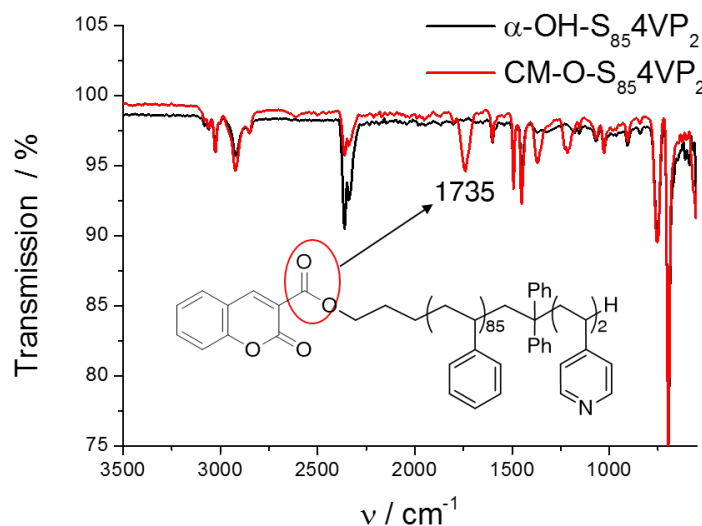


Figure 4.61: IR spectrum of CM-O-S₈₅4VP₂ ester in comparison to $\alpha\text{-OH-S}_{85}\text{4VP}_2$.

Further characterization of the successful click-reaction was done via GPC coupled with a diode array detector. The ester was screened with a wavelength range between 260 nm and 400 nm to observe the absorption of the coumarin. Figure 4.62a shows a 3D chromatogram of the CM-O-S₈₅4VP₂ ester. By plotting the intensity against the elution volume in dependence of the UV signal it was possible to detect the coupling of the coumarin group with the functional polymer. In contrast, the $\alpha\text{-OH-S}_{85}\text{4VP}_2$ polymer did not show any UV signal (Figure 4.62b).

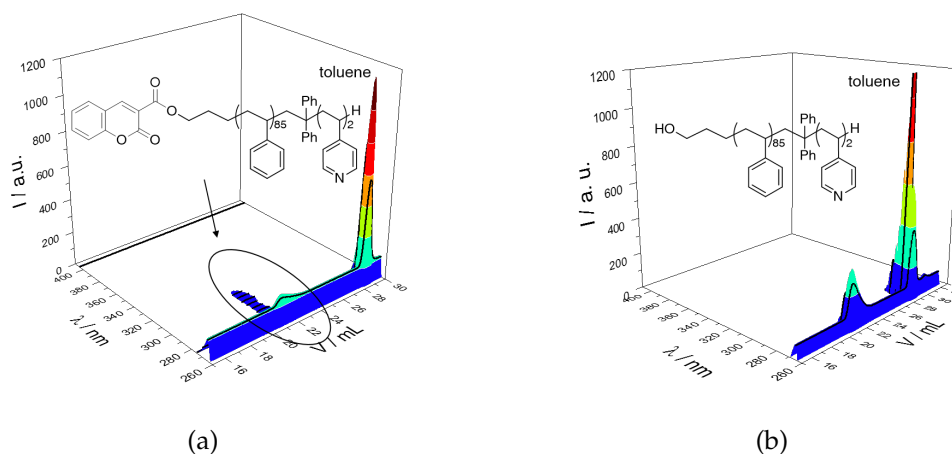


Figure 4.62: (a) GPC-DAD 3D chromatogram of the CM-O-S₈₅4VP₂ ester with (b) α -OH-S₈₅4VP₂ as reference in DMF-LiBr screened in a range between 260 nm and 400 nm.

According to the GPC-DAD results, which showed absorption of the coumarin group at around 310 nm, the ester was also characterized by means of Fluorescence spectroscopy. By excitation at $\lambda_{ex} = 310$ nm, the ester emitted fluorescence at $\lambda_{em} = 419$ nm. In contrast the α -OH-S₈₅4VP₂ did not show any fluorescence by excitation at 310 nm. Instead α -OH-S₈₅4VP₂ showed an emission at $\lambda_{em} = 282$ nm due to the aromatic rings of polystyrene, which absorb at a wavelength around 240 nm. Figure 4.63 shows the fluorescence spectra of CM-O-S₈₅4VP₂ ester in comparison to α -OH-S₈₅4VP₂.

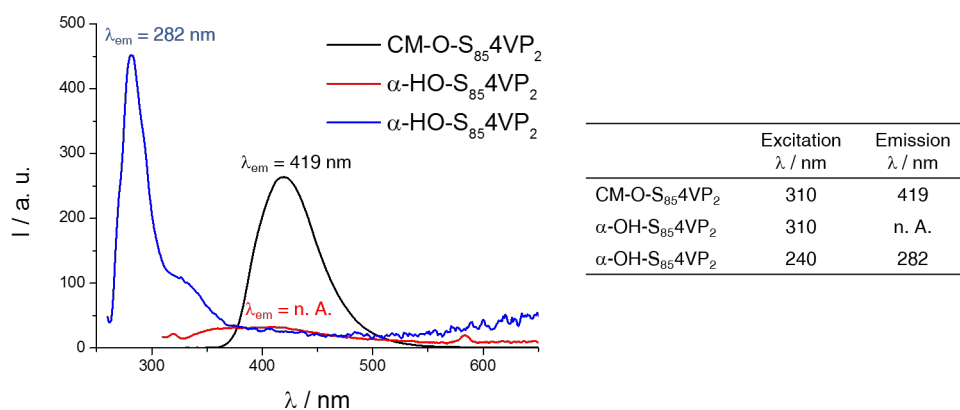


Figure 4.63: Fluorescence spectra of CM-O-S₈₅4VP₂ ester in comparison to α -OH-S₈₅4VP₂ in CHCl₃.

To conclude this section the click reaction between α -OH-S₈₅4VP₂ and coumarin-3-carboxylic chloride was successful under mild reaction conditions. The synthesized functional block copolymer CM-O-S₈₅4VP₂ was used for a further functionalization with gold- and silver nanoparticles respectively.

4.7 Ligand Exchange Reactions of Citrate@AuNP with CM-O-S₈₅4VP₂

A ligand exchange reaction of Citrate@AuNP with CM-O-S₈₅4VP₂ was performed following the procedure described in section 4.4. The ligand exchange was performed with an equal molar ratio of both reactants (1:1). Figure 4.64 shows the UV/Vis spectra before and after ligand exchange. After ligand exchange the UV/Vis spectrum showed an absorption band at $\lambda = 330$ nm, which belongs to the absorption of coumarin and a shift of the SPR of AuNP from $\lambda = 520$ nm to $\lambda = 533$ nm. From the UV/Vis spectrum it is possible to observe, that the SPR of AuNP is influenced by the absorption of the coumarin end-group, as the SPR of AuNP is diminished.

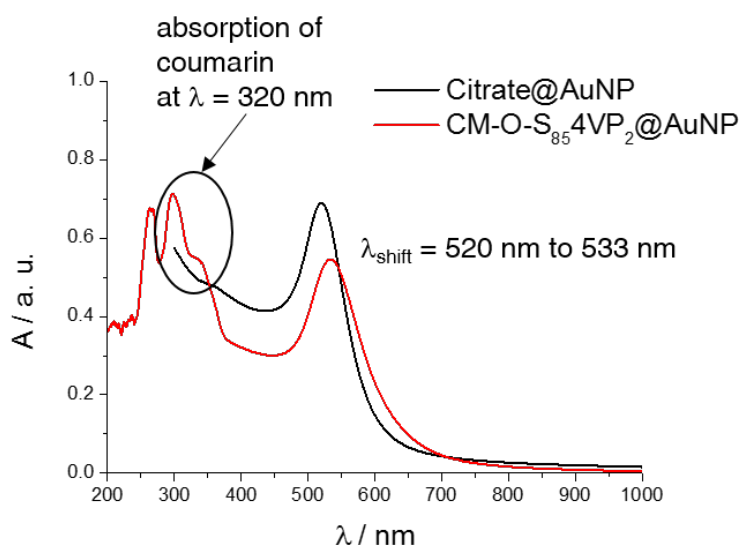


Figure 4.64: UV/Vis spectra of CM-O-S₈₅4VP₂@AuNP before and after ligand exchange of Citrate@AuNP.

By excitation of CM-O-S₈₅4VP₂@AuNP at $\lambda = 330$ nm an emission band at $\lambda = 419$ nm was observed (Figure 4.65a). The sample was also excited at $\lambda = 533$ nm to demonstrate

a successful attachment of AuNP with the polymer (Figure 4.65b). A weak emission band at $\lambda = 590$ nm was observed, which belongs to the SPR of AuNP.

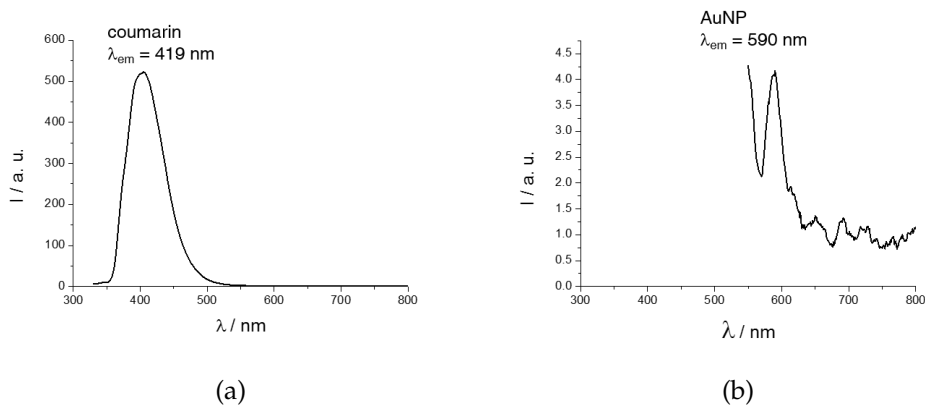


Figure 4.65: (a) Fluorescence spectrum of CM-O-S₈₅4VP₂@AuNP with an emission band of the coumarin end-group at $\lambda = 419$ nm. (b) Fluorescence spectrum of CM-O-S₈₅4VP₂@AuNP with an emission band of AuNP at $\lambda = 590$ nm.

TEM images of CM-O-S₈₅4VP₂@AuNP supported the successful ligand exchange with no observable aggregation (Figure 4.66).

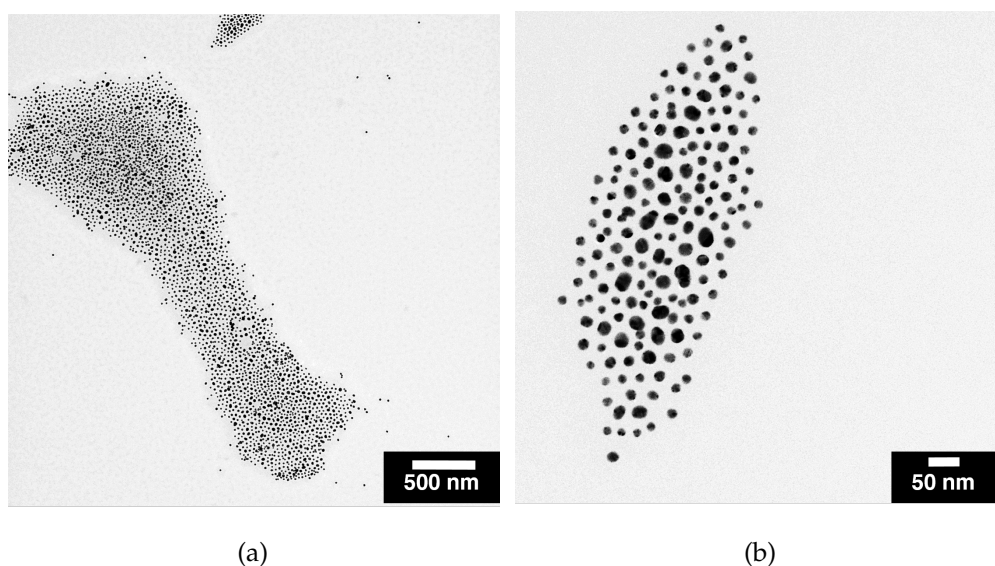


Figure 4.66: (a) TEM image of CM-O-S₈₅4VP₂@AuNP. (b) TEM image of CM-O-S₈₅4VP₂@AuNP at a higher magnification.

4.8 Ligand Exchange Reactions of Citrate@AgNP with CM-O-S₈₅4VP₂

A ligand exchange reaction was also tested with Citrate@AgNP. The silver nanoparticles were freshly prepared prior to the ligand exchange according to a procedure described by PEREIRA^[132]. They were characterized using UV/Vis Spectroscopy and showed a SPR of $\lambda = 393$ nm, which is according to literature. For this ligand exchange reaction, the same process as for the AuNP was used. The transfer of AgNP was also successful and showed a shift of the SPR of AgNP from $\lambda = 393$ nm to $\lambda = 415$ nm. However, the strong absorption band of the coumarin end-group was not possible to observe.

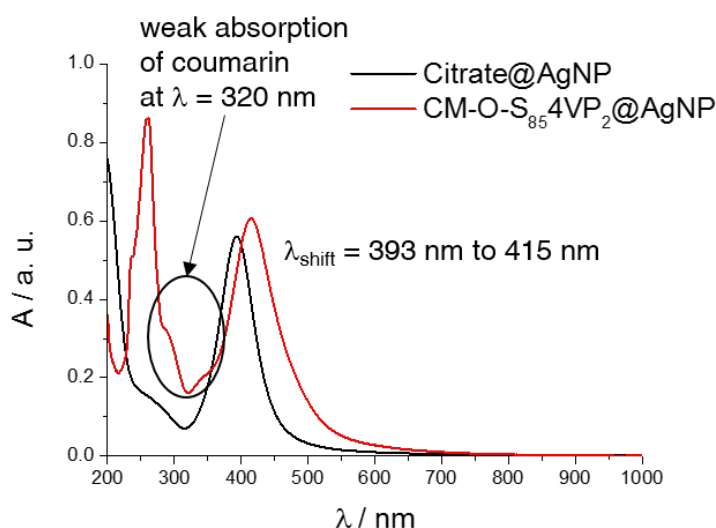


Figure 4.67: UV/Vis spectra of CM-O-S₈₅4VP₂@AgNP before and after ligand exchange of Citrate@AgNP.

In contrast the fluorescence spectrum of CM-O-S₈₅4VP₂@AgNP showed a strong, but broader emission band at $\lambda = 419$ nm after excitation at $\lambda = 320$ nm (Figure 4.68a), while the AgNP showed a weak emission band at $\lambda = 448$ nm after excitation at $\lambda = 415$ nm (Figure 4.68b). A possible explanation for this weak absorption of the coumarin end-group might be due to the overlap between the emission band of the coumarin group at $\lambda = 419$ nm with the SPR of AgNP at $\lambda = 415$ nm.

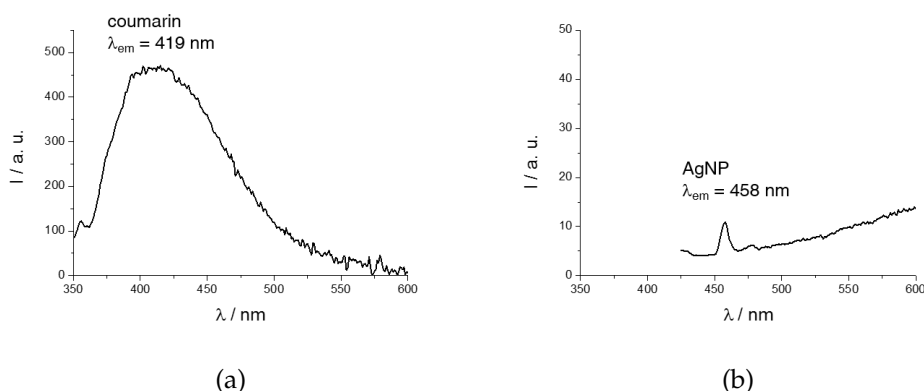


Figure 4.68: (a) Fluorescence spectrum of CM-O-S₈₅4VP₂@AgNP with an emission band of the coumarin end-group at $\lambda = 419$ nm. (b) Fluorescence spectrum of CM-O-S₈₅4VP₂@AgNP with an emission band of AuNP at $\lambda = 458$ nm.

TEM analysis also showed no aggregation of AgNP (Figure 4.69).

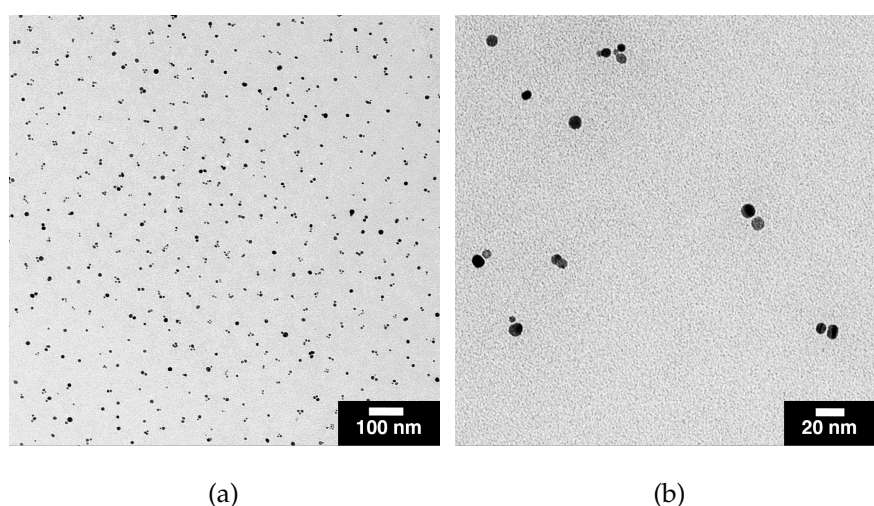


Figure 4.69: (a) TEM image of CM-O-S₈₅4VP₂@AgNP. (b) TEM image of CM-O-S₈₅4VP₂@AgNP at a higher magnification.

In this section the use of CM-O-S₈₅4VP₂ as functional polymer was successfully presented by performing ligand exchange reactions of gold and silver nanoparticles. The use of a polymer with a chromophore attached at the end-chain of the polystyrene block and a further functionalization of metal nanoparticles can be of great interest in the field of FRET due to the close energy observed by the emission band of the coumarin group to the absorption band of the metal nanoparticles.

A manuscript of these results is in preparation and will be submitted.

5 Summary

In the present work three different research projects regarding the functionalization and self-assembly of gold nanoparticles (AuNP) with functional block copolymers of styrene and 4VP in solution were presented. S4VP block copolymers with different block lengths of 4VP were synthesized *via* sequential living anionic polymerization. Two different approaches of functionalized AuNP with S4VP polymers were exposed. Pyridyl-terminated polystyrenes were employed as monodentate ligands for AuNP, while longer blocks of 4VP were used as multidentate ligands. The control of selectivity and distribution of metal nanoparticles within the S4VP block copolymer domains were probed by two different methods, namely ligand exchange reactions and *in situ* reactions of AuNP by reduction of a metal salt with NaBH₄. The optical properties of these S4VP/AuNP nanocomposites were thoroughly studied. Furthermore a telechelic α -OH-S4VP block copolymer was synthesized using the living anionic polymerization technique. Each research project is summarized independently.

In the first part ligand exchange reactions of Citrate@AuNP with a diameter size of $d_{AuNP} = 15$ nm with monodentate and multidentate ligands of S4VP polymers were performed. The reaction was carried out in the biphasic system water/chloroform. The variation of AuNP to the 4VP and viceversa showed strong differences on the self-assembly of S4VP/AuNP nanocomposites. The use of monodentate ligands showed a tremendous influence on the formation of highly ordered structures of AuNP within S4VP, which was not observed in the case of multidentate ligands. It was shown, that the amount of ligands relative to the amount of AuNP was crucial for the formation of ordered supramolecular S4VP/AuNP nanocomposites. The formation of self-assembly of AuNP was followed by measuring the hydrodynamic diameter of the nanocomposites by means of DLS, which showed a systematic increase by increasing the AuNP ratio. The self assembly of the AuNP agglomerates in suspension showed an uniformly order

of AuNP, while in the solid state a perfect hexagonal order of AuNP. This was carefully analyzed by TEM and cryo-TEM, which proved the stabilization of AuNP agglomerates in suspension and hexagonal ordered AuNP in the solid state. The interparticle distance of AuNP could be controlled by simply changing the length of the polystyrene block, which also acted as a repulsion agent between the nanoparticles to avoid aggregation of the system. Due to the narrow interparticle distance of AuNP, interplasmonic interactions in the SPR were observed. The use of an external stimulus, such as variation of temperature or further addition of polymer led to disintegration of these agglomerates, which exhibited an irreversible effect on AuNP self-assembly. This was verified by means of UV/Vis spectroscopy, in which the interplasmonic interactions vanished and the color of the suspension changed. DLS measurements showed an alteration of the hydrodynamic diameter as a function of temperature. TEM images showed no self-assembly AuNP after treating the AuNP agglomerates by an external stimulus.

In the second part, the stabilization and particle size distribution of AuNP in solution generated *in situ* by using different S4VP block copolymers as monodentate and multidentate ligands were investigated. In these studies a series of experiments by varying the molar ratio of the polymer were performed and carefully analyzed by means of TEM and UV/Vis spectroscopy. It was shown, that the particle size distribution as well as the particle diameter is crucially influenced by the length of the 4VP moiety, the polymer concentration, and the reducing agent. The size distribution of AuNP with monodentate ligands was almost constant ($d_{AuNP} = 8$ nm) over all molar ratios. The multidentate ligands showed a distinct different formation mechanism. Increasing the 4VP/HAuCl₄ ratio resulted in the formation of micelles at high polymer concentrations and small AuNP ($d_{AuNP} = 2.5$ nm) with no signs of optical properties. Low polymer concentrations showed the formation of narrowly distributed AuNP with diameters of around $d_{AuNP} = 8$ nm, which showed SPR. It was demonstrated, that block copolymers with different 4VP block lengths can lead to the formation of AuNP in different sizes with narrow size distributions by *in situ* reactions.

The third and last part of this work, the synthesis and characterization of a functional telechelic α -OH-S4VP polymer *via* anionic polymerization was presented. Furthermore a functionalization with coumarin as well as the stabilization of AuNP and AgNP by lig-

and exchange reactions in a biphasic system was probed, in order to enhance the optical properties of functional S4VP/AuNP nanocomposites. Prior to this synthesis, a bifunctional initiator for the anionic polymerization was prepared. This initiator was achieved by protecting the hydroxyl group of 3-chloropropane-1-ol, subsequently by a lithiation. Since this synthesis was very sensitive to air, moisture, and light and unstable it was difficult to control the molecular weight of the polymer. Three different functional α -OH-S4VP polymers were successfully synthesized and analyzed by GPC-DAD and IR. However, the control of molar mass of polystyrene was difficult to achieve. It varied from $9000 \text{ g} \cdot \text{mol}^{-1}$ over $18000 \text{ g} \cdot \text{mol}^{-1}$ to $35000 \text{ g} \cdot \text{mol}^{-1}$. The polymer with a molar mass of $9000 \text{ g} \cdot \text{mol}^{-1}$ was preferred for further functionalizations. The polymer was used to attach the chromophore coumarin-3-hydroxy chloride in α position of the polystyrene. This reaction showed successful results and the coumarin-functionalized block copolymer was employed in ligand exchange reactions with AuNP and AgNP. The reaction showed a full transfer of metal nanoparticles into the organic phase. The Coumarin-functionalized S4VP/AuNP nanocomposites were characterized by means of fluorescence spectroscopy, which showed a weak absorption of the Coumarin, though a strong emission light by excitation at 310 nm. Also AuNP and AgNP showed a strong SPR, respectively. TEM analysis confirmed a successful stabilization of the metal nanoparticles with the functional block copolymer.

6 Zusammenfassung

Im Rahmen dieser Arbeit wurden drei verschiedene Forschungsprojekte hinsichtlich der Funktionalisierung und Selbstanordnung, oder sogenannten „Self-Assembly“ von Goldnanopartikeln (AuNP) mit funktionalen Blockcopolymeren aus Styrol und 4-Vinylpyridin (S4VP) durchgeführt. S4VP Blockcopolymeren wurden mittels lebender anionischer Polymerisation hergestellt. Durch Steuerung des 4VP Blocks fungieren diese als monodentate bzw. multidentate Liganden für AuNP. Sowohl die Kontrolle und Selektivität der AuNP Verteilung als auch die optischen Eigenschaften des S4VP/AuNP Nanokomposit Materials wurden sorgfältig untersucht. Desweiteren wurde ein telecheles α -OH-S4VP hergestellt. Dabei wurde die Methode der anionischen Polymerisation angewendet. Jedes Forschungsprojekt wird in Folge einzeln zusammengefasst.

Das erste Forschungsprojekt beschäftigt sich mit der Funktionalisierung von AuNP mit S4VP Blockcopolymeren als monodentaten und multidentaten Liganden für AuNP. Es wurden Ligandenaustauschreaktionen von citrat-stabilisierten AuNP mit S4VP in einem zwei-Phasen System (Wasser/Chloroform) durchgeführt, wobei eine Versuchsreihe durch Variation des molaren Verhältnisses von AuNP erstellt wurde. Im Vergleich zu multidentaten Liganden besitzen monodentate Liganden einen starken Einfluss auf die Self-Assembly von S4VP/AuNP Nanokomposit Materialien. Je nach Verhältnis von Polymer zu AuNP konnte die Self-Assembly der AuNP gesteuert werden. Die Self-Assembly konnte durch DLS nachgewiesen werden, wobei eine systematische Zunahme des hydrodynamischen Durchmessers beobachtet wurde. Durch cryo-TEM Messungen wurde keine hochgeordnete Anordnung der Partikel gezeigt, jedoch eine Zusammenlagerung der Nanopartikel ohne Aggregation beobachtet. Dies war aufgrund des vorhandenen Lösungsmittels, das auch einen Einfluss auf die Anordnung der AuNP zeigte. Im festen Zustand wurde eine hexagonale Anordnung der AuNP mittels TEM beobachtet. Durch Anwendung eines externen Stimulus für die Self-Assembly der AuNP, zum

Beispiel einfü von Temperatur oder durch Zugabe von extra Polymer war es möglich die Self-Assembly der AuNP aufzulösen. Dies wurde durch Änderungen der optischen Eigenschaften mit Hilfe von UV/Vis Messungen und Anhand der Farbänderung der Probe als auch von TEM und DLS Messungen bestätigt.

Im zweiten Forschungsprojekt wurden AuNP durch *in situ* Reaktionen in Gegenwart des S4VP Blockcopolymer durchgeführt. Dabei wurde ebenfalls eine Versuchsreihe erstellt, in der die Polymerkonzentration variiert wurde. Es wurde gezeigt, daß die Verteilung und Größe der AuNP sowohl von der Anzahl der Koordinationsteile des 4VP Blocks, als auch von der Polymerkonzentration, und dem benutzten Reduktionsmittel stark beeinflusst wird. Monodentate Liganden zeigten keine starke Änderung der Partikelgröße und eine enge Verteilung der AuNP mit einem Durchmesser von $d = 8$ nm mit starken SPR im Wellenlängenbereich $\lambda = 530$ nm. Im Gegensatz dazu zeigten multidentate Liganden keinen Einfluss auf die optischen Eigenschaften des S4VP/AuNP Nanokomposit Materials. Durch Variation der Polymerkonzentration konnte die Partikelgröße gesteuert werden. Aufgrund von Mizellen Bildung bei höheren Polymerkonzentrationen wurden Partikel in Größe von $d = 2$ nm hergestellt. Niedrige Polymerkonzentrationen lieferten AuNP in Größe $d = 8$ nm mit guten optischen Eigenschaften.

Ziel des dritten Forschungsprojekts war die Synthese und Charakterisierung eines telechelen α OH-S4VP Blockcopolymer für eine weitere Funktionalisierung mit Farbstoffmolekülen. Durch anschließende Stabilisierung von AuNP mit dem 4VP Block wurden die Wechselwirkungen zwischen beiden Funktionalitäten mittels UV/Vis- und Fluoreszenzspektroskopie untersucht, wobei der Polystyrol Block als Abstandhalter fungierte. Die Herstellung des funktionalen α -OH-S4VP Blockcopolymer erfolgte mittels anionische Polymerisation. Aus diesem Grund wurde einen bi-funktionellen Initiator für die lebende anionische Polymerisation hergestellt. Ein funktionales HO-S4VP Blockcopolymer mit dem gewünschten Molekulargewicht von ca. $9000 \text{ g} \cdot \text{mol}^{-1}$ wurde erfolgreich hergestellt und als Templat für weitere Funktionalisierungen mit Chromophoren getestet. Als Farbstoffmolekül wurde Coumarin gewählt, das durch Veresterungsreaktionen mit dem funktionalen Polymer verknüpft wurde und mittels GPC-DAD charakterisiert wurde. Die anschließende Funktionalisierung von Gold- und Silbernanopartikeln wurde erfolgreich durchgeführt und mittels Fluoreszenz Spektroskopie charakterisiert. Man

beobachtete dabei ein schwaches Absorptionssignal des Coumarinmoleküls, jedoch ein starkes Emissionssignal durch Anregung des Farbstoffs bei 310 nm. Eine starke Plasmonenbande von AuNP und AgNP wurde ebenso detektiert. Durch TEM Messungen konnte eine erfolgreiche Stabilisierung von den Metallnanopartikeln mit dem funktionalen Blockcopolymer bestätigt werden.

7 Outlook

The precise control of block copolymer morphologies and the selectivity of metal nanoparticles in different domains of BCPs are currently of major interest, since they provide the possibility to build nanodevices with desirable properties and stimuli-responsiveness, that can extend their applications in the field of nanotechnology, which is also required in everyday life. Basic requirements for future developments in the field include further seeking and optimization of controlled synthesis of the nanoparticle based building blocks. Size-control of AuNP, design and synthesis of functional materials with simple coating needs contribution of organic and polymer synthetic chemists. Also the contributions of inorganic and physical chemists would enhance the fabrication of metal nanoparticle-based nanocomposites. This territory envisions an interdisciplinary team (field), that will lead to the next industrial revolution^[153]. A full potential of polymer/metal nanocomposites remains largely unexplored and will always deliver new and simple strategies to enhance the chemical and physical properties of nanodevices at low costs.

The method of ligand exchange reactions in a biphasic system, without the utilization of a phase transfer catalyst, affords a versatile approach to get controllable formation of self-assembled AuNP within S4VP polymers in solution. The direct functionalization of presynthesized AuNP with 4VP moieties makes the system unique, since the system contains less impurities, which can distort the stability and properties of AuNP. Due to the fact that the interparticle distance of AuNP can be tuned (depending on the length of the polystyrene chain), it is possible to control and manipulate the optical properties of these nanocomposites. The use of an external stimulus (temperature or additives) shows an irreversible disintegration of the self-assembly of AuNP as well as an induced-color change of the AuNP. Nevertheless these S4VP/AuNP nanocomposites could be exploited as potential devices in the field of optical-, temperature-, and bio-sensor de-

vices. Moreover the concept is applicable for many other metal nanoparticles, since 4VP is a suitable coordination agent for almost all metal nanoparticles.

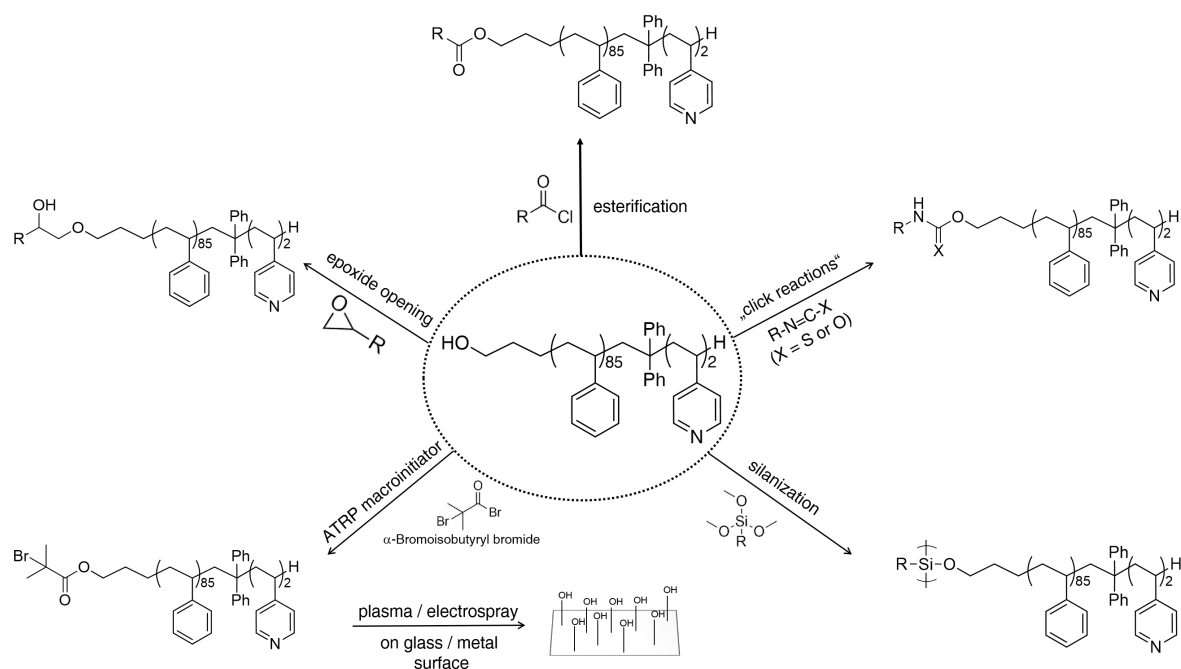
The research projects presented in this work show different concepts and methods for the feasibility in designing well-defined functional S4VP/AuNP nanocomposites, where their morphology is mainly driven by the self-assembly of AuNP. Key for the defined control ordered formation of AuNP was the employment of 4VP as monodentate ligands as well as the modulation of the ratio AuNP versus ligands.

The *in situ* method shows a simple concept with favorable results for size-controlled AuNP towards multidentate 4VP ligands, depending on the concentration used for S4VP block copolymers. Tuning the molecular composition of the block copolymer allows the possibility to create different morphologies of the S4VP/AuNP nanocomposites with desirable properties, which can be used as multifunctional devices. The polystyrene block acting as repulsion agent between the AuNPs is not directly involved in structure-forming mechanisms and is easy to tailor and replaceable with any other polymer desirable for functional applications. The size control by synthetic protocols may have impact on the fields of optoelectronics and catalysis, where small AuNP with controllable size and high surface area are required.

The „grafting to“ method often requires the addition of a functional groups to the surface of inorganic nanoparticles, allowing then for conventional chemical reactions to graft other polymers or molecules to the modified inorganic particles. A prior modification of the S4VP block copolymer, that contains an additional reactive group in α position of the polystyrene chain, opens wide possibilities for the enhancement of „grafting to“ methods. „Click chemistry“ is useful in attaching chains to the surface of particles, as it can be carried out with high efficiency under relatively mild conditions^[154].

In the present work a telechelic polystyrene α -OH-S4VP was successfully synthesized. On the one hand the 4VP moiety is established to functionalize AuNP. On the other hand a hydroxyl group can be further modified and be used in many different reactions for further functionalizations. In other words, this polymer can be used straightforward as a template to build hierarchical multifunctional devices by combining any kind of metal nanoparticles and reactive molecules, respectively.

Scheme 21 displays an overview of the most common reactions that can be achieved using the telechelic polystyrene as template for „grafting to“ or post-functionalization of S4VP/AuNP nanocomposites.



SCHEME: 21 Overview of possible reactions of α -OH-S4VP used as template.

In this work the chromophore Coumarin was successfully attached to α -OH-S4VP@AuNP nanocomposites, which improved the optical properties of the material. This concept was extended by using AgNP, which also showed outstanding optical properties. Since the absorption band of AgNP overlaps with the emission band of Coumarin, and the molar mass of polystyrene is relative low, the material is suitable for FÖRSTER resonance energy transfer (FRET) experiments^[155–157]. Analogous the post-functionalization of α -OH-S4VP@AuNP with Rhodamine B would attract particular interest in the enhanced energy transfer efficiency. Furthermore this system could also be applied as substrates for surface-enhanced RAMAN scattering^[158,159].

Other modifications by „click reactions“ of the polymer with epoxides or iso(thio)cyanates are possible. The conversion of the polymer to a macroinitiator *via* ATRP is also achievable.

8 Acknowledgments

First of all, my gratefulness goes to my supervisor Prof. Dr. Andreas Greiner, who welcomed me first to the department of Macromolecular Chemistry in Marburg and afterwards to go along with his new adventure at the department of Macromolecular Chemistry II in Bayreuth. I would like to thank him, for giving me the opportunity to accomplish my PhD degree within his chair and therefore for trusting me along those three and a half years. I grandly appreciate the precious time he granted me with his help, his advices, and long talks regarding manuscripts. Also his support by sending me to an international conference in Thailand, where I had the chance to present my work and meet polymer chemists from all over the world. Also the opportunity to go to Finland and explore the world of microscopy in the department of applied physics. Thank you for providing me a great academic career in the field of Polymer Chemistry and Nanotechnology!

I would like to thank Prof. Dr. Seema Agarwal for the extensive discussions about my work and the nice talks in the kitchen „while waiting until tea“ was ready.

Directly related to my work, I would like to thank my mentor Dr. Holger Schmalz for introducing me to the difficult and duty of anionic polymerization in our great anionic lab. I am grateful for all the wise talks that we had concerning the theory, synthesis-, and analytical-part of my (functional) block copolymers. Dr. André Gröschel for all brainstorming, crazy and useful ideas about my projects.

My special thank goes to Dr. Markus Drechsler for introducing me the duty of TEM, Melanie Müller for TEM measurements, Dr. Tobias König for his help on UV/Vis simulations, M. Sc. Bianca Uch and Marietta Böhm for GPC measurements, and Dr. Marina Krekhova for all TEM advices.

To the University of Bayreuth Graduate School, thank you for the financial support, that arose the opportunity to live new adventures overseas.

Of course, I would like to thank the old and new members of the MC2 group for creating an amusing atmosphere full of surprises. My lab partners Mitsunobu Doimoto for his great friendship and Peter Ohlendorf for his kindness.

My special thank goes to the lab 785, Viola Buchholz and Markus Langner for all kind of discussions; great-, bad-, sad-, angry-, and happy moments that we experienced. You rock guys! Thank You for making the PhD life a little easier in a way...

Oliver Hauenstein for fixing my computer problems and being patient at all „internet break-down“times.

Florian Käfer, Judith Schöbel, and Viola Buchholz thank you, thank you, thank you for taking the time and patience to proof-read my thesis. Thank you for the extensive discussions!!!

I can never thank enough our both Secretaries, Edith Schmid (Marburg) and Gaby-Rösner-Oliver (Bayreuth) for all the energy they put on paper-work and administration duties, their kindness and for being always ready to help and to answer my questions. Gaby, thank you for listening.

My sincere thanks are given to Tina Löbling and Viola Buchholz: **„we started as a group of people and we finished as a group of friends“**. I will always be grateful for meeting you. Thank you for not giving up on me, for accepting me just the way I am, and for always being there.

I also want to thank a very special group of friends: „Crossbunker-Polers“(Chrissi, Geli, Tasja, Miriam, Julia, Alena, Eva, Nicy, Thomas, Philipp, Andy, Alex, Jörg, Uwe), thank you for showing me how great life can be outside the academic world.

I want to thank my parents Elizabeth Serrano Grosvenor and Johnny Köhn Weiss for their unconditional support, who always believed I would make it.

Finally I would like to thank Ralf Krüll for keeping faith in me when I did not myself, for his wholehearted support, his patience and his love.

9 Experimental section

9.1 Materials and Methods

9.1.1 Chemicals and Solvents

<i>sec</i> -Butyllithium	Acros, used as received
<i>tert</i> -Butyldimethylsilyloxychloride	Sigma-Aldrich, stored under Ar
1,1-Diphenylethylene	Sigma-Aldrich, dried over CaH ₂ , distilled under vacuum, stored under Ar
3-Chloropropane-1-ol	Sigma-Aldrich, washed with saturated NHCl ₄ -Solution
4-Vinylpyridine	Sigma-Aldrich, dried over triethylaluminum, condensed under vacuum, stored under Ar
Ammoniumchloride	Grüssing GmbH, used as received
N(<i>tert</i> -butoxycarbonyl)glycine	Sigma-Aldrich, stored at 4 °C, used as received
Calciumhydride	Alfa Aesar, used as received
1,1'-Carbonyldiimidazole	Sigma-Aldrich, stored under Ar, used as received
Celite Filter Pad	Fluka, dried at 120 °C
Coumarin-3-carboxylic acid	Sigma-Aldrich, used as received
Deuterated Chloroform	Deutero GmbH, used as received
N,N'-Dicyclohexylcarbodiimide	Sigma-Aldrich, used as received
Di- <i>n</i> -Butylmagnesium	Sigma-Aldrich, used as received
Dimethyl amino pyridine	Sigma-Aldrich, used as received
Ethylendiamine	Sigma-Aldrich, dried over CaH ₂ , distilled under Ar
Fluorescein isothiocyanate	Sigma-Aldrich, stored at -20 °C, used as received
Hydrochloric acid (conc.)	Sigma-Aldrich, used as received

Imidazole	Sigma-Aldrich, used as received
Lithium 4-10 mesh particle size high sodium, 99 %	Sigma-Aldrich, stored under Ar
Magnesium sulfate anhydrous	Grüssing GmbH, used as received
Nitric acid (conc.)	Sigma-Aldrich, used as received
Phosphorus pentoxide	Merck, used as received
Rhodamine B	Sigma-Aldrich, used as received
Silver nitrate	Sigma-Aldrich, used as received
Sodium hydrogen carbonate	Grüssing GmbH, used as received
Silica gel pore size 60	University supply, used as received
Sodium chloride	VWR, used as received
Sodium borohydride	Fluka, used as received
Styrene	Sigma-Aldrich, dried over di- <i>n</i> -butylmagnesium, condensed under vacuum, stored under Ar
Tetra- <i>n</i> -Butylammoniumfluoride	Sigma-Aldrich, used as received
Tetrachloroauric acid trihydrate	Alfa Aesar, used as received
Trifluoroacetic acid	Sigma-Aldrich, used as received
Thionylchloride	Sigma-Aldrich, dried over CaH ₂ , distilled under Ar
Triethylaluminum	Acros, used as received
Triethylamine	Sigma-Aldrich, dried over CaH ₂ , distilled under argon
Trisodium citrate dihydrate	Merck, used as received
Chloroform	Aldrich (p.a.), used as received
Cyclohexane	Aldrich (p.a.), dried over CaH ₂ , potassium and distilled under nitrogen
Dichloromethane	Aldrich (p.a.) dried over P ₂ O ₅ , distilled
Diethylether	University supply (technical grade), distilled
Dimethyl sulfoxide (DMSO)	Aldrich, used as received
Ethyl acetate (EtOAc)	University supply (technical grade), distilled
iso-Hexane	University supply (technical grade), distilled
Methanol	University supply, distilled

Milli-pore water	MILLIPORE, used as received
Pentane	University supply (technical grade), distilled
Tetrahydrofuran p.a.	Aldrich, dried over CaH ₂ , potassium and distilled under nitrogen
Tetrahydrofuran	University supply (technical grade), distilled

9.1.2 Instrumentation

Nuclear Magnetic Resonance (NMR) spectroscopy

¹H-NMR spectra were recorded at 300 MHz on a Bruker AC300 spectrometer using tetramethylsilane (TMS) as an internal standard. The chemical shifts were referred to the residual protons of the deuterated solvent (CDCl₃). NMR-spectra were analyzed with the MesReNova software (version 6.1.0).

Gel Permeation Chromatography (GPC)

For polystyrene precursors (PS-Precursor) GPC measurements were performed on a set of 30 cm SDV-gel column of 5 μm particle size having a pore size of 10⁵, 10⁴, 10³, and 10² Å with refractive index and UV (λ = 254 nm) detection. GPC was measured at an elution rate of 1 mL · min⁻¹ with THF as eluent, calibrated with polystyrene standards, and toluene internal standard.

S4VP copolymer measurements were performed on a Knauer System equipped with a PSS-SDV gel columns of 10 μm particle size with a 8 x 50 mm² precolumn and two columns 8 x 300 mm² at 30 °C, a Knauer UV detector at a wavelength of 260 nm and a Agilent differential refractive index detector. DMF (containing 5 g · L⁻¹ of lithium bromide as an additive) was used as eluent at a flow rate of 0.5 mL · min⁻¹ using toluene as an internal standard and calibrated with a linear polymethylmethacrylat (PMMA) standards.

Chomophor-functionalized S4VP block copolymers were analyzed using a Gel permeation chromatograph coupled with a diode array detector in DMF (DMF-GPC-DAD). Measurements were carried out using five different wavelengths in the range between 260 nm and 600 nm. GPC chromatograms were analyzed with the software WinGPC

(version 7.2.1).

Gas Chromatography (GC)

GC measurements were carried out on a Shimadzu 2010 Plus GC-FID system of the type QP-5050 with nitrogen as carrier gas (Pressure 77.7 kPa, total flow 54.1 mL·min⁻¹, column flow 1 mL·min⁻¹) and a ZB-5MS capillary column with a length of 30 m, inner diameter of 0.25 mm, and a film thickness of 0.25 μm. Samples were diluted in cyclohexane (0.01 %) and 1 μl was injected with a split ratio of 50. All samples were measured with a standard method measured from 50-300 K with a heating rate of 15 K. GC Chromatograms were analyzed with the LabSolutions software (version 5.54 SPL).

Dynamic Light Scattering (DLS)

DLS measurements were performed on an ALV Correlator System equipped with ALV-SP 125 compact goniometer, an ALV 5000/E cross correlator, and a He-Ne Laser ($\lambda = 632.8$ nm). Cylindrical scattering cells with a diameter of $d = 10$ mm were used. Samples were measured at a fixed scattering angle of $\theta = 90^\circ$ or multiple angles ranging from $\theta = 30^\circ$ - 150° in 10° increment steps at a temperature of $T = 20^\circ\text{C}$ for 120 s. Temperature dependent DLS measurements were recorded at different angles between 30° and 150° in 20° increments steps. All samples were measured three times for 120 s. The CONTIN algorithm was applied to analyze the obtained correlation functions. The apparent hydrodynamic diameter (D_H) was calculated according to the Stokes-Einstein equation. All CONTIN plots were intensity weighted. Citrate@AuNP were measured in milli pore water. All S4VP@AuNP samples were measured in chloroform. The data was analyzed with the ALV Correlator software (version 3.0).

UV/Vis Spectroscopy

UV/Vis spectra were recorded using a JASCO V630 Spectrophotometer. All measurements were analyzed in solution at a wavelength between $\lambda = 1000$ nm-300 nm. Citrate@AuNP were diluted and recorded on milli pore water. S4VP@AuNP were diluted and performed on chloroform and on THF solutions for ligand exchange and *in situ* reactions respectively. The samples were diluted until an absorbance below 1 was detected at the absorption maximum of the AuNP at $\lambda_{max} \approx 520$ nm.

Fluorescence Spectroscopy

Fluorescence measurements were carried out on a JASCO Spectrofluorometer FP-8600. All measurements were carried out in solutions. All samples were measured in emission mode with an excitation and emission band width of 5 nm.

Transmission Electron Microscopy (TEM)

TEM images were performed on a LEO 922 OMEGA electron microscope with an acceleration voltage of 200 kV and integrated CCD camera. TEM samples were prepared by dropping 2 μL of the nanoparticle solution diluted in CHCl_3 on a carbon coated copper grid and instantly plated on a filter paper to remove excess solvent. Sample images were analyzed with ImageJ software using 500 nanoparticles (version 1.48).

Cryogenic Transmission Electron Microscopy (cryo-TEM)

Cryo-TEM measurements were performed at Aalto University, Finland. Imaging was carried out using a JEOL JEM 3200SFC emission field microscope operated at 300 kV in bright field mode with OMEGA type-Zero-loss energy filter. The images were acquired with ORIUS SC200 CCD camera (GATAN) and with GATAN DIGITALMICROGRAPH software while the specimen temperature was maintained at -187°C . Vitrified samples were prepared using a FEI VIRIBOT MARK IV. Due to the low enthalpy of vaporization, preparation of vitrified chloroform films turned out to be very difficult on lacey and holey carbon films. Therefore 3 μL of samples solution was placed on 200 mesh carbon only copper grids under ambient conditions, then blotted with filter paper 0.5 s and immediately plunged to -170°C ethane/propane mixture and cryo transferred to the microscope. The samples were tilted between $\pm 20^\circ$.

Electron Tomography (ET)

ET measurements were carried out at Aalto University, Finland on a transmission electron microscope FEI Tecnai 12 at 120 kV. A series of projection images was recorded with TEM at various angles between $\pm 60^\circ$ with 2° increment steps. Tilted images were acquired with SerialEM software package (version 3.2.2). Pre-alignment of tilt image series was done with IMOD^[160] and the fine alignment and cropping with custom-made Silicon Graphics JPEGANIM-software package^[161]. The images were binned twice to reduce noise and computation time and maximum entropy method (MEM) reconstruction

scheme was carried out with custom-made script on Mac or Linux cluster with regularization parameter value of $\delta = 1.0E^3$ ^[160].

Visualization of 3D Reconstruction

Volumetric graphics and analyses were performed with the UCSF Chimera Package^[162].

Finite Difference Time Domain Simulations (FDTD)

Simulations of the extinction cross-section spectra were done using commercial software from Lumerical Solutions, Inc. (FDTD Solutions, Version 8.7.3). AuNP were modelled in chloroform ($n = 1.44$). The AuNP dimensions were evaluated using TEM images. For a broad band source simulation (total-field scattered-field (TFSF) source, $\lambda = 300$ -1000 nm), the FDTD software approximates the refractive index of the materials by a polynomial function. For the optical constants of Au, a fitting of the experimental data by *Johnson and Christy* (JC) was applied (6 coefficients, 2 imaginary weight, which results in 0.21 root mean square error)^[163]. A simulation mesh size of 0.25 nm was chosen for the particle and 0.5 nm mesh was chosen for the TFSF source box. The zero-conformal-variant mesh refinement was used. For the best simulation stability, the TFSF source box was chosen to be 50 nm larger than the existing structure in all three principal directions. All simulations reached the auto shut off level of 10^{-7} before reaching 150 fs simulation time. Anti-symmetric boundary conditions (BC) were used normal to the polarization plane and symmetric BC were used parallel to the polarization plane only at single particle conditions. In radiation direction we used always in both directions the perfect match layer (PML) BCs. Simulation for more than one particle we used PML at all BCs. Single AuNP simulation results from FDTD method are in excellent agreement with simulation results from MIE Theory (mean square error is below 0.4)^[164].

Multi Reax Shaker

Ligand exchange reactions were performed on a Heidolph Multi Reax Shaker. Samples were shaken at 1000 rpm for 10 min and at 500 rpm for 12 h.

Thermogravimetric Analysis (TGA)

The thermal decomposition of block copolymer samples was measured with thermobalance from NETZSCH TG 209F1 Libra. 5 - 10 mg of the sample was placed in an alu-

minum oxide (Al_2O_3) crucible and measured under nitrogen atmosphere with a flow of $50 \text{ ml} \cdot \text{min}^{-1}$ and a heating rate of $10 \text{ K} \cdot \text{min}^{-1}$ in a temperature range of 25 - 800 °C. Data were analyzed with the software Proteus (version 6.1.0).

Infrared Spectroscopy (IR)

IR measurements were recorded on a Digilab IR-Spectrometer (Excalibur series) equipped with an ATR-unit containing a ZnSe crystal. Data evaluation was performed with WinIR-Pro software.

9.2 General Synthetic Procedures

Anionic polymerization reactions and lithiation reactions were carried out in a reactor or schlenkflasks under strict prevention of moisture, water, and oxygen. All glassware was heated under vacuum, and flushed with argon.

For reactions with AuNP all glassware and magnetic stir bars were cleaned with *aqua regia* and ultra pore water and dried at 120 °C prior to use.

9.2.1 Synthesis of S4VP Block Copolymers

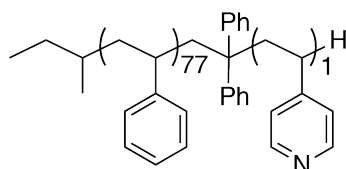
Block copolymers of styrene (S) and 4-vinylpyridine (4VP) (S4VP) were synthesized *via* a sequential living anionic polymerization. The anionic polymerization was carried out in a thermostated laboratory autoclave (1 L, Büchi) at a temperature of -78 °C using 400 mL of THF_{abs} as a solvent. *sec*-BuLi was used as initiator. One batch of polystyrene was synthesized to keep a constant molecular weight, while the molecular weight of 4VP was varied by taking aliquots of the mixture consecutively during the reaction process. Before adding the actual amount of the initiator to the THF solution, 1 mL *sec*-BuLi was added and a yellow color was observed. The solution was allowed to warm up to room temperature prior to reaction begin. This step was required to remove all impurities of the solvent and avoid side reactions during the polymerization process. A pyridyl-terminated polystyrene $\text{S}_{77}\text{4VP}_1$, and two S4VP block copolymers $\text{S}_{77}\text{4VP}_{17}$, and $\text{S}_{77}\text{4VP}_{34}$ were prepared in one batch. 2.41 mL (3.6 mmol, 1.48 M, 1 eq.) *sec*-BuLi were used for the syntheses of S4VP block copolymers. 29.6 g (284 mmol, 79 eq.) of

styrene were transferred into the reactor *via* a glass ampoule under vigorously stirring and the typical orange color of the polystyryl anion was observed. After 10 minutes stirring an aliquot of the reaction mixture was withdrawn for NMR and GPC analysis. 0.63 mL (3.6 mmol, 1 eq.) DPE were added to end cap the polystyryl anion and stirred for 30 minutes. The color of the solution changed immediately to deep red. Then 0.4 g (3.6 mmol, 1 eq.) 4VP was added *via* a syringe to the reaction mixture and the color changed in a few minutes from red to yellow. After one hour 100 mL of the solution were pumped out of the reactor and precipitated from degassed methanol. Further 4VP (7.5 g, 71.4 mmol, 20 eq) was added *via* a syringe to the remaining solution of the still living S4VP polymer. After one hour 150 mL of the solution were again pumped out of the reactor and precipitated from degassed pentane. At last 15.3 g (145 mmol, 40 eq) 4VP were added and stirred for one hour. Afterwards the reaction mixture was terminated by degassed methanol and the reaction mixture was allowed to warm up to room temperature. The resulting block copolymer was precipitated from pentane. The molecular weight of polystyrene was determined by GPC-THF, while the units of the 4VP block were calculated by $^1\text{H-NMR}$ -spectroscopy.

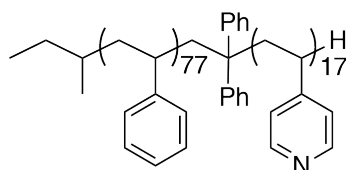
The syntheses of pyridyl-terminated polystyrenes $\text{S}_{26}4\text{VP}_1$ and $\text{S}_{49}4\text{VP}_1$ were carried out in 250 mL Schlenkflasks with 150 mL dried THF as solvent at a temperature of -78°C using a acetone/dry-ice bath. *sec*-BuLi was used as initiator. Prior to reaction begin, 0.1 mL initiator was added to remove all impurities of the solvent and allowed to warm up at room temperature. The solvent was again cooled down at -78°C . For $\text{S}_{26}4\text{VP}_1$ 3.25 mL (4.54 mmol, 1.4 M, 1 eq) *sec*-BuLi were added to dried THF. 10.49 g (100 mmol, 22 eq.) styrene were added to the vigorously stirring solution. After 10 minutes 2 mL of the reaction mixture were taken and precipitated from degassed methanol and prepared for NMR and GPC analysis. 0.80 mL (4.54 mmol, 1 eq.) DPE was added and stirred for 30 minutes. Afterwards 0.51 g (4.8 mmol, 1 eq.) 4VP was added and stirred for 20 minutes. The reaction mixture was terminated by adding a few drops of degassed methanol. The reaction mixture was precipitated from methanol.

For the synthesis of $\text{S}_{49}4\text{VP}_1$ 1.45 mL (1.88 mmol, 1 eq.) *sec*-BuLi were used. 10.82 g (104 mmol, 55 eq.) styrene were added and stirred for 10 minutes. 2 mL of the reaction mixture were withdrawn and prepared for NMR and GPC analysis. 0.33 mL (1.88 mmol, 1 eq) DPE were added and stirred for 30 minutes. Afterwards, 0.2 g (1.90 mmol, 1 eq.) 4VP were added and stirred for 20 minutes. The reaction mixture was terminated with

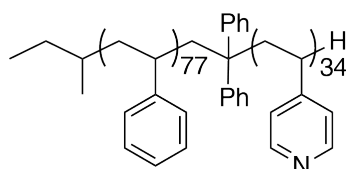
degassed methanol followed by precipitation from methanol. All synthesized BCPs were dried in vacuum at 50 °C and characterized by means of NMR-spectroscopy and GPC-DMF analysis.



$S_{77}4VP_1$, 300 MHz, $CDCl_3$, δ in ppm: 8.66-7.98 (m, 2H of aromatic system of 4VP), 7.23-6.14 (m, 2H of aromatic system of 4VP, 5H of aromatic system of S, 10H of aromatic system of DPE), 2.38-0.96 (CH_2CH PS backbone, CH_2CH of initiator, CH_2 of DPE, CH_2CH P4VP backbone), 0.79-0.51 (m, 6H of initiator).

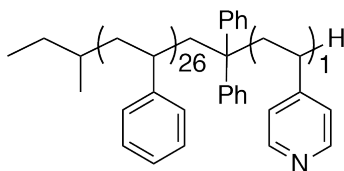


$S_{77}4VP_{17}$, 300 MHz, $CDCl_3$, δ in ppm: 8.65-8.05 (m, 2H of aromatic system of 4VP), 7.24-6.09 (m, 2H of aromatic system 4VP, 5H of aromatic system of S, 10H of aromatic system of DPE), 2.39-0.98 (CH_2CH PS backbone, CH_2CH of initiator, CH_2 of DPE, CH_2CH P4VP backbone), 0.98-0.48 (m, 6H of initiator).

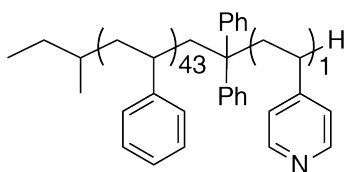


$S_{77}4VP_{34}$, 300 MHz, $CDCl_3$, δ in ppm: 8.62-7.98 (m, 2H of aromatic system of 4VP), 7.24-5.81 (m, 2H of aromatic system 4VP, 5H of aromatic system of S, 10H of aromatic system of DPE), 2.58-0.78 (CH_2CH PS backbone, CH_2CH of initiator, CH_2 of DPE, CH_2CH P4VP

backbone), 0.80-0.45 (m, 6H of initiator).



$S_{26}4VP_1$, 300 MHz, $CDCl_3$, δ in ppm: 8.47-8.16 (m, 2H of aromatic system of 4VP), 7.27-6.12 (m, 2H of aromatic system of 4VP, 5H of aromatic system of S, 10H of aromatic system of DPE), 2.45-1.21 (CH_2CH PS backbone, CH_2CH of initiator, CH_2 of DPE, CH_2CH P4VP backbone), 0.85-0.47 (m, 6H of initiator).



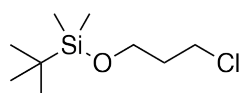
$S_{43}4VP_1$, 300 MHz, $CDCl_3$, δ in ppm: 8.34-8.22 (m, 2H of aromatic system of 4VP), 7.27-6.25 (m, 2H of aromatic system of 4VP, 5H of aromatic system of S, 10H of aromatic system of DPE), 2.55-1.18 (CH_2CH PS backbone, CH_2CH of initiator, CH_2 of DPE, CH_2CH P4VP backbone), 0.83-0.49 (m, 6H of initiator).

9.2.2 Synthesis of *t*BDMSOPrCl

A solution of 3-Chloropropan-1-ol (10 mL) in DCM (10 mL) was washed with 2 mL deionized water, 2 mL of a 5% $NaHCO_3$ solution (until the washes were basic), and a saturated $NaCl$ solution (2 mL). The organic layer was dried over $MgSO_4$, filtered, and distilled at $73^\circ C$ under vacuum (100 mmbar)^[165].

In a 500 mL Schlenkflask 4.32 g (63.5 mmol 1.5 eq.) imidazole and 3.5 mL (42 mmol, 1 eq.) freshly distilled 3-chloropropane-1-ol were dissolved in 100 mL dried DCM. After 5 minutes stirring, the solution was cooled down to $0^\circ C$. 9.57 g (63.5 mmol, 1.5 eq) *tert*-BDMSCl were dissolved in 60 mL dried DCM and added dropwise over 15 minutes to the reaction mixture. The reaction was allowed to rise to room temperature and stirred

for 16 h before being diluted with 100 mL diethyl ether and washed with 50 mL saturated NH_4Cl solution. The aqueous phase was further extracted three times with diethyl ether (50 mL), the organic phases were gathered and washed with 100 mL brine, dried over anhydrous MgSO_4 and reduced to dryness. The resultant sirup was purified by column chromatography with gradient elution (hexane/EtOAc 9:1) to yield a clear liquid (7.3 g, 83 %)^[166].



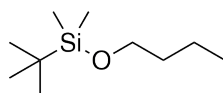
*t*BDMSOPrCl, 300 MHz, CDCl_3 , δ in ppm: 3.75 (t, 2H, $J = 3.7$ Hz, $\text{CH}_2\text{-O}$), 3.65 (t, 2H, $J = 3.7$ Hz, CH_2Cl), 1.95 (pentet, 2H, $J = 1.9$ Hz, $\text{CH}_2\text{-CH}_2\text{-CH}_2$), 0.9 (s, 9H, CH_3), 0.06 (s, 6H, CH_3).

GC-FID (50-300 K in 15 K): 8.9 minutes.

9.2.3 Synthesis of *t*BDMSOPr as an Internal Standard for GC

tert-Butyldimethylsiloxy-propane (*t*BDMSOPr) was used as an internal standard for GC to calculate the concentration of the synthesized *t*BDMSOPrCl.

In a 50 mL schlenkflask 4.6 g (68.75 mmol, 2.5 eq.) imidazole and 5 g (33 mmol, 1.2 eq) *t*BDMSCl were dissolved in 12 mL DMF. Afterwards 1.5 g (2.07 mL, 27.5 mmol, 1 eq.) 1-propanol was added drop wise. The reaction was allowed to stir for 12 h at room temperature.

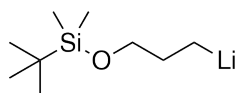


*t*BDMSOPr, 300 MHz, CDCl_3 , δ in ppm: 3.57 (t, 2H, $J = 3,6$ Hz, $\text{CH}_2\text{-O}$), 1.54 (pentet, 2H, $J = 1.6$ Hz, $\text{CH}_2\text{-CH}_3$), 0.89 (q, 12H, $J = 0.9$ Hz, CH_3), 0.05 (s, 6H, CH_3).

GC-FID (50-300 K in 15 K): 6.1 minutes.

9.2.4 Synthesis of *t*BDMSOPrLi

The functional initiator *tert*-butyldimethylsilyloxy-1-propyllithium (*t*BDMSOPrLi) was synthesized following a similar procedure by Bates^[57]. Lithium (0.77 g, 111 mmol, 4.6 eq.) was placed in a 100 mL three-neck round bottom flask equipped with an egg-shaped magnetic stir bar and a condenser using an argon balloon. The surface of the lithium metal was activated by mechanical abrasion by adding 6 mL dried cyclohexane and stirred vigorously at room temperature over night. Further 17 mL of fresh dried cyclohexane were added and stirred for 1 h. 3-chloro-1-*tert*-butyldimethylsilyloxy-propane (5.2 g, 24 mmol, 1 eq.) was added drop wise through a septum to the lithium in cyclohexane at 40 °C over 0.5 h. Upon complete addition the reaction mixture was heated at 60 °C for 22 h. The lithiation was followed by taking aliquots of the sample and quenching the product to analyze the degradation products and reagent by means of GC. After 22 h the reaction was cooled down at room temperature and schlenk filtered through a pad of celite filter pad to yield a transparent faint brown solution of the organolithium reagent.



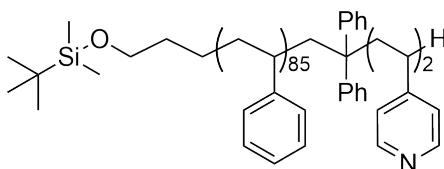
GC-FID (50-300 K in 15 K): 6.1 minutes. Yield 60 %.

9.2.5 Synthesis of α -HO-S4VP Block Copolymer

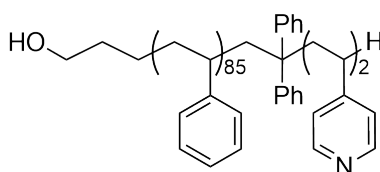
The anionic polymerization of α -HO-S₈₅4VP₂ was initiated with *t*BDMSOPrLi in THF at -78 °C. Prior to reaction begin, 0.5 mL of *sec*-BuLi was added to the dried THF and allowed to warm up at room temperature. The reaction was carried out in a 250 mL Schlenk flask using an acetone/dry ice bath to cool down the reaction mixture. 12 mL *t*BDMSOPrLi (0.07 M, 0.8 mmol, 1 eq.) was added. 7.7 g (81 mmol 101 eq.) styrene were added and a yellow color was observed. After 45 minutes stirring, 2 mL aliquot was withdrawn, precipitated from degassed methanol, and used for NMR and GPC analysis. 0.14 mL (0.8 mmol, 1 eq.) DPE were added and the color changed from yellow to orange-red. After one hour 0.1 g (0.8 mmol, 1 eq.) 4VP were added and the color

changed again to yellow. The reaction was allowed to stir for 30 minutes. Afterwards a few drops degassed methanol were added to terminate the reaction. The functional BCP was precipitated from hexane and dried in vacuum at 50 °C.

2 g of the resultant functional BCP was dissolved in 30 mL dried THF and treated with an excess of tetra-*n*-butylammoniumfluoride (TBAF) for 24 h at room temperature. The reaction mixture was dialyzed using dialysis tubes with a MWCO of 3500 Da changing the solvent from THF to water (two times per day) for two days and at last to THF to remove any residual salts. The polymer was recovered by precipitation from hexane and dried at 50 °C in vacuum. The α -OH-S4VP was characterized by means of GPC-DMF and $^1\text{H-NMR}$ spectroscopy.

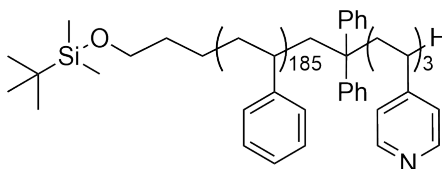


$t\text{BDMSOPrS}_{85}\text{4VP}_2$, 300 MHz, CDCl_3 , δ in ppm: 8.66-8.14 (m, 2H of aromatic system of 4VP), 7.27-6.16 (m, 2H of aromatic system of 4VP, 5H of aromatic system of S, 10H of aromatic system of DPE), 3.56-3.33 (m, 2H, $\text{CH}_2\text{-O}$), 2.41-1.27 ($\text{CH}_2\text{-CH}_2$ of Propyl group, $\text{CH}_2\text{-CH}$ PS backbone, CH_2 of DPE, CH_2CH P4VP backbone), 0.96-0.81 (9H, CH_3), 0.05-(-)0.01 (m, 6H, $\text{CH}_3\text{-Si}$).

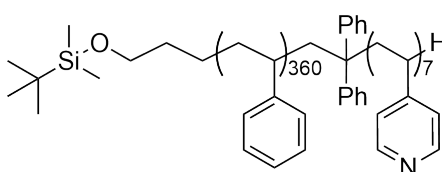


$\text{HO-S}_{84}\text{4VP}_2$, 300 MHz, CDCl_3 , δ in ppm: 8.71-8.15 (m, 2H of aromatic system of 4VP), 7.27-6.11 (m 2H of aromatic system of 4VP, 5H of aromatic system of S, 10H of aromatic system of DPE), 3.60-3.35 (m, 2H, $\text{CH}_2\text{-O}$), 2.51-1.23 ($\text{CH}_2\text{-CH}_2$ of Propyl group, $\text{CH}_2\text{-CH}$ PS backbone, CH_2 of DPE, $\text{CH}_2\text{-CH}$ P4VP backbone).

The block copolymers *t*BDMSOPr-S₁₈₅4VP₃ and *t*BDMSOPr-S₃₆₀4VP₇ were synthesized analogous to *t*BDMSOPr-S₈₅4VP₂.



*t*BDMSOPrS₁₈₅4VP₃, 300 MHz, CDCl₃, δ in ppm: 8.62-8.01 (m, 2H of aromatic system of 4VP), 7.24-5.78 (m, 2H of aromatic system of 4VP, 5H of aromatic system of S, 10H of aromatic system of DPE), 3.56-3.31 (m, 2H, CH₂-O), 2.46-1.22 (CH₂-CH₂ of Propyl group, CH₂-CH PS backbone, CH₂ of DPE, CH₂CH P4VP backbone), 0.97-0.55 (9H, CH₃), 0.03-(-)0.07 (m, 6H, CH₃-Si).

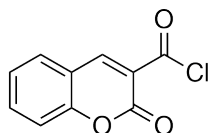


*t*BDMSOPrS₃₆₀4VP₇, 300 MHz, CDCl₃, δ in ppm: 8.73-8.11 (m, 2H of aromatic system of 4VP), 7.35-6.00 (m, 2H of aromatic system of 4VP, 5H of aromatic system of S, 10H of aromatic system of DPE), 3.58-3.34 (m, 2H, CH₂-O), 2.37-1.26 (CH₂-CH₂ of Propyl group, CH₂-CH PS backbone, CH₂ of DPE, CH₂CH P4VP backbone), 0.96-0.83 (9H, CH₃), 0.05-(-)0.06 (m, 6H, CH₃-Si).

9.2.6 Synthesis of Coumarin-3-Carboxylic Chloride

The synthesis of coumarin-3-carboxylic chloride was performed according to the procedure of Sebe^[167]. In a three-neck flask, equipped with a condenser 2 g (10.5 mmol, 1 eq.) of coumarin-3-carboxylic acid were placed and dried under vacuum at room temperature for two hours. 30 mL of toluene (abs.) and 3 drops of DMF were added under argon. To the suspension 1.52 mL (21 mmol, 2 eq.) thionylchloride (SOCl₂) were given drop wise under vigorously stirring and the reaction mixture was allowed to stir under

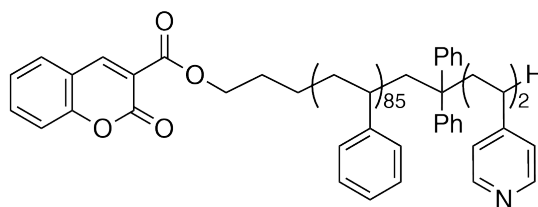
reflux for three hours. Afterwards the reaction was cooled down at room temperature and the resulted crystals were filtered. After recrystallization from toluene the product was dried under vacuum at room temperature and characterized by IR, UV/Vis spectroscopy, and fluorescence spectroscopy (yield = 80 %).



IR (ν/cm^{-1}) = aromatic system (1763-1300), lactone (1720), C-Cl (1763), C=O (2358).

9.2.7 Synthesis of CM-O-S₈₅4VP₂

The synthesis of CM-O-S₈₅4VP₂ was performed by an esterification of the coumarin-3-carboxylic chloride and the hydroxyl group of α -OH-S₈₅4VP₂ in dried DCM. 0.3 g (0.033 mmol, 1 eq.) α -OH-S₈₅4VP₂ was dissolved in 5 mL dried DCM. 4.6 μ L (0.033 mmol, 1 eq.) Triethylamine (TEA) was added and the solution was cooled down at 0 °C. 6.86 mg (0.033, 1 eq) coumarin-3-carboxylic chloride dissolved in 5 mL dried DCM were drop wise added and the solution was allowed to warm up to room temperature. After 24 h stirring the product was precipitated from hexane. The product was purified by dialysis using dialysis tubes with a cutoff of MWCO = 3500 Da in THF for two days. THF was changed every 12 h. Finally CM-O-S₈₅4VP₂ was dried under vacuum at room temperature and analyzed by IR, GPC-DAD in DMF, and fluorescence spectroscopy (yield 86 %).



IR (ν/cm^{-1}) = aromatic system (1763-1300), lactone (1720), C-O-C (1739), C=O (2356).

9.2.8 Synthesis of Citrate@AuNP

Citrate-stabilized gold nanoparticles (Citrate@AuNP) with an average diameter of $d = 15$ nm were synthesized by the Turkevich method^[78]. 100 mg (0.4 mmol, 1 eq.) tetrachloroauric acid trihydrate ($\text{HAuCl}_4 \cdot 3 \text{H}_2\text{O}$) were dissolved in 200 mL ultra-pure water. To the boiling solution a 1 w% (1.36 mmol, 3.4 eq.) solution of trisodium citrate dihydrate ($\text{Na}_3\text{C}_6\text{H}_5\text{O}_7 \cdot 2 \text{H}_2\text{O}$) was added. A change of color from yellow over dark grey to deep red was observed. The solution was stirred for 10 min. Afterwards, the colloidal dispersion was cooled down to room temperature and stored at 4 °C in a dark place. The mean diameter D_H of Citrate@AuNP was determined by TEM image analysis, using 500 nanoparticles.

9.2.9 Ligand Exchange Reactions of Citrate@AuNP with S4VP

The ligand exchange of Citrate@AuNP was performed in a two phase system, using 40 mL glass bottles. Chloroform was used as the organic phase. 1 μmol with respect to the 4VP block of the block copolymers S4VPs was dissolved in chloroform to get a concentration of $c = 1 \text{ g} \cdot \text{L}^{-1}$. A given amount of Citrate@AuNP was added to the chloroform solution and diluted with ultra-pure water to equal the same volume of the chloroform solution. The glass bottles were covered with aluminum foil and the reaction mixture was allowed to shake initially at 1000 rpm for 10 minutes to form a homogenous mixture and afterwards overnight at 500 rpm at room temperature. The polymer functionalized AuNP (S4VP@AuNP) were separated from the aqueous phase and prepared for analysis.

9.2.10 *In situ* Synthesis of S4VP@AuNP

Gold nanoparticles were prepared *in situ* in the presence of S4VP block copolymers using NaBH_4 as reducing agent. The reactions were performed in THF at room temperature. $\text{HAuCl}_4 \cdot 3 \text{H}_2\text{O}$ (20 mg, 0.05 mmol, 1 eq.) and a given amount of polymer with an adequate molar ratio of the 4VP block were dissolved in THF to get a final concentration of $\text{HAuCl}_4 \cdot 3 \text{H}_2\text{O}$ of $c = 0.2 \text{ g} \cdot \text{L}^{-1}$. The solution was allowed to stir for one hour to achieve a complexation of the gold acid with the pyridine groups. A solution of NaBH_4 (0.125 mmol, 1.0 M, 2.5 eq.) in water was rapidly added to the stirring solution, causing

a color change from yellow to red, deep violet, or brown, depending on the given molar ratio of the polymer. After ten minutes stirring the reaction was stopped. Afterwards the samples were purified by dialysis using dialysis tubes with a cutoff of MWCO = 3500 Da against water for two days (water was changed every twelve hours) and finally against THF. The polymer-functionalized AuNP S4VP@AuNP were stored at 4 °C with exclusion of light.

9.2.11 Synthesis of Citrate@AgNP

Citrate-stabilized silver nanoparticles (Citrate@AgNP) with an average diameter of $d = 5$ nm were synthesized according to the published results of Pereira^[132]. NaBH_4 was used as reduction agent, while trisodium citrate dihydrate ($\text{Na}_3\text{C}_6\text{H}_5\text{O}_7 \cdot 2 \text{H}_2\text{O}$) was used as stabilizing agent. A 100 mL solution of AgNO_3 and $\text{Na}_3\text{C}_6\text{H}_5\text{O}_7 \cdot 2 \text{H}_2\text{O}$ with a concentration of 0.25 mM for both reagents was prepared and stirred for one minute. Afterwards 3 mL of a 1 mM NaBH_4 solution (fresh prepared) was added quickly to the mixture. The solution turned immediately to yellow. After 10 minutes stirring the Citrate@AgNP were stored at 4 °C under exclusion of light. The mean diameter was determined by TEM analysis, using 500 particles.

9.2.12 Ligand Exchange Reactions of Citrate@AuNP and Citrate@AgNP with CM-O-S₈₅4VP₂

The ligand exchange of Citrate@AuNP and Citrate@AgNP was performed using the same procedure as described in section 9.2.9. 1 μmol with respect to the 4VP block of CM-O-S₈₅4VP₂ was dissolved in chloroform to get a concentration of $c = 1 \text{ g} \cdot \text{L}^{-1}$. A given amount of Citrate@AuNP and Citrate@AgNP respectively was added to the chloroform solution and diluted with ultra-pure water to equal the same volume of the chloroform solution. The glass bottles were covered with aluminum foil and the reaction mixture was allowed to shake initially at 1000 rpm to form a homogenous mixture for 10 minutes and afterwards overnight at 500 rpm at room temperature. The polymer functionalized AuNP and AgNP (CM-O-S₈₅4VP₂@AuNP, CM-O-S₈₅4VP₂@AgNP) were separated from the aqueous phase and prepared for analysis.

List of Abbreviations

α	alpha
α -OH-S4VP	alpha-hydroxy-polystyrene- <i>block</i> -poly-4(vinylpyridine)
δ	delta
μ L	micro liter
μ m	micro meter, 10^{-6}
$^{\circ}$ C	degree Celsius
1 H-NMR	Proton-Nuclear Magnetic Resonance Spectroscopy
<i>sec</i> -BuLi	sec-Butyllithium
<i>t</i> BDMSCl	<i>tert</i> -Butyldimethylsilyl chloride
<i>t</i> -BDMSOPr	<i>tert</i> -Butyldimethylsilyloxy-propane
<i>t</i> BDMSOPrCl	<i>tert</i> -Butyldimethylsilyl-oxy-propylchloride
<i>t</i> BDMSOPrLi	<i>tert</i> -Butyldemethylsilyl-oxy-propyllithium
3D	three dimensional
4VP	4-vinylpyridine
abs.	absolute
AgNP	silver nanoparticles
Ar	argon
AuNP	gold nanoparticles
BCPs	block copolymers
CaH ₂	Calciumhydride
CDCl ₃	deuterated chloroform
CDI	1,1'-Carbonyldiimidazole
CHCl ₃	Chloroform
Citrate@AgNP	citrate-functionalized silver nanoparticles
Citrate@AuNP	citrate-functionalized gold nanoparticles

CM	Coumarin
CM-Cl	Coumarin-3-carboxylic chloride
CM-COOH	Coumarin-3-carboxylic acid
CM-O-S4VP	Coumarin-oxy-polystyrene- <i>block</i> -poly-4(vinylpyridine)
cryo	cryogenic
Da	Dalton
DAD	Diode Array Detector
DCC	N,N'-Dicyclohexylcarbodiimide
DCM	Dichloromethane
DLS	Dynamic Light Scattering
DMAP	Dimethyl amino pyridine
DMF	Dimethyl formamide
DMSO	Dimethyl sulfoxide
DP	Degree of polymerization
DPE	1,1-Diphenylethylene
e.g.	exempli gratia, for example
eq.	equivalent
ET	electron Tomography
et. al	et alii, and others
FDTD	Finite Difference Time Domain
FITC	Fluorescein isothiocyanate
GC	Gas Chromatography
GPC	Gel Permeation Chromatography
h	hours
IR	Infrared spectroscopy
K	Kelvin
L	Liter
M_n	Number average molecular weight
M_w	weight average molecular weight
MALDI	Matrix-assisted laser desorption/ionization
MgSO ₄	Magnesium sulfate
min	minutes

mL	milliliter
mM	milli molar
nm	nanometer, 10^{-9}
NaHCO ₃	Sodium hydrogen carbonate
p	pressure
Pa	Pascal
PDI	Polydispersity index
ppm	parts per million
s	seconds
S	styrene
S4VP	polystyrene- <i>block</i> -poly-4(vinylpyridine)
S4VP@AuNP	polystyrene- <i>block</i> -poly-4(vinylpyridine)-functionalized AuNP
SOCl ₂	thionylchloride
SPR	Surface Plasmon Resonance
TBAF	tetrabutylammonium fluoride
TEA	triethylamine
TEM	Transmission Electron Microscopy
TFA	trifluoroacetic acid
TGA	thermogravimetric analysis
THF	tetrahydrofuran
TMS	tetramethylsilyl
TOAB	tetraoctyl ammonium bromide
UV/Vis	Ultraviolet-visible spectroscopy
wt %	weight percent

Bibliography

- [1] M. A. Hood, M. Mari and R. Munoz-Espi, *Materials* **2014**, 7, 4057.
- [2] R. Mezzenga and J. Ruokolainen, *Nature Materials* **2009**, 8, 926.
- [3] O. V. Borisov, E. B. Zhulina, F. A. M. Leermakers and A. H. E. Müller, *Adv. Polym. Sci.* **2011**, 241, 57.
- [4] E. Manias, *Nature Materials* **2007**, 6, 9.
- [5] W. Schlenk, J. Appenrodt, A. Michael and A. Thal, *Ber. Deut. Chem. Ges.* **1914**, 47, 473.
- [6] S. R. Sandler and W. Karo, *Polymer Syntheses*, Band 1, Academic Press, Inc. New York and London **1974**.
- [7] M. Szwarc, *J. Polym. Sci.* **1998**, 36, ix.
- [8] M. Szwarc, M. Levy and R. Milkovich, *J. Am. Chem. Soc.* **1956**, 78, 2656.
- [9] M. Maurice, *Anionic Polymerization: Principles and Practice*, Academic Press New York **1983**.
- [10] M. Szwarc, *Living Polymers and Mechanism of Anionic Polymerization*, Band 1, Berlin: Springer-Verlag **1983**.
- [11] O. W. Webster, *Science* **1991**, 251, 887.
- [12] M. Morton, E. E. Bostick and R. Livigni, *Rubber Plastic Age* **1961**, 42, 397.
- [13] M. Morton and F. R. Ells, *J. Polym. Sci.* **1962**, 61, 25.
- [14] M. Morton and L. J. Fetters, *Macromolecular Reviews* **1967**, 2, 71.

- [15] D. Baskaran and A. H. E. Müller, *Controlled and Living Polymerizations: From Mechanism to Applications*, Band 1, Wiley-VCH Verlag GmbH und Co. KGaA, Weinheim **2010**.
- [16] M. W. Matsen and F. S. Bates, *Macromolecules* **1996**, *29*, 1091.
- [17] M. Lazzari, G. Liu and S. Lecommandoux, *Block Copolymers in Nanoscience*, Band 1, WILEY-VCH Verlag GmbH und Co. KGaA, Weinheim **2006**.
- [18] A. J. Meuler, M. K. Mahanthappa, M. A. Hillmyer and F. S. Bates, *Macromolecules* **2007**, *40*, 760.
- [19] Y. Mai and A. Eisenberg, *Chem. Soc. Rev.* **2012**, *41*, 5969.
- [20] K. Matyjaszewski and N. V. Tsarevsky, *Nature Chemistry* **2009**, *1*, 276.
- [21] M. C. Orilall and U. Wiesner, *Chem. Soc. Rev.* **2011**, *40*, 520.
- [22] F. S. Bates, *Science* **1991**, *251*, 898.
- [23] G. H. Fredrickson and F. S. Bates, *Annu. Rev. Mater. Sci.* **1996**, *26*, 501.
- [24] V. Abetz and P. F. W. Simon, *Adv. Polym. Sci.* **2005**, *189*, 125.
- [25] L. Leibler, *Macromolecules* **1980**, *13*, 1602.
- [26] G. M. Whitesides, J. P. Mathias and C. T. Seto, *Science* **1991**, *254*, 1312.
- [27] F. S. Bates and G. H. Fredrickson, *Phys. Today* **1999**, *32*, 898.
- [28] P. Alexandridis and B. Lindman, *Amphiphilic Block Copolymers: Self-Assembly and Applications*, Band 1, Elsevier, Amsterdam **2000**.
- [29] L. Zhang and A. Eisenberg, *Science* **1995**, *268*, 1728.
- [30] L. Zhang, K. Yu and A. Eisenberg, *Science* **1996**, *272*, 1777.
- [31] T. P. Lodge, J. Bang, Z. Li, M. A. Hillmyer and Y. R. Talmon, *Faraday Discuss.* **2005**, *128*, 1.
- [32] N. S. Cameron, M. K. Corbierre and A. Eisenberg, *Can. J. Chem.* **1999**, *77*, 1311.

- [33] J. F. Ding, G. J. Liu and M. L. Yang, *Polymer* **1997**, *38*, 5497.
- [34] J. Bang, S. M. Jain, Z. B. Li, T. P. Lodge, J. S. Pedersen, E. Kesselman and Y. Talmon, *Macromolecules* **2006**, *39*, 1199.
- [35] P. Rempp, E. Franta and J. E. Herz, *Adv. Polym. Sci.* **1988**, *86*, 145.
- [36] L. Zhang and A. Eisenberg, *Polym. Adv. Technol.* **1998**, *9*, 677.
- [37] D. M. P. Mingos, *Structure and Bonding: Gold Clusters, Colloids and Nanoparticles I*, Band 1, Springer **2014**.
- [38] S. Roland, R. E. Prudhomme and C. G. Bazuin, *ACS Macro Lett.* **2012**, *1*, 973.
- [39] M. Antonietti, S. Heinz, M. Schmidt and C. Rosenauer, *Macromolecules* **1994**, *27*, 3276.
- [40] S. O. Driscoll, G. Demireal, R. A. Farrell, T. G. Fitzgerald, C. O. Mahony, J. D. Holmesa and M. A. Morris, *Polym. Adv. Technol.* **2011**, *22*, 915.
- [41] L. Song and Y. M. Lam, *J. Nanosci. Nanotechnol.* **2006**, *6*, 3904.
- [42] C. Menodza, N. Gindy, J. S. Gutmann, A. Fromsdorf, S. Förster and A. Fahmi, *Langmuir* **2009**, *25*, 9571.
- [43] A. Fahmi, T. Pietsch, C. Mendoza and N. Cheval, *Mat. Today* **2009**, *12*, 44.
- [44] G. Kästle, H. G. Boyen, F. Weigl, G. Lengl, T. Herzog, P. Ziemann, S. Tiethmüller, O. Mayer, C. Hartmann, J. P. Spatz, M. Möller, M. Ozawa, F. Banhart, M. G. Garnier and P. Oelhafen, *Adv. Funct. Mat.* **2013**, *13*, 853.
- [45] F. H. Schacher, P. A. Rugar and I. Manners, *Angew. Chem. Int. Ed.* **2012**, *51*, 7898.
- [46] D. E. Sutton and J. A. Schwindemann, *ACS Symp. Ser.* **1998**, *704*, 58.
- [47] A. M. Breul, M. D. Hager and U. S. Schubert, *Chem. Soc. Rev.* **2013**, *42*, 5366.
- [48] N. Shepherd and M. J. Stewart, *Pat. Appl. GB 2241239* **1991**.
- [49] R. P. Quirk, S. H. Jang, K. Han, H. Yang, B. Rix and Y. Leed, *ACS Symp. Ser.* **1998**, *704*, 71.

- [50] P. Zhang and J. S. Moore, *J. Polym. Sci. Part A* **2000**, *38*, 207.
- [51] E. M. Frick and M. A. Hillmyer, *Macromol. Rapid Commun.* **2000**, *21*, 1371.
- [52] J. Tong, C. Zhou, S. Ni and M. A. Winnik, *Macromolecules* **2001**, *34*, 696.
- [53] X. Wang, M. A. Winnik and I. Manners, *Macromol. Rapid Commun.* **2002**, *23*, 210.
- [54] R. P. Quirk, F. You, C. Wesdemiotis and M. A. Arnould, *Macromolecules* **2004**, *37*, 1234.
- [55] A. K. Brannan and F. S. Bates, *Macromolecules* **2004**, *37*, 8816.
- [56] L. R. Hutchings and S. Roberts-Bleming, *Macromolecules* **2006**, *39*, 2144.
- [57] A. J. Meuler, M. K. Mahanthappa, M. A. Hillmyer and F. S. Bates, *Macromolecules* **2007**, *40*, 760.
- [58] G. Schmid, *Microwaves in Nanoparticle Synthesis: Fundamentals and Application*, Band 1, Wiley-VCH GmbH and Co KGaA, Weinheim **2013**.
- [59] S. Horikoshi and N. Serpone, *Nanoparticles: From Theory to Applications*, Band 1, Wiley-VCH GmbH and Co KGaA, Weinheim **2004**.
- [60] E. Roduner, *Chem. Soc. Rev.* **2006**, *35*, 583.
- [61] D. Buceta, Y. Pineiro, C. Vazquez-Vazquez, J. Rivas and M. A. Lopez-Quintela, *Catalysts* **2014**, *4*, 356.
- [62] S. K. Gosh and T. Pal, *Chem. Rev.* **2007**, *107*, 4797.
- [63] C. L. Choi and A. P. Alivisatos, *Annu. Rev. Phys. Chem.* **2010**, *61*, 369.
- [64] G. Schmid and B. Corain, *Eur. J. Inorg. Chem.* **2003**, 3081.
- [65] A. Tomar and G. Garg, *Global J. Pharmacol.* **2013**, *7*, 34.
- [66] Y. Zhang, W. Chu, A. D. Foroushani, H. Wang, D. Li, J. Liu, C. J. Barrow, X. Wang and W. Yang, *Materials* **2014**, *7*, 5169.
- [67] M. C. Daniel and D. Astruc, *Chem. Rev.* **2004**, *104*, 293.

- [68] M. Faraday, *Philos. Trans. R. Soc. Lond.* **1857**, 147, 145.
- [69] J. C. M. Garnett, *Philos. Trans. R. Soc., A* **1904**, 203, 385.
- [70] G. Mie, *Ann. Phys.* **1908**, 25, 377.
- [71] K. L. Kelly, E. Coronado, L. L. Zhao and G. C. Schatz, *J. Phys. Chem. B* **2003**, 107, 668.
- [72] A. Link and M. A. El-Sayed, *J. Phys. Chem. B.* **1999**, 103, 4212.
- [73] G. Schmid, *Chem. Rev.*, Band 92, Wiley-VCH GmbH and Co KGaA, Weinheim **1992**.
- [74] L. D. Pachon and G. Rothenberg, *Appl. Organometal. Chem.* **2008**, 22, 288.
- [75] P. Zhao, N. Li and D. Astruc, *Coord. Chem. Rev.* **2013**, 257, 638.
- [76] P. W. Voorhees, *J. Statist. Phys.* **1885**, 38, 231.
- [77] W. Ostwald, *Zeitschrift für Physikalische Chemie* **1900**, 34, 495.
- [78] J. Turkevich, P. C. Stevenson and J. Hillier, *Discuss. Faraday Soc.* **1950**, 8, 352.
- [79] G. Frens, *Nature* **1973**, 241, 20.
- [80] L. M. Liz-Marzan, *Langmuir* **2006**, 22, 32.
- [81] J. Kimling, M. Maier, B. Okenve, V. Kotaidis, H. Ballot and A. Plech, *J. Phys. Chem. B* **2006**, 110, 15700.
- [82] B. K. Pong, H. I. Elim, J. X. Chong, W. Ji, B. L. Trout and J. Y. Lee, *J. Phys. Chem. C* **2007**, 111, 6281.
- [83] J. Polte, T. T. Ahner, F. Delissen, S. Sokolov, F. Emmerling, A. F. Thunemann and R. Kraehnert, *J. Am. Chem. Soc.* **2010**, 132, 1296.
- [84] S. Kumar, K. S. Gandhi and R. Kumar, *Ind. Eng. Chem. Res.* **2007**, 46, 3128.
- [85] I. Ojea-Jimenez, F. M. Romero, N. G. Bastus and V. Puentes, *J. Phys. Chem. C* **2010**, 114, 1800.

- [86] M. Brust, M. Walker, D. Bethell, D. J. Schiffrin and R. J. Whyman, *J. Chem. Soc, Chem. Comm.* **1994**, 801.
- [87] R. Sardar, A. M. Funston, P. Mulvaney and R. W. Murray, *Langmuir* **2009**, *25*, 13840.
- [88] A. C. Templeton, W. . Wuelfing and R. W. Murray, *Acc. Chem. Res.* **2000**, *33*, 27.
- [89] C. A. Mirkin, R. L. Letsinger, R. C. Mucic and J. J. Storhoff, *Nature* **1996**, *382*, 607.
- [90] J. S. Bradley, *The Chemistry of Transition Metal Colloids, Cluster and Colloids: From Theory to Applications*, Wiley VCH: Weinheim **1994**.
- [91] H. H. Helcher, *Aurum Potabile Oder Gold Tinstur*, Breslau and Leipzig, Germany **2718**.
- [92] J. Shan and H. Tenhu, *Chem. Commun.* **2007**, *44*, 4580.
- [93] N. Uehara, *Anal. Sci* **2010**, *26*, 1219.
- [94] K. Ohno, K. Koh, Y. Tsujii and T. Fukuda, *Macromolecules* **2002**, *35*, 8989.
- [95] S. Bokern, J. Getze, S. Agarwal and A. Greiner, *Polymer* **2011**, *912*, 179.
- [96] C. Krüger, S. Agarwal and A. Greiner, *J. Am. Chem. Soc.* **2008**, *130*, 2710.
- [97] S. Bokern, K. Gries, H.-H. Görtz, V. Warzelhahn, S. Agarwal and A. Greiner, *Adv. Funct. Mater.* **2011**, *21*, 3753.
- [98] M. K. Corbierre, N. S. Cameron and R. B. Lennox, *Langmuir* **2004**, *20*, 2867.
- [99] P. J. G. Goulet, G. R. Bourret and R. B. Lennox, *Langmuir* **2008**, *28*, 2909.
- [100] H. Pletsch, L. Peng, F. Mitschang, A. Schaper, M. Hellwig, D. Nette, A. Seubert, A. Greiner and S. Agarwal, *Small* **2014**, *10*, 201.
- [101] M. Sastry, *Curr. Sci.* **2003**, *85*, 1735.
- [102] J. Tian, J. Jin, F. Zheng and H. Zhao, *Langmuir* **2010**, *26*, 8762.
- [103] A. C. V. Chechik, *Phys. Chem. Chem. Phys* **2008**, *10*, 5029.
- [104] J. J. Chiu, B. J. kim, E. J. Kramer and D. J. Pine, *J. Am. Chem. Soc.* **2005**, *127*, 5036.

- [105] J. Shan, M. Nupponen, H. Jiang, T. Viitala, E. Kauppinen, K. Kontturi and H. Tenhu, *Macromolecules* **2005**, *38*, 2918.
- [106] C. Gentilini, F. Evangelista, P. Rudolf, P. Franchi, M. Lucarini and L. Pasquato, *J. Am. Chem. Soc.* **2008**, *130*, 15678.
- [107] H. Pletsch, M. J. Schnepf and S. Agarwal, *Chem. Mater.* **2014**, *26*, 4805.
- [108] J. P. Spatz, S. Mössmer and M. Möller, *Chem. Eur. J.* **1996**, *2*, 1552.
- [109] A. C. Balazs, T. Emrick and R. P. Russell, *Science* **2006**, *314*, 1107.
- [110] B. Ebeling and P. Vana, *Macromolecules* **2013**, *46*, 4862.
- [111] S. Bokern, Z. Fan, C. Mattheis, A. Greiner and S. Agarwal, *Macromolecules* **2005**, *38*, 2918.
- [112] P. Alexandridis, *Chem. Eng. Technol.* **2011**, *34*, 15.
- [113] S. Förster and M. Antonietti, *Adv. Mater.* **1998**, *10*, 195.
- [114] H. Cho, H. Park, S. Par, H. Choi, H. Huang and T. Chang, *J. Coll. Inter. Sci.* **2011**, *356*, 1.
- [115] B. J. Kim, J. Bang, C. J. Hawker, J. J. Chiu, D. J. Pine, S. G. Jang, S.-M. Yang and E. J. Kramer, *Langmuir* **2007**, *23*, 12693.
- [116] W. Hamley, *Nanotechnology* **2003**, *14*, R39.
- [117] M. Grzelcak and L. M. Liz-Marzan, *Langmuir* **2013**, *29*, 4652.
- [118] M. Grzelcak, J. Vermant, E. M. Furst and L. M. Liz-Marzan, *ACS Nano* **2010**, *4*, 3591.
- [119] X. Chen, D. Zhao, Y. An, L. Shi, W. Hou and L. Chen, *J. Nanopart. Res.* **2010**, *12*, 1877.
- [120] W. L. Leong, P. S. Lee, A. Lohani, Y. M. Lam, T. Chen, S. Zhang, A. Dodabalapur and S. G. Mhaisalkar, *Adv. Mater.* **2008**, *20*, 2325.
- [121] S. Ren, S.-K. Lim and S. Gradecak, *Chem. Comm.* **2010**, *46*, 6246.

- [122] A. Haryono and W. H. Binder, *Small* **2006**, *2*, 600.
- [123] C. Mendoza, T. Pietsch, N. Gindy and A. Fahmi, *Adv. Mater.* **2008**, *20*, 1179.
- [124] L. Bronstein, M. Antonietti and P. Valetsky, *Metal Colloids in Block Copolymer Micelles: Formation and Material Properties, Nanoparticles and Nanostructured Films*, Wiley VCH: Weinheim **1998**.
- [125] A. B. R. Mayer, *Polym. Adv. Technol.* **2001**, *12*, 96.
- [126] J. J. Chiu, B. J. Kim, G.-R. Yi, J. Bang, E. J. Kramer and D. J. Pine, *Macromolecules* **2007**, *40*, 3361.
- [127] T. Ye, X. Chen, X. Fan and Z. Shen, *Soft. Mater.* **2013**, *9*, 4715.
- [128] Y. Zhao, K. Thorkelsson, A. J. Mastroianni, T. Schilling, J. M. Luther, B. J. Rancatore, K. Matsunaga, H. Jinnai, Y. Wu, D. Poulsen, J. M. J. Fréchet, A. P. Alivisatos and T. Xu, *Nat. Mater.* **2009**, *8*, 979.
- [129] R. Liang, J. Xu, W. Li, Y. Liao, K. Wang, J. You, J. Zhu and W. Jiang, *Macromolecules* **2015**, *48*, 256.
- [130] W. Li, S. Liu, R. Deng and J. Zhu, *Angew. Chem. Int. Ed.* **2011**, *50*, 5865.
- [131] W. Li, S. Liu, R. Deng, J. Wang, Z. Nie and J. Zhu, *Macromolecules* **2013**, *46*, 2282.
- [132] V. V. Pinto, M. J. Ferreira, R. Silva, H. A. Santos, F. Silva and C. M. Pereira, *Coll. Surf. A: Physicochem. Eng. Aspects* **2010**, *364*, 19.
- [133] C. Liu and B. Li, *Anal. Bioanal. Chem.* **2011**, *401*, 229.
- [134] A. Janz, A. Köckritz, L. Yao and A. Martin, *Langmuir* **2010**, *26*, 6783.
- [135] D. Mollenhauer, N. Gaston, E. Voloshina and B. Paulus, *J. Phys. Chem. C* **2013**, *117*, 4470.
- [136] V. Myroshnychenko, J. Rodriguez-Fernandez, I. Pastoriza-Santos, A. M. Funston, C. Novo, P. Mulvaney, L. M. Liz-Marzan and F. J. G. de Abajo, *Chem. Soc. Rev.* **2008**, *37*, 1792.

- [137] J. Kottmann, O. Martin, D. Smith and S. Schultz, *Opt. Exp.* **2000**, *6*, 213.
- [138] P. K. Jain, K. S. Lee, I. H. El-Sayed and M. A. El-Sayed, *J. Phys. Chem. B* **2006**, *110*, 7238.
- [139] P. K. Jain, W. Huang and M. A. El-Sayed, *Nano Lett.* **2007**, *7*, 2080.
- [140] D. S. Citrin, *Nano Lett.* **2005**, *5*, 985.
- [141] B. Willingham and S. Link, *Opt. Express* **2011**, *19*, 6450.
- [142] C. Hanske, M. Tebbe, C. Kuttner, V. Bieber, V. V. Tsukruk, M. Chanana, T. A. F. König and A. Fery, *Nano Lett.* **2014**, *14*, 6863.
- [143] T. A. F. König, R. Kodiyath, Z. A. Combs, M. A. Mahmoud, M. A. El-Sayed and V. V. Tsukruk, *Part. Part. Syst. Charact.* **2014**, *31*, 274.
- [144] S. Ehlert, S. M. Taheri, D. Pirner, M. Drechsler, H. W. Schmidt and S. Förster, *ACS Nano* **2014**, *8*, 6114.
- [145] M. K. Corbierre, N. S. Cameron, M. Sutton, S. G. J. Mochrie, L. B. Lurio, A. Rü and R. B. Lennox, *J. Am. Chem. Soc.* **2001**, *123*, 10411.
- [146] C. K. Yee, R. Jordan, A. Ulman, H. White, A. King, M. Rafailovich and J. Sokolov, *Langmuir* **1999**, *30*, 1674.
- [147] C. Mendoza, T. Pietsch, N. Gindy and A. Fahmi, *Adv. Mater.* **2008**, *20*, 1179.
- [148] C. Lee, S. H. Kim and T. P. Russell, *Macromol. Rapid Commun.* **2009**, *30*, 1674.
- [149] X. Zu, W. Tu and Y. Deng, *J. Nanopart. Res.* **2011**, *13*, 1.
- [150] B. H. Sohn and B. H. Seo, *Chem. Mater.* **2001**, *13*, 1752.
- [151] T. W. Greene and P. G. M. Wuts, *Protective Groups in Organic Synthesis*, Band 2, Wiley-Interscience: New York **1991**.
- [152] H. G. O. Becker, W. Berger and G. Domschke, *Organikum*, Band 20, Heidelberg **1996**.

- [153] N. N. Y. Chujo, *Nanohybridization of Organic-Inorganic Materials*, Band XVII, Springer **2009**.
- [154] H. C. Kolb, M. G. Finn and K. B. Sharpless, *Angew. Chem. Int. Ed.* **2001**, *40*, 2004.
- [155] C. Li and S. Liu, *Chem. Comm.* **2012**, *48*, 3262.
- [156] A. S. Al-Kady, M. Gaber, M. M. Hussein and E. M. Ebeid, *J. Phys. Chem. A* **2009**, *113*, 9474.
- [157] D. Ghosh and N. Chattopadhyay, *OPJ* **2013**, *3*, 18.
- [158] G. Chumanov, K. Sokolov, B. W. Gregory and T. M. Cotton, *J. Phys. Chem.* **1995**, *99*, 9466.
- [159] S. Nie and S. R. Emory, *Science* **1997**, *275*, 1102.
- [160] J. R. Kremer, D. N. Mastronade and J. R. McIntosh, *J. Struct. Biol.* **1996**, *116*, 71.
- [161] P. Engelhardt, *Encycl. Anal. Chem.* **2000**, *6*, 4948.
- [162] E. F. P. et al., *J. Comput. Chem.* **2004**, *25*, 1605.
- [163] P. B. Johnson and R. W. Christy, *Phys. Rev. B* **1972**, *6*, 4370.
- [164] M. B. Müller, C. Kuttner, T. A. F. König, V. V. Tsukruk, S. Förster, M. Karg and A. Fery, *ACS Nano* **2014**, *8*, 9410.
- [165] S. T. Hill and M. Mokotoff, *J. Org. Chem.* **1984**, *49*, 1441.
- [166] L. B. Poole, B. B. Zeng, S. A. Knaggs, M. Yakubu and S. B. King, *Bioconjug. Chem.* **2005**, *16*, 1624.
- [167] E. G. H. Shahinian and I. Sebe, *Rev. Chim.* **2011**, *11*, 1098.

(Eidesstattliche) Versicherungen und Erklärungen

(§8 S. 2 Nr. 6 PromO)

Hiermit erkläre ich mich damit einverstanden, dass die elektronische Fassung meiner Dissertation unter Wahrung meiner Urheberrechte und des Datenschutzes einer gesonderten Überprüfung hinsichtlich der eigenständigen Anfertigung der Dissertation unterzogen werden kann.

(§8 S. 2 Nr. 8 PromO)

Hiermit erkläre ich eidesstattlich, dass ich die Dissertation selbständig verfasst und keine anderen als die von mir angegebenen Quellen und Hilfsmittel benutzt habe.

(§8 S. 2 Nr. 9 PromO)

Ich habe die Dissertation nicht bereits zur Erlangung eines akademischen Grades anderweitig eingereicht und habe auch nicht bereits diese oder eine gleichartige Doktorprüfung endgültig nicht bestanden.

(§8 S. 2 Nr. 10 PromO)

Hiermit erkläre ich, dass ich keine Hilfe von gewerblichen Promotionsberatern bzw. -vermittlern in Anspruch genommen habe und auch künftig nicht nehmen werde.

Bayreuth, den 21.07.2015,.....